Masterarbeit im Fach Physik

# NNLO-Beiträge zur Photoproduktion von Jets

# NNLO Contributions to Jet Photoproduction

vorgelegt von
Markus Michael

17. September 2013

*"You must learn to listen,"* he says. If particles, forces, and fields obey the curve that binds the flow of numbers, then they must sound like harmonies in time. *"You think with your eyes; this is your problem. No one can see four independent variables mapping out a surface in five or more dimensions. But the tuned ear can hear chords."*

---

Richard Powers, *The Time of Our Singing*

# Contents

# 1. Introduction

Higher order calculations in perturbative Quantum Chromodynamics (pQCD) have become a powerful predictive tool in the realms of high energy particle physics. Regardless of the efforts that are put into the evaluation of partonic cross sections in the perturbative regime, the parton world remains inaccessible for direct observation. The quantities that can be measured relate to detected hadrons and leptons, in the same way as information on the initial particle is merely available at hadron level. This calls for the calculation of hadronic cross sections, for which we cannot avoid to leave pQCD: Hadrons, e.g. a proton, have a spacial extent that is much larger than the typical distance in hard scattering processes. Moreover, the scattering off a proton in the parton model is equivalent to the incoherent sum of the scattering processes off the different constituent partons, whose description is of an inherently non-perturbative nature, since the energy scales inside the proton is to low to allow for the application of pQCD. Hence, any perturbative calculation at any order whatsoever needs a link to long distance soft QCD and eventually to observable states.

This link is provided by the so-called parton density functions (PDFs), which cannot be calculated in QCD but need to be determined experimentally. In the case of the proton, information on the inner parton distribution is usually collected in deep inelastic electron-proton scattering (DIS) [1, 2], a process in which the much smaller electron serves to probe the inner structure. The analysis then basically consists in finding parametrizations for the different parton densities and to fit them to the data. As the resulting structure functions, which are universal for all processes, depend on the energy scale at which the underlying data was taken, they have to be evoluted to the scale of interest if they are used in other processes. The evolution prescription is again given by theory, where the corresponding scale dependence arises due to factorization and leads to the DGLAP evolution equations. Further input for the analysis is contributed by inclusive-jet measurements and fixed target experiments [2] that cover kinematical ranges complementary to DIS.

The kinematical region of electron-proton collisions in which the exchanged photon has a small virtuality $Q \simeq 0$ is refered to as photoproduction. This region is of great importance because it exhibits the largest event rates and well observable hadronic final states, and it was widely studied in the context of jet production by the experiments H1 and ZEUS at HERA even after the shutdown of the accelerator in 2007 [3, 4, 5, 6]. The quasireal, spacelike photons are well-suited for the investigation of the proton substructure, but they can also dissolve on their part into partons that scatter off the partons in the proton. Therefore, photoproduction is another promising source of knowledge about the photon structure and serves as a complement to the rarely existing information that has been extracted from deep inelastic $\gamma\gamma^*$ scattering at $e^+e^-$ colliders.

A recently published analysis of ZEUS inclusive-jet data [3] shows a mismatch of experimental values and next-to-leading order (NLO) perturbative calculations [7] for the differential inclusive jet cross section at low transverse momenta and high rapidities. These discrepancies are mostly related to non-perturbative effects and point out the need for a further study of the photon structure function. The latter can be accomplished with the help of the photoproduction data mentioned above. An essential requirement for this kind of study is to have a very accurate theoretical prediction; for this reason, it is of great interest to include higher order, i.e. next-to-next-to-leading order (NNLO) contributions in the calculations.

In theory, the evaluation of partonic cross sections leads to a number of divergent integrals.

Beyond leading order (LO), the virtual corrections are evaluated from Feynman amplitudes that contain at least one inner particle loop. The integration over the loop momenta causes so-called infrared and ultraviolet singularities, of which the latter are absorbed into the fields and couplings by renormalizing the QCD Lagrangian. This renormalization procedure causes the QCD coupling to run and gives rise to a very important feature which is the asymptotic freedom of QCD. The energy-scale-dependent coupling strength tends to zero as the energy becomes very large. It is this feature which makes pQCD valid at high energies, at which the expansion parameter of the perturbative series is sufficiently small and quarks can be described as independent particles. On the other hand, at low energies the coupling becomes large; this provides an explanation of the confinement of coloured states in QCD.
Processes in which the LO amplitude is extended by the emission of one or more real particles, are called real corrections. Here, another class of singularities arises. Emitted particles whose momenta tend to zero, produce soft divergences in the final state phase space integration, which cancel against the infrared divergences from the loop corrections. If a particles radiates further particles with parallel momenta and zero mass, combinations of so-called collinear divergences and splitting functions occur, which have to be absorbed into the structure functions by introducing renormalized parton densities and cross sections. The latter renormalization gives rise to a running also of the PDFs, which has been mentioned above.

A similar procedure would yield fragmentation functions describing the transformation of the scattered final state particles into hadrons. Inclusive jet cross sections, which are considered in this thesis, are characterized by not taking into account specific hadrons or partons, but only beams of them. Both the reconstruction of jets from detected particle showers on the experimental side, as well as the construction of the former from final state partons on the theoretical side, are realized by the application of jet or cluster algorithms. Of the several prescriptions that have been developed [8, 9, 10, 11], each leads to different final results.

Apart from the fact that the coefficients of the perturbative series have to be non-divergent, they should decrease towards higher orders, as otherwise any finite-order truncation of the expansion would be meaningless. Because of the incomplete cancellation of the soft terms stemming from real corrections by the infrared poles of the virtual contributions, logarithmic expressions are left over at each order in the series which in a certain region of phase space grow large, and in particular lead to the fact that all coefficients of the expansion have the same order of magnitude. Consequently, all these logarithmic terms should be considered even if the evaluation of the perturbative series is stopped at some finite order. This is achieved through the method of resummation, in which the logarithms are summed up to all orders in a soft limit, yielding a closed exponentiated form for the all-order soft and virtual corrections.

In the case of threshold resummation, only those logarithms that become large at threshold are resummed. Two different kinds of threshold can be distinguished: The hadronic threshold marks the limiting case in which all hadronic center-of-mass energy is found in the final state jets. However, most of the detected events occur relatively far from this hadronic threshold. Of relevance for threshold resummation is the partonic threshold, the region in phase space where the energy of an emitted particle becomes zero and the final state jets carry the complete partonic center-of-mass energy.
The corresponding soft and virtual corrections for this order are found by expanding the resummed cross section into a perturbative series up to NNLO; these can be added to a fixed order NLO calculation such as in [7] after a matching has been performed in order to avoid double-counting of any terms. The NNLO corrections are given at next-to-next-to-leading logarithm

(NNLL) accuracy in a general form, to be adapted to the particular processes of interest, in a publication of N. Kidonakis [12].

The aim of this thesis is to incorporate these NNLO corrections into the full NLO calculation of Klasen and Kramer [7] in order to provide higher accuracy in the calculation of inclusive jet cross sections in photoproduction. As pointed out before, improved precision is needed for a better determination of the proton and photon density functions. Another goal is to obtain the best fitting value of the strong coupling constant $\alpha_s$ one the basis of NNLO-NNLL-improved calculations, using the different PDF sets of the CT10 NNLO series [13].

After giving an overview of some important aspects of QCD and photoproduction, Sec. 2 examines the calculation of partonic cross sections in pQCD as well as their connection to initial state hadrons and final state jets. An introduction to the philosophy of resummation marks the beginning of Sec. 3 and leads to a general discussion of resummation at next-to-leading logarithm (NLL) accuracy. Afterwards, the derivation of the NLO and NNLO master formulæ for soft and virtual corrections [12] is sketched, and the NLO results are compared to those in [7]. The forth section contains the description of our approach in the implementation of the higher order terms in the existing full NLO calculation, whereupon the numerical results are presented and compared to the data of different experiments. Finally, in Sec. 5, the results are summarized and conclusions are drawn.

# 2. Photoproduction in the QCD-improved parton model

We start by providing the theoretical base for our study. Rather than giving a complete review, we aim at giving an overview of the features of photoproduction and its quantum chromodynamical description which play a major role for the calculations presented in the following chapters. Furthermore, we use this section state which notations will be used. After a brief introduction to Quantum Chromodynamics in Sec. 2.1, which follows in parts the corresponding introductory section in [14], we turn to the foundations of *ep* scattering at HERA in Sec. 2.2, which will be discussed first in the framework of the naïve parton model. We then give a preview of the QCD-improved parton model by introducing the non-perturbative parton densities of the proton (Sec. 2.2.2) and the photon (Sec. 2.2.3), discussing their experimental determination and quoting their evolution equations. This subsection is partly based on [7].
Sec. 2.3 deals with the calculation of inclusive jet cross sections. Before the needed master formula for inclusive jet cross sections is derived in Sec. 2.3.2 [15, 7], a link between final state partons and observed jets is provided by a review of several cluster algorithms (Sec. 2.3.1). Leading order partonic cross sections of the processes relevant in photoproduction are finally presented in Sec. 2.4. This first glimpse at perturbative QCD is followed by a discussion of two central sources of QCD corrections, which are renormalization (Sec. 2.5) and factorization (Sec. 2.6). In both sections, we treat the different divergences which arise at higher order QCD and shortly explain the origin of renormalization [16] and factorization scales [16, 7].

## 2.1. Basics of Quantum Chromodynamics

The theory underlying most of our calculations is QCD, a non-Abelian gauge field theory describing the strong interaction in the Standard Model (SM). It is based on a SU(3) gauge group; the corresponding massless gauge bosons mediating the interaction are called gluons. The charge associated to the gauge group is called colour, while the fermions carrying the colour charge are the quarks. Until now, 6 quarks have been discovered which have different masses, fractional electromagnetic charge, and which are also distinguished by an additional quantum number called flavour. They can be grouped in three families of two quarks in each case, as can be seen in the following table:

| family | 1 | | 2 | | 3 | |
|---|---|---|---|---|---|---|
| flavour | d | u | s | c | b | t |
| name | down | up | strange | charm | bottom | top |
| el. charge | $-1/3$ | $2/3$ | $-1/3$ | $2/3$ | $-1/3$ | $2/3$ |
| mass ($\overline{\text{MS}}$) | $\sim 4.8\,\text{MeV}$ | $\sim 2.3\,\text{MeV}$ | $\sim 0.1\,\text{GeV}$ | $\sim 1.3\,\text{GeV}$ | $\sim 4.1\,\text{GeV}$ | $\sim 173\,\text{GeV}$ |

Table 1: Summary of the basic properties of the three quark families. The quark masses are taken from [17].

Apart from these three quark families, there might be more at higher masses, but current research (e.g. by the CMS Collaboration [18]) has not found any new quarks up to a limit of 675 GeV. See also [17] for lower mass limits of possible 4th generation quarks. In this thesis we will always assume all particles to be massless, which is a very good approximation at the energy scale we are considering. However, the heavy top quark is too massive to play a role in photoproduction. Therefore, we set the number of flavours $n_f = 5$.
As the three lightest quarks have very small and similar masses, the QCD Lagrangian,

$$\mathcal{L} = \mathcal{L}_\text{G} + \mathcal{L}_\text{F} + \mathcal{L}_\text{GF} + \mathcal{L}_\text{FP}, \tag{2.1}$$

has an approximate U(3) flavour symmetry. On this symmetry the ancient quark model was build even before the theory of QCD was established. A better approximation would be a U(2) symmetry, i.e. if we only considered the up and down quark. In the massless limit, the two chiral components of the quarks become completely independent, leaving us actually with two U(2) symmetries, $\mathrm{U}(2)_\mathrm{L} \times \mathrm{U}(2)_\mathrm{R}$. Alternatively, this can be expressed as the symmetry of vector and axial combinations, $\mathrm{U}(2)_\mathrm{V} \times \mathrm{U}(2)_\mathrm{A}$. The vector component can be decomposed into $\mathrm{SU}(2)_\mathrm{I} \times \mathrm{U}(1)_\mathrm{B}$, thereby expressing isospin and baryon number conservation which is also observed in nature. However, $\mathrm{SU}(2)_\mathrm{A} \times \mathrm{U}(1)_\mathrm{A}$ is spontaneously broken, so one would expect four Goldstone bosons to be observed. Three of them, belonging to $\mathrm{SU}(2)_\mathrm{A}$, are the pions, while the $\mathrm{U}(1)_\mathrm{A}$ symmetry is indeed explicitly broken. This means that CP invariance is violated in the strong sector, which has not been observed so far and is known as the strong CP problem.
The first two parts on the left-hand side of Eq. (2.1) contain the kinematic terms of the gluon and quark fields $G_a^{\mu\nu}$ and $\psi_f$ as well as their interactions [19]:

$$\begin{aligned}
\mathcal{L}_\mathrm{G} + \mathcal{L}_\mathrm{F} &= -\frac{1}{4} G_a^{\mu\nu} G^a_{\mu\nu} + \sum_f \bar{\psi}_f (i\gamma^\mu D_\mu - m_f)\psi_f \\
&= -\frac{1}{4}(\partial^\mu G_a^\nu - \partial^\nu G_a^\mu)(\partial_\mu G^a_\nu - \partial_\nu G^a_\mu) + \sum_f \bar{\psi}_f (i\gamma^\mu \partial_\mu - m_f)\psi_f \\
&\quad + g_s G_a^\mu \sum_f \bar{\psi}_f \gamma_\mu T^a \psi_f \\
&\quad - \frac{g_s}{2} f^{abc}(\partial^\mu G_a^\nu - \partial^\nu G_a^\mu) G^b_\mu G^c_\nu - \frac{g_s^2}{4} f^{abc} f_{ade} G^\mu_b G^\nu_c G^\mu_d G^e_\nu
\end{aligned} \tag{2.2}$$

Here, explicit sums run over the different quark flavours, $T^a$ are the generators of the SU(3) colour symmetry and $f^{abc}$ the corresponding structure functions. In perturbative QCD, the second line of Eq. (2.2) gives rise to the gluon and quark propagators, the third line to quark-gluon vertices, whereas the last line contains the three and four gluon coupling.
The remaining two terms in Eq. (2.1) are the gauge fixing and the Faddeev-Popov term respectively. They have the form

$$\mathcal{L}_\mathrm{GF} = -\frac{1}{2\xi}(\partial^\mu G^a_\mu)(\partial_\nu G^\nu_a), \tag{2.3}$$

with the gauge parameter $\xi$, and

$$\mathcal{L}_\mathrm{FP} = -\partial_\mu \bar{\phi}_a D^\mu \phi^a, \tag{2.4}$$

where $\phi$ is a scalar field obeying fermion statistics, the so-called ghost field. Both are introduced in order to handle unphysical polarizations of the gluon field which cause problems while dealing with field quantization and gluon loops.

## 2.2. Electron proton collisions and parton densities

When in 1992 HERA, the largest particle accelerator at DESY in Hamburg, was put into operation, it was the first storage ring in the world that could accelerate two different types of particles. Electrons (or their anti-particles, the positrons) and protons were accelerated in different devices, travelling in opposite directions through the 6.3 km long storage ring, before colliding at high energies in one of the huge detectors belonging to the experiments of ZEUS and H1. Together with Tevatron, the storage ring at Fermilab in Chicago it was also the first accelerator using superconducting coils to provide the strong magnetic fields needed in order to bend the proton beam. Data taking continued until 2007, when the experiment was shut down. However, the data analysis is still in progress. In this section, we will review some important features of $ep$ scattering and see how experimental data enters into our calculations.

### 2.2.1. Neutral current $ep$ collisions

First, we will give a short overview of general kinematics. A collision between an electron and a proton is said to be inelastic if the inner structure of the proton is destroyed and the final state apart from a lepton merely contains hadronized proton remnants. If the final state lepton is an electron,

$$e^-(k) + p(p) \to e^-(k') + X, \tag{2.5}$$

the process is called a neutral current (NC) process, mediated by the exchange of a neutral boson such as the photon or the $Z^0$ boson from weak interaction. However, the contribution of the weak gauge bosons is largely suppressed due to their high mass ($m_Z \simeq 91\,\text{GeV}$), and possible multiple photon exchanges due to additional powers of the electromagnetic coupling $\alpha$. Hence, we only take single photon exchange into account, see Fig. 2.1. By

$$S = (k+p)^2 \simeq 4E_eE_p \tag{2.6}$$

we denote the hadronic center-of-mass energy squared, which at HERA in the later stage was $\sqrt{S} \simeq 318\,\text{GeV}$, when electrons of energy $E_e = 27.5\,\text{GeV}$ collided with a proton beam of energy $E_p = 920\,\text{GeV}$. The virtuality of the exchanged photon is given by

$$Q^2 = -q^2 = -(k-k')^2 \tag{2.7}$$

and determines the resolution available to probe the proton with the electron. Together with the Bjorken-x scaling variable,

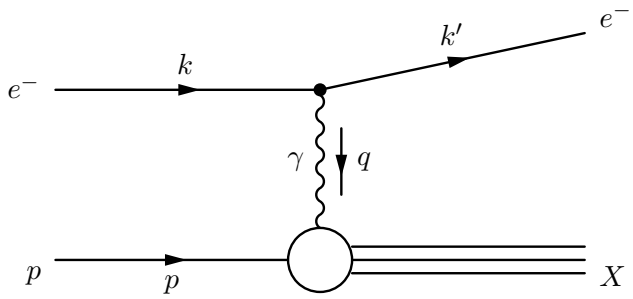


Figure 2.1: Electron-proton scattering with exchange of a single photon.

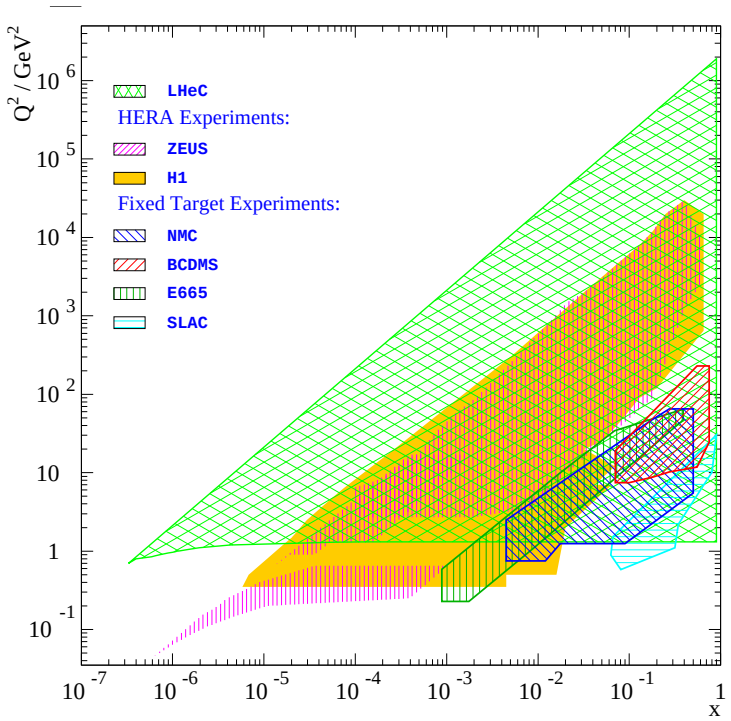


Figure 2.2: The coverage of the kinematic plane in different experiments. [20]

$$x = \frac{Q^2}{2pq}, \tag{2.8}$$

which gives the momentum fraction of the proton carried by the interacting parton, it provides a complete description of the scattering kinematics. Fig. 2.2 displays the covered range of HERA in the $(x, Q^2)$ plane. It is clearly visible that the area reached with two accelerated particles at HERA exceeds the range of fixed target experiments. Yet, the improvements at the LHC enable us to gain more information about the proton substructure with LHeC especially at high $Q^2$, i.e. in the deep inelastic scattering (DIS) regime.
DIS implies a virtuality $Q^2 \gg 1\,\text{GeV}$ much larger than the proton mass. The photoproduction regime lies at lower photon virtualities $Q \leq 1\,\text{GeV}$. These quasireal photons are very suitable to investigate the proton structure. They can either interact directly with the partons in the proton, or equally contribute a parton to the interaction, as they also fluctuate into hadronic parts like $q\bar{q}$ pairs. Therefore, we distinguish between *direct* processes, which dominantly contribute to the cross section at high transverse energies, and *resolved* processes, which are more likely to produce jets of low transverse energy. It is because of the latter resolved interactions that photoproduction is also an important tool for gaining knowledge about the hadronic nature of the photon. In pre-HERA times, information on the photon structure was rare and came solely from $\gamma^*\gamma$ scattering at $e^+e^-$ colliders.
A significant simplification for theoretical calculations is to use the *Weizsäcker-Williams approximation* to describe the photon spectrum in the electron. The electron-proton cross section then factorizes in the following way:

$$d\sigma_{ep}(ep \to eX) = \int_0^1 dx_a\, F_{\gamma/e}(x_a)\, d\sigma_{\gamma p}(\gamma p \to X), \tag{2.9}$$

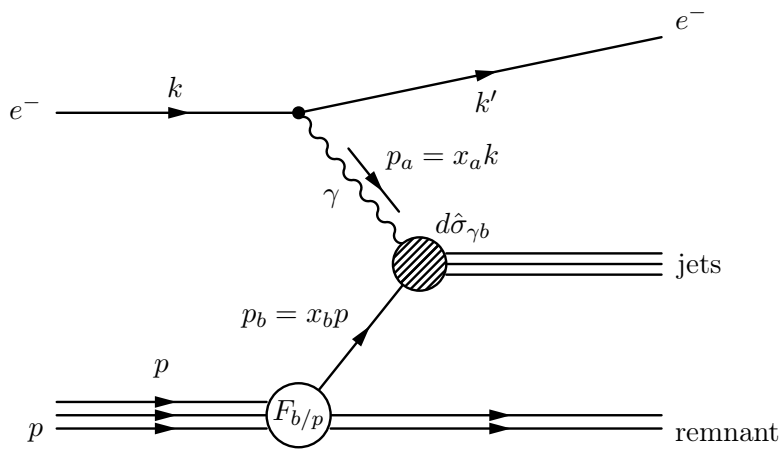


Figure 2.3: Electron-proton scattering in the parton model.

where $F_{\gamma/e}(x_a)$ denotes the probability to find a photon carrying the fraction $x_a$ of the initial electron momentum. It is given in the approximation mentioned above by

$$F_{\gamma/e}(x_a) = \frac{\alpha_s}{2\pi} \frac{1 + (1 - x_a)^2}{x_a} \ln\left(\frac{Q^2_{\max}(1 - x_a)}{m_e^2 x_a^2}\right). \tag{2.10}$$

$Q^2_{\max}$ is determined from the maximum scattering angle $\theta_{\max}$ of the electrons,

$$Q^2_{\max} = E_e^2(1 - x_a)\theta^2_{\max}, \tag{2.11}$$

taking into account that at HERA they have to disappear into the beam pipe after scattering as they are anti-tagged.
According to Eq. (2.9), we have to calculate the photon proton cross section in order to evaluate the hadronic cross section. For this purpose we will proceed to the QCD-improved parton model of both the photon and the proton, as both are no pointlike objects. Protons consist of valence and sea quarks as well as gluons, and their size constitutes a length scale to large to allow for perturbative calculations. Also, the resolved nature of the photon underlies a non-perturbative description. We will therefore introduce the concept of parton densities in the following.

### 2.2.2. Parton density of the proton

As has been mentioned, the proton interacts with the photon via its partonic substructure. The first indications for this substructure came from deep inelastic electron-proton scattering. In the parton model, the scattering off a hadron is described as an incoherent sum over scattering processes off the single massless and pointlike partons. Information about the momentum distribution of the different partons is provided by yet another $F$ function. In case that the scattering proceeds at a large scale $\mu_p$, the parton of interest will carry only low transverse momentum, and its longitudinal momentum is given as a fraction

$$x_b = \frac{qp_b}{qp} \in [0, 1] \tag{2.12}$$

of the initial proton momentum, whereas the proton remnant has the momentum fraction $1 - x_b$. Then, the photon-proton cross section factorizes again, leaving us with

$$d\sigma_{\gamma p}(\gamma p \to \text{jets} + \text{remnant}) = \sum_b \int_0^1 dx_b \, F_{b/p}(x_b, \mu_b^2) \, d\hat{\sigma}_{\gamma b}(\gamma b \to \text{jets}), \tag{2.13}$$

where the sum is over all different partons $b$ in the proton, which carry the momentum fraction $x_b$ with a probability $F_{b/p}(x_b, \mu_b^2)$. The scale dependence is due to factorization, which will be discussed later in Sec. 2.6. Usually, the chosen scale is of the order of the transverse energy of the outgoing partons or jets. While $d\hat{\sigma}_{\gamma b}$, as indicated by its hat, is a partonic hard cross section and can be calculated in perturbative QCD, the parton densities $F_{b/p}(x_b, \mu_b^2)$, which somehow provide the link between hadron and parton level, are non-perturbative quantities and have to be obtained experimentally.
If we work in the leading twist approximation and consider only contributions that factorize properly (like in Eq. (2.13)), the parton densities gained from deep inelastic scattering are universal, which means that they can be used for other processes which have incoming nucleons as well, such as photoproduction. The PDF set we used for this thesis is the ZEUS2002_ZM [1] set taken from the LHAPDF library. These parton densities were extracted from fixed target DIS data (BCDMS, NMC, E665, CCFR) and ZEUS cross section data by fitting at a chosen input scale $Q_0^2 = 7\,\mathrm{GeV}$ with a general fitting function of the form

$$xf(x) = p_1 x^{p_2}(1-x)^{p_3}(1+p_5 x), \tag{2.14}$$

which becomes zero or diverges as $x \to 0$ and vanishes for $x \to 1$. It was employed to determine five parton densities, namely u valence ($xu_{\mathrm{val}}$), d valence ($xd_{\mathrm{val}}$), total sea quark ($xS$), and gluon ($xg$) density, as well as the difference between u and d contributions to the sea ($x\Delta$). The resulting parameter values are given in Tab. 2, and Fig. 2.4 visualizes the corresponding densities.

| PDF | $p_1$ | $p_2$ | $p_3$ | $p_5$ |
|---|---|---|---|---|
| $xu_{\mathrm{val}}(x)$ | $1.69 \pm 0.07$ | 0.5 | $4.00 \pm 0.09$ | $5.04 \pm 0.73$ |
| $xd_{\mathrm{val}}(x)$ | $0.96 \pm 0.09$ | 0.5 | $5.33 \pm 0.57$ | $6.2 \pm 2.7$ |
| $xS(x)$ | $0.603 \pm 0.055$ | $-0.235 \pm 0.014$ | $8.9 \pm 1.4$ | $6.8 \pm 2.4$ |
| $xg(x)$ | $1.77 \pm 0.58$ | $-0.20 \pm 0.05$ | $6.2 \pm 1.4$ | 0 |
| $x\Delta(x)$ | $0.27 \pm 0.07$ | 0.5 | $10.9 \pm 1.4$ | 0 |

Table 2: PDF parameters at $Q_0^2$, evaluated by the ZEUS-S fit. The values without error were fixed, see [1] for further details.

For the gluon and the sea quark density, $p_2$ takes a negative value, so these functions are enhanced for small $x$. This fact is also reflected in the $x \to 0$ poles of the $gq$ and $gg$ splitting functions, see Eqs. (2.112) and (2.114). As $p_3 > 0$ throughout, all distributions tend to zero for $x \to 1$.
However, all PDFs depend on the scale $Q_0^2$, at which the underlying data was taken. Their evolution to any scale $Q^2$ of interest that is not too low and therefore spoils perturbativity is described theoretically by the DGLAP equations found by Dokshitzer [21], Gribov and Lipatov [22, 23], and Altarelli and Parisi [24]:

$$\frac{dF_{q/p}(x,Q^2)}{d\ln Q^2} = \frac{\alpha_s}{2\pi}\int_x^1 \frac{dz}{z}\left[P_{q\leftarrow q}\left(\frac{x}{z}\right)F_{q/p}(z,Q^2) + P_{q\leftarrow g}\left(\frac{x}{z}\right)F_{g/p}(z,Q^2)\right], \tag{2.15}$$

$$\frac{dF_{g/p}(x,Q^2)}{d\ln Q^2} = \frac{\alpha_s}{2\pi}\int_x^1 \frac{dz}{z}\left[P_{g\leftarrow q}\left(\frac{x}{z}\right)F_{q/p}(z,Q^2) + P_{g\leftarrow g}\left(\frac{x}{z}\right)F_{g/p}(z,Q^2)\right]. \tag{2.16}$$

The so-called splitting functions $P_{b\leftarrow b'}$ appearing in the latter equations can only be calculated order by order of a perturbative series

$$P_{b\leftarrow b'} = P^{(0)}_{b\leftarrow b'} + \alpha_s P^{(1)}_{b\leftarrow b'} + \alpha_s^2 P^{(2)}_{b\leftarrow b'} + \ldots. \tag{2.17}$$

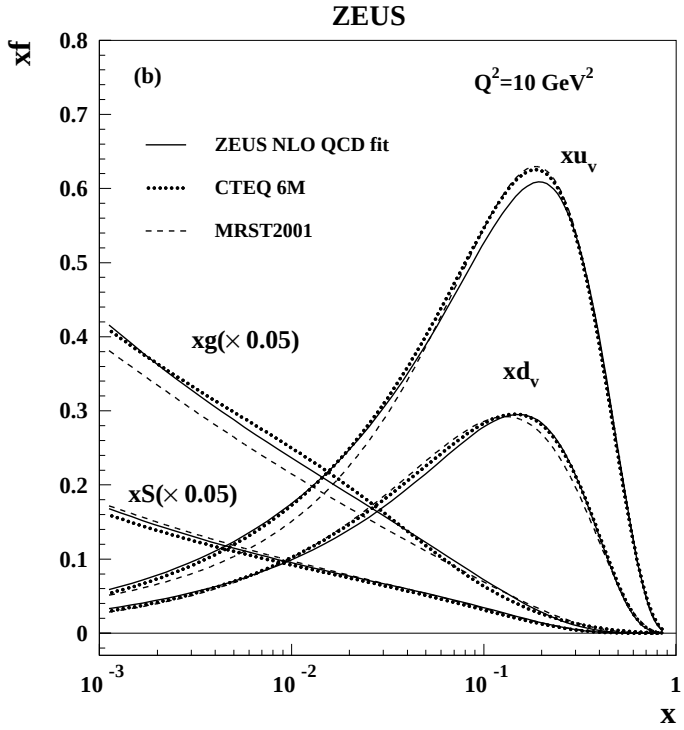


Figure 2.4: The gluon, sea, u and d valence distributions extracted from the ZEUS-S NLO QCD fit at $Q^2 = 10\,\mathrm{GeV}^2$ [1], compared to those extracted from the fits MRST2001 and CTEQ6.

Of this coefficients, $P^{(0)}_{b\leftarrow b'}$ and $P^{(1)}_{b\leftarrow b'}$ have been known for a long time [25, 26], $P^{(2)}_{b\leftarrow b'}$ was evaluated only a few years ago [27, 28].

### 2.2.3. Parton density of the photon

So far, we have discussed the photon spectrum in the scattering electrons and how these photons interact directly with the constituents of the proton. Yet we have not taken into account the fluctuation of the photon into $q\bar{q}$ pairs, which on their part can enter the hard scattering process. Applying again the factorization theorem, we state

$$d\hat{\sigma}_{\gamma b}(\gamma b \to \text{jets}) = \sum_a \int_0^1 dy_a\, F_{a/\gamma}(y_a, \mu_a^2)\, d\hat{\sigma}_{ab}(ab \to \text{jets}). \tag{2.18}$$

The resolved photon thus requires an additional integration, and $F_{a/\gamma}(y_a, \mu_a^2)$ gives the probability of finding a parton $a$ with momentum fraction $y_a$ in the photon. The scale dependence again arises from factorization (see Sec. 2.6), and usually one assumes $\mu_a \sim \mathcal{O}(E_T)$ where $E_T$ is the transverse energy of the outgoing particles or jets. We can include the case of the directly interacting photon in the last equation by setting

$$F_{\gamma/\gamma}(y_a, \mu_a^2) = F_{\gamma/\gamma}(y_a) = \delta(1 - y_a). \tag{2.19}$$

Experimental data for the determination of the distribution functions is provided, as mentioned before, by deep inelastic $\gamma^*\gamma$ scattering at $e^+e^-$ colliders. However, finding an appropriate fitting function is not as simple as in the case of the proton. This can be attributed to the fact that the photon is the QED gauge boson and therefore goes hand in hand with corresponding

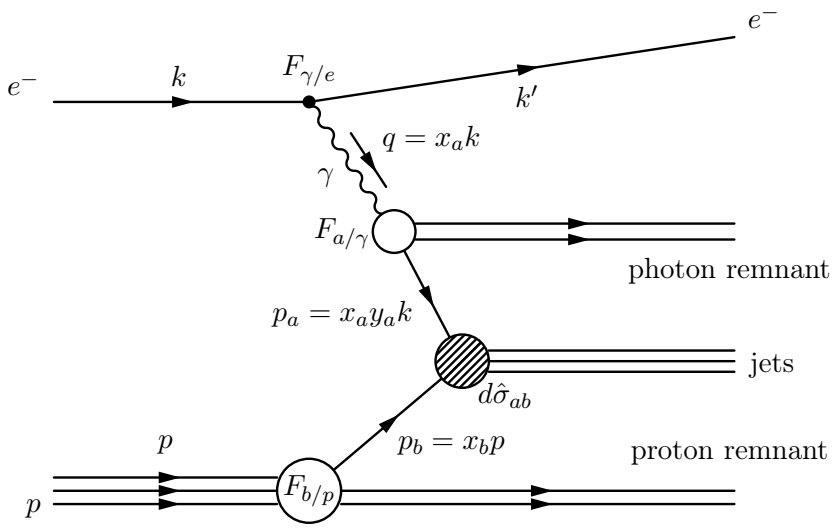


Figure 2.5: Electron-proton scattering in the parton model with resolved photon.

electrodynamical contributions. This leads to a violation of Bjorken scaling for the structure functions even at LO, and the purely perturbative ansatz diverges at small $y_b$ for the quark densities as well as for its gluon counterpart. Also, we cannot apply the momentum sum rule to the photonic parton densities, as they are QED quantities. See [29] for a more detailed discussion. The photon PDF set used in this thesis is the GRV-G NLO [30] set, which is based on the so-called Vector Meson Dominance (VMD) model [31] and uses as a fit function:

$$\frac{1}{\alpha} x f(x, Q^2) = \left[ x^a (A + B\sqrt{x} + C x^b) + s^{\alpha'} \exp\left( -E + \sqrt{E' s^\beta \ln\left(\frac{1}{x}\right)} \right) \right] (1-x)^D, \qquad (2.20)$$

with the QED coupling constant $\alpha = \frac{e^2}{4\pi}$ and

$$s \equiv \ln\left( \frac{\ln\left[Q^2/(0.248\,\mathrm{GeV})^2\right]}{\ln[\mu^2_{\mathrm{HO}}/(0.248\,\mathrm{GeV})^2]} \right) \qquad \text{with} \qquad \mu^2_{\mathrm{HO}} = 0.3\,\mathrm{GeV}^2. \qquad (2.21)$$

In Fig. 2.6, one sees different parametrizations of the u quark distribution in the photon at LO and NLO, including the GRV distribution employed for our calculations. All functions are given in the $\overline{\mathrm{MS}}$ scheme and exhibit a behaviour at NLO which differs significantly from the behaviour at LO, whereas for the gluon such a problem does not occur. A possibility to fix this is to absorb the direct photon contributions at NLO into the photonic quark distribution, which is done in the $\mathrm{DIS}_\gamma$ factorization scheme. As a consequence, the photon is always accompanied by potential quarks it can split up into as a higher order effect, and the initial "pure" photon only exists at leading order. In other words, the separation between direct and resolved photons is not physical but rather an artefact of finite order perturbation theory. Especially at NLO, where divergences get absorbed into the photon structure function due to factorization, we encounter a scale-dependent mixing of both direct and resolved contributions.
The PDFs obtained from the fit again have to be evoluted to the scale of interest, which is achieved within the perturbative regime using the inhomogeneous DGLAP equations

$$\frac{dF_{\gamma/\gamma}(y, Q^2)}{d \ln Q^2} = 0, \qquad (2.22)$$

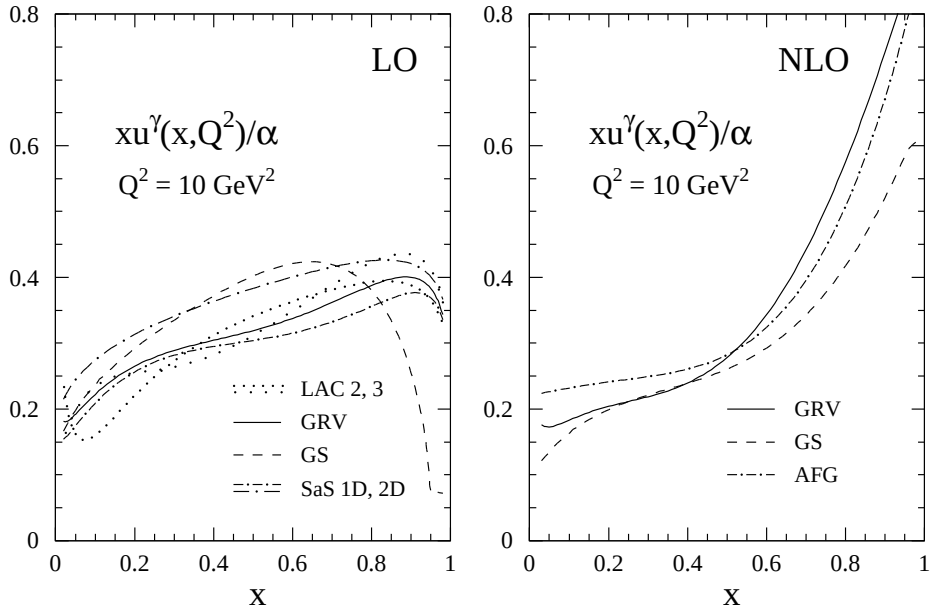


Figure 2.6: Different parametrizations of the photonic u quark distribution. The NLO densities are given in the $\overline{\text{MS}}$ scheme [29].

$$\frac{dF_{q/\gamma}(y,Q^2)}{d\ln Q^2} = \frac{\alpha_s}{2\pi}\int_y^1 \frac{dz}{z}\left[P_{q\leftarrow q}\left(\frac{y}{z}\right)F_{q/\gamma}(z,Q^2) + P_{q\leftarrow g}\left(\frac{y}{z}\right)F_{g/\gamma}(z,Q^2)\right] + \frac{\alpha}{2\pi}P_{q\leftarrow\gamma}(y) \tag{2.23}$$

and

$$\frac{dF_{g/\gamma}(y,Q^2)}{d\ln Q^2} = \frac{\alpha_s}{2\pi}\int_y^1 \frac{dz}{z}\left[P_{g\leftarrow q}\left(\frac{y}{z}\right)F_{q/\gamma}(z,Q^2) + P_{g\leftarrow g}\left(\frac{y}{z}\right)F_{g/\gamma}(z,Q^2)\right]. \tag{2.24}$$

## 2.3. Inclusive jet cross sections in photoproduction

Up to this point, we have described the cross section at parton level by perturbative QCD and discussed the linking between the unobservable partons and the observable initial hadron states. For these states, our lack of knowledge about the transition between the perturbative and non-perturbative regime has been parametrized in the parton distribution functions. Now, we will deal with the connection between the observed final states and the partonic world. The hadronization of partons is usually described via so-called fragmentation functions, following a concept similar to that of the splitting functions and looking for factorization properties. Although factorization requires some kind of universality of the hadronization part, the latter varies significantly if one compares $e^+e^-$ scattering to cases where initial hadrons are involved. This is due to the remnants of the hadrons, that also interfere in the hadronization process. Therefore, we restrict ourselves to the mere observation of hadron beams, i.e. a high number of hadrons going more or less in the same direction forming a jet. However, there is no unique prescription for defining the set of particles belonging to one of these jets. In the following, we will review several techniques that have been developed over the past 40 years.

### 2.3.1. Jet definitions

Hadrons are grouped to constitute a jet by applying a cluster algorithm, which decides whether a particle belongs to a jet or not. Important features for any of such algorithms are [32]

- to be simply implementable in experimental analysis,
- to be simply implementable in theoretical calculations,
- to be defined at any order of perturbation theory,
- to result in a finite cross section at any order of perturbation theory,
- to yield a cross section insensitive to hadronization.

On the theoretical side, we have to decide in which way the outgoing particles of the hard partonic scattering process should be combined to form two jets. This is trivial at LO, at which we deal only with two final partons, which leads to an insensitivity of the leading order cross section to any modelling of hadronization or resolution parameters. At NLO, the situation becomes more interesting, as the emission of an additional parton leads to a first substructure of one of the jets, which now consist of two particles. Finally, the NNLO corrections discussed in this thesis will not bring any new insight into the performance of any algorithm, for we deal only with soft and virtual corrections, which have two parton final states, and therefore exhibit the same insensitivity observed at LO.
Experimental jet finding starts on the other side of hadronization. Departing from the detected hadrons in the calorimeter cells, the algorithm tries to combine the groups to stable ensembles. The "seed" for starting the algorithm can either be a single cell or already an entire cluster of them. For both theorists and experimentalists it is important to work with an infrared and collinear (IRC) safe criterion. Single soft gluons should not give rise to a new jet configuration even if they are emitted in larger angles with respect to the jet axis. In any case, collinearly emitted particles should be attributed to the same jet as their source. If these conditions are met, a stable configuration can be found.

The concept of a Sterman-Weinberg jet is based on the resolution criterion proposed in [8] for $e^+e^-$ hadron production. The jet cross section is calculated from events in which all but a small

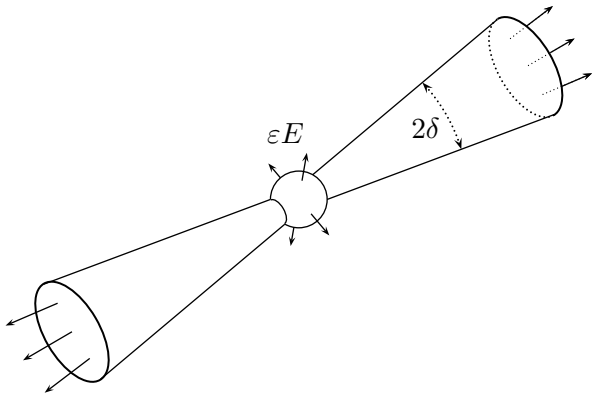


Figure 2.7: Jet criterion developed by Sterman and Weinberg [8].

fraction $\varepsilon$ of the total energy $E$ is emitted in two oppositely directed cones of opening angle $2\delta$ (see. Fig 2.7). The cones are supposed to lie within a fixed solid angle range with respect to the beam axis. This first algorithm guarantees the required IRC safety. In $e^+e^-$ collisions at NLO, the outgoing particles will typically be a quark, an anti-quark and possibly a gluon. The possible combinations this algorithm will create are:

a) Jet 1 is a quark (anti-quark) plus a hard ($E_g \geq \varepsilon E$) gluon, jet 2 is an anti-quark (quark).
b) Jet 1 is a quark, jet 2 is an anti-quark; a soft ($E_g < \varepsilon E$) gluon might or might not belong to one of them.
c) Jet 1 is a quark, jet 2 is an anti-quark (virtual diagram).

However, it is not suitable for hadron collisions with remnant hadrons, which are in general not correlated with the hard process. The algorithm tends to include the latter into the current jets, as it cannot handle multi-jet events with possibly overlapping cones. A more convenient choice for this type of issues are the so-called cone algorithms, which work in $(\eta, \phi)$ space.

$$\eta = -\ln\left[\tan\left(\frac{\theta}{2}\right)\right] \tag{2.25}$$

is the pseudo-rapidity, which measures the angle $\theta$ and thereby the distance between jet and beam axis, while $\phi$ is the usual azimuthal angle. Infrared safety can only be ensured in the case of inclusive cross sections, where radiated soft particles (i.e. those softer than the hard jet) do not disturb the jet finding process. Starting with one particle or calorimeter cell $i$, we define the jet transverse energy

$$E_{T_J} = \sum_{R_i \leq R} E_{T_i}, \tag{2.26}$$

and the jet axis

$$\eta_J = \frac{1}{E_{T_i}} \sum_{R_i \leq R} E_{T_i}\eta_i, \tag{2.27}$$

$$\phi_J = \frac{1}{E_{T_i}} \sum_{R_i \leq R} E_{T_i}\phi_i, \tag{2.28}$$

whereas, of course, in the first step the sums are not present and therefore $(E_{T_J}, \eta_J, \phi_J) = (E_{T_i}, \eta_i, \phi_i)$ (see Fig. 2.8 *a*)). In the following, one adds particles to the jet which are in a distance

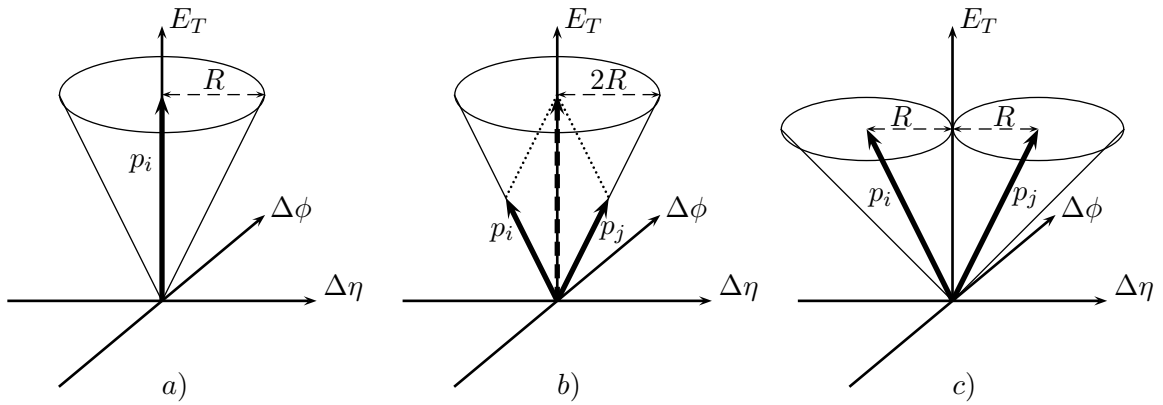


Figure 2.8: Jet cone definition for *a*) a single parton, *b*) two combined partons, each with distance $R$ from the jet axis, *c*) the same partons, interpreted as single ones.

$$R_i = \sqrt{(\eta_i - \eta_J)^2 + (\phi_i - \phi_J)^2} \leq R \tag{2.29}$$

from the current jet axis. The Snowmass meeting in 1990 brought a standardization in the parameter use for the cone algorithm, stating that the resolution parameter $R$ should lie in the range from 0.4 to 1, with 0.7 as the standard choice. If we enclose a second parton to the jet, its axis will move. Due to the $E_T$ weighting in Eqs. (2.27) and (2.28), it always represents the center-of-transverse-momentum axis such that $(E_{T_i}, \Delta\eta_i, \Delta\phi_i)$ and $(E_{T_j}, \Delta\eta_j, \Delta\phi_j)$ can be replaced by a single jet $(E_{T_J}, 0, 0)$ in the newly defined $(E_T, \Delta\eta, \Delta\phi)$ space, as can be seen in Fig. 2.8 *b*).
Eq. (2.29) only fixes the distance between the single partons and the jet axis. By inserting Eqs. (2.27) and (2.28) into (2.29), we find for $p_i$ and $p_j$:

$$R_{i/j} = \frac{E_{T_{i/j}}}{E_{T_i} + E_{T_j}} \sqrt{(\eta_i - \eta_j)^2 + (\phi_i - \phi_j)^2} \leq R. \tag{2.30}$$

The square root is nothing else than the distance $R_{ij}$ of $p_i$ and $p_j$ in the $(\Delta\eta, \Delta\phi)$ plane. As the condition has to be fulfilled for both $i$ and $j$, we find

$$R_{ij} = \sqrt{(\eta_i - \eta_j)^2 + (\phi_i - \phi_j)^2} \leq \frac{E_{T_i} + E_{T_j}}{\max(E_{T_i}, E_{T_j})} R. \tag{2.31}$$

This means that if the transverse energy of two partons is similar or equal (see Figs. 2.8 *b*) and *c*)), they are allowed to have the distance $2R$ from each other and are still attributed to the same cone. Equally, one could assign a separate cone of radius $R$ to each of them without having any overlap. If this is the case, one has to pay attention in highest-$E_T$ jet studies to avoid double counting. Whereas situations like these do not cause any problems in theoretical calculations, they do so in experimental analysis, as the "seed-finding" will not combine such particles because of the missing seed in the jet center. Nevertheless, one can compare theoretical and experimental results if one manages to model the difficulties in the calculations. The latter is achieved through introducing an additional parameter $R_{\text{sep}}$, which restricts the distance between two outgoing partons. Eq. (2.31) now reads

$$R_{ij} \leq \min \left[ \frac{E_{T_i} + E_{T_j}}{\max(E_{T_i}, E_{T_j})} R, R_{\text{sep}} \right], \tag{2.32}$$

in which $R \leq R_{\text{sep}} \leq 2R$ is usually chosen to be $R_{\text{sep}} \simeq 1.3$ and becomes the limiting parameter if $E_{T_i}$ and $E_{T_j}$ are similar. This algorithm is infrared safe; but since collinear partons will be merged with their source and soft partons hardly influence the jet axis because of the $E_T$ weighting, it has the disadvantage that cones can overlap, so one would basically have to find all possibilities to match Eq. (2.29) before deciding on the resulting jet configuration.

Another possible algorithm of a successive combination type was proposed by Ellis and Soper [10]. It starts with a set of so-called protojets, which are in general single calorimeter cells or partons, and consists of the following steps:

1. For each protojet, define
$$d_i = E_{T_i}^2, \tag{2.33}$$
and for each pair of protojets
$$d_{ij} = \min(E_{T_i}, E_{T_j}) \frac{R_{ij}}{R}. \tag{2.34}$$
2. Assign $d_{\min}$ to the smallest of all $d_i$ and $d_{ij}$.
3. If $d_{\min}$ is a $d_{ij}$, merge the particles to a new protojet according to Eqs. (2.26) - (2.28).
4. If $d_{\min}$ is a $d_i$, the corresponding protojet should not be merged but removed from the list of protojets and added to the list of jets.
5. Repeat from step 1.

This procedure is also IRC safe and produces a long list of jets for each event. But only the highest $E_T$ jets, the last jets to be added to the list, will be of interest for inclusive cross sections, whereas the others are rather "minijets" or some kind of beam debris.
In the case of small opening angles $R_{ij} \ll 1$ and high transversality of the jet, we can set $R_{ij} \simeq \Delta\theta$ and $E_T \simeq E$, which results in
$$d_{ij} \simeq \min(E_i, E_j) \frac{\Delta\theta}{R} \simeq \frac{k_T^2}{R}. \tag{2.35}$$
Here, $k_T$ denotes the relative transverse momentum of the two particles in the jet, and the algorithm is therefore also called $k_T$ or $k_\perp$ algorithm. $R$ is usually chosen to be of $\mathcal{O}(1)$. The similarity between this successive combination and the cone algorithm is obvious. The jets which both algorithms find are quite similar as long as $R \simeq R_{\text{sep}}$.
A severe problem for each of the procedures is the large number of computational steps, which grows in the case of the $k_T$ algorithm for $N$ particles with $N^3$. While at theoretical parton level only a few outgoing particles occur, this is a time-consuming issue for experimentalists, who have to deal with thousands of detected hadrons. More recent publications presented a way to reduce the amount of steps remarkably from $\mathcal{O}(N^3)$ to $\mathcal{O}(N \ln(N))$ [11]. This improvement is primarily based on the insight that for a given particle $i$ $d_{ij}$ becomes minimal if $j$ is its nearest neighbour. Thus, step 1 of the $k_T$ algorithm has to be fully executed only once if one creates an array in which for every particle $i$ just $d_i$ and the nearest neighboured particle $j$, i.e. the one with the smallest $d_{ij}$, are stored. After merging two particles $i$ and $j$, step 1 only has to be repeated as an update for those particles whose nearest neighbour had been $j$. Apart from the number of steps, this improvement also reduces the amount of data that has to be processed.

### 2.3.2. Calculation of photoproduction cross sections

After discussing the links of the partonic cross section to both the initial and final hadronic states, we will now fix the kinematics of the complete photoproduction process. We combine

Eqs. (2.9), (2.13) and (2.18) to [15, 7]

$$\begin{aligned} &d\sigma_{ep}(ep \to e + \text{jets} + \text{remnants}) \\ &= \sum_{a,b} \int_0^1 dx_a \, F_{\gamma/e}(x_a) \int_0^1 dy_a \, F_{a/\gamma}(y_a, \mu_a^2) \int_0^1 dx_b \, F_{b/p}(x_b, \mu_b^2) \, d\hat{\sigma}_{ab}(ab \to \text{jets}), \end{aligned} \tag{2.36}$$

using the momentum fractions $x_a$, $y_a$ and $x_b$ as assigned in Fig. 2.5. If we change the integration over the momentum fraction $x_a$ for the photon in the electron into an integration over $X_a = y_a x_a$, the momentum fraction of the parton $a$ in the electron which we newly define to be $x_a$, we arrive at

$$\begin{aligned} &d\sigma_{ep}(ep \to e + \text{jets} + \text{remnants}) \\ &= \sum_{a,b} \int_0^1 dx_a \int_{x_a}^1 \frac{dy_a}{y_a} F_{\gamma/e}\left(\frac{x_a}{y_a}\right) F_{a/\gamma}(y_a, \mu_a^2) \int_0^1 dx_b \, F_{b/p}(x_b, \mu_b^2) \, d\hat{\sigma}_{ab}(ab \to \text{jets}); \end{aligned} \tag{2.37}$$

the lower bound of the $y_a$ integration changed due to the convolution with $F_{\gamma/e}$, which returns zero as its argument exceeds unity. In order to be able to compare our calculations to experimental results, it is convenient to transform the integration variables mentioned above into a set of jet variables accessible to measurement. This will facilitate the calculation of corresponding differential cross sections and also the implementation of technical constraints on the kinematic range.
The HERA beam axis is taken to be along the $z$ axis of our coordinate system, and the positive direction is defined to be parallel to the initial proton momentum. By a simple shift in rapidity,

$$\eta_{\text{boost}} = \frac{1}{2} \ln\left(\frac{E_e}{E_p}\right), \tag{2.38}$$

we can change into the $ep$ center-of-mass system, in which our perturbative calculation will be performed. Measurements, however, took place in the HERA laboratory system, where we define the momenta of the incoming (massless) particles

$$k = E_e(1, 0, 0, -1) \qquad \text{and} \qquad p = E_p(1, 0, 0, 1) \tag{2.39}$$

as well as those of the outgoing partons and hard jets respectively,

$$p_i = E_{T_i}(\cosh(\eta_i), \cos(\phi_i), \sin(\phi_i), \sinh(\eta_i)). \tag{2.40}$$

Exploiting momentum conservation, we find that the jet variables $(E_{T_i}, \eta_i)$ are related to the initial momentum fractions $(x_a, x_b)$ in the following way:

$$x_a = \frac{1}{2E_e} \sum_i E_{T_i} e^{-\eta_i}, \tag{2.41}$$

$$x_b = \frac{1}{2E_p} \sum_i E_{T_i} e^{\eta_i}. \tag{2.42}$$

The focus of this thesis is clearly on two particle final states, i.e. we are interested in the case of two jets which then have to balance their transverse energy, so that $E_{T_1} = E_{T_2} = E_T$, and hence

$$x_a = \frac{E_T}{2E_e}(e^{-\eta_1} + e^{-\eta_2}), \tag{2.43}$$

$$x_b = \frac{E_T}{2E_p}(e^{\eta_1} + e^{\eta_2}). \tag{2.44}$$

Due to tagging issues at HERA, the range of $x_a$ is restricted to $x_{a,\min} \leq x_a \leq x_{a,\max} < 1$, which is usually given as an interval $\sqrt{x_{a,\min} kp} \leq W_{\gamma p} \leq \sqrt{x_{a,\max} kp}$. This constrains the rapidity $\eta_2$ of the second jet, since it is calculated via

$$\eta_2 = -\ln\left(\frac{2x_a E_e}{E_T} - e^{\eta_1}\right), \tag{2.45}$$

and therefore kinematically fixed by $E_T$, $x_a$ and $\eta_1$.
The partonic cross section $d\hat{\sigma}(ab \to \text{jets})$ in Eq. (2.37) is expressed in terms of the usual Mandelstam variables $s$, $t$ and $u$, which are related to the initial and final state variables by

$$s = (p_a + p_b)^2 = 4x_a x_b E_e E_p = 4E_T^2 \cosh^2\left(\frac{\eta_1 - \eta_2}{2}\right), \tag{2.46}$$

$$t = (p_a - p_1)^2 = -2x_a E_e E_T e^{\eta_1} = -2x_b E_p E_T e^{\eta_2} = -E_T^2(1 + e^{\eta_1 - \eta_2}) \tag{2.47}$$

and

$$u = (p_a - p_2)^2 = -2x_a E_e E_T e^{-\eta_2} = -2x_b E_p E_T e^{-\eta_1} = -E_T^2(1 + e^{\eta_2 - \eta_1}). \tag{2.48}$$

We can now perform the variable change $(x_a, x_b, t) \to (\eta_1, \eta_2, E_T^2)$ in Eq. (2.37), where the differential volume transforms according to

$$\det(J) = \frac{E_T^2}{4E_e E_p}(e^{\eta_1 - \eta_2} + e^{\eta_2 - \eta_1} + 2) = x_a x_b, \tag{2.49}$$

and thus

$$dx_a\, dx_b\, dt = x_a x_b\, d\eta_1\, d\eta_2\, dE_T^2. \tag{2.50}$$

Accordingly, we obtain

$$\frac{d^3\sigma}{d\eta_1 d\eta_2 dE_T^2} = \sum_{a,b} x_a \int_{x_a}^1 \frac{dy_a}{y_a} F_{a/\gamma}(y_a, \mu_a^2)\, F_{\gamma/e}\left(\frac{x_a}{y_a}\right) x_b F_{b/p}(x_b, \mu_b^2)\, \frac{d\hat{\sigma}}{dt}(ab \to \text{jets}). \tag{2.51}$$

## 2.4. Leading order cross sections

Before we come to the discussion of higher order effects and divergences in the perturbative calculation of partonic cross sections, we give in this section a brief summary of the results at leading order. The relevant processes for direct and resolved photoproduction are shown in Figs. 2.9 and 2.10, where only those diagrams are exhibited that we actually need to calculate.
The unpolarized Born matrix elements for direct photons are [33, 34, 7]

$$\overline{|\mathcal{M}|^2}_{\gamma q\to gq}(s,t,u) = 2e^2e_q^2g_s^2C_F\left(-\frac{u}{s}-\frac{s}{u}\right), \tag{2.52}$$

which is the so-called "QCD Compton Scattering" (see Fig. 2.9), and

$$\overline{|\mathcal{M}|^2}_{\gamma g\to q\bar{q}}(s,t,u) = e^2e_q^2g_s^2\left(\frac{u}{t}+\frac{t}{u}\right) \tag{2.53}$$

for the "Boson Gluon Fusion" process. The latter is obtained from crossing the initial quark with the final gluon in the Compton scattering, which yields a factor $(-1)$ for crossing a fermion line and requires the exchange $s \leftrightarrow t$. In both equations we encounter the fractional charge $e_q$ of the quark involved, and in Eq. (2.52) we used

$$C_F = \frac{N_C^2-1}{2N_C} = \frac{4}{3}, \tag{2.54}$$

with $N_C = 3$ for SU(3) colour symmetry. Of course, the first process can also take place with an anti-quark instead of a quark. The corresponding matrix element is found after the crossing $s \leftrightarrow u$, leaving Eq. (2.52) invariant.

In the case of resolved photons, the number of contributing Born processes is somewhat higher. Nevertheless, only those processes displayed in Fig. 2.10 have to be evaluated, the rest again is obtained by crossing. We find [35]:

$$\overline{|\mathcal{M}|^2}_{qq'\to qq'}(s,t,u) = g_s^4\frac{C_F}{N_C}\frac{s^2+u^2}{t^2}, \tag{2.55}$$

where $q$ and $q'$ are quarks of different flavour so that the depicted t-channel (Fig. 2.10 a)) is the only possible topology, and the resulting matrix element is of a rather simple form. Next, we have

$$\overline{|\mathcal{M}|^2}_{q\bar{q}'\to q\bar{q}'}(s,t,u) = \overline{|\mathcal{M}|^2}_{qq'\to qq'}(u,t,s), \tag{2.56}$$

related to Eq. (2.55) by the exchange $s \leftrightarrow u$, and

$$\overline{|\mathcal{M}|^2}_{q\bar{q}\to q'\bar{q}'}(s,t,u) = \overline{|\mathcal{M}|^2}_{qq'\to qq'}(t,s,u), \tag{2.57}$$

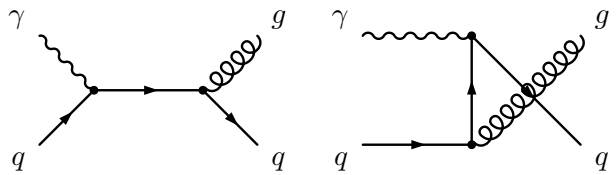

Figure 2.9: Born diagrams for direct photoproduction.

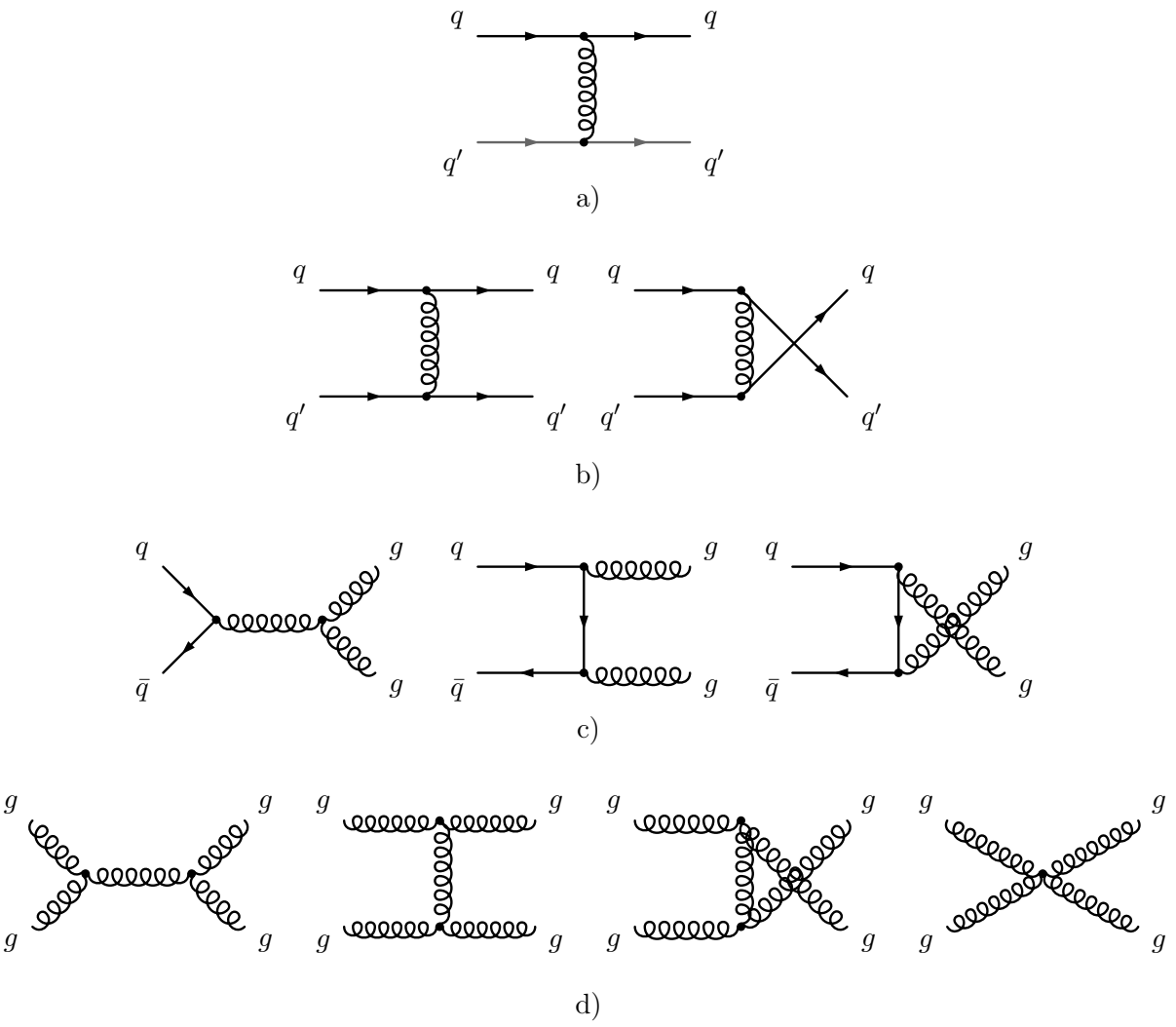


Figure 2.10: Born diagrams for resolved photoproduction.

which is obtained from the same process after crossing $s \leftrightarrow t$. For identical quarks (Fig. 2.10 b)), the matrix element is given by

$$\overline{|\mathcal{M}|^2}_{qq\to qq}(s,t,u) = g_s^4 \frac{C_F}{2N_C}\left(\frac{s^2+u^2}{t^2} + \frac{s^2+t^2}{u^2} - 2\frac{s^2}{tu}\right), \tag{2.58}$$

an expression symmetric with respect to $t$ and $u$, as the final state particles cannot be distinguished. This fact also requires an additional factor $\frac{1}{2}$ which has already been included. Exchanging $s$ and $u$, we also get

$$\overline{|\mathcal{M}|^2}_{q\bar{q}\to q\bar{q}}(s,t,u) = g_s^4 \frac{C_F}{N_C}\left(\frac{s^2+u^2}{t^2} + \frac{t^2+u^2}{s^2} - 2\frac{u^2}{st}\right). \tag{2.59}$$

The first resolved process involving gluons (Fig. 2.10 c)) has the matrix element

$$\overline{|\mathcal{M}|^2}_{q\bar{q}\to gg}(s,t,u) = g_s^4 \frac{C_F}{N_C}\left(C_F\left(\frac{t}{u}+\frac{u}{t}\right) - N_C\frac{t^2+u^2}{s^2}\right), \tag{2.60}$$

and constitutes a base for the calculation of

$$\overline{|\mathcal{M}|^2_{qg\to qg}}(s,t,u) = \overline{|\mathcal{M}|^2_{\bar{q}g\to\bar{q}g}}(u,t,s) = -\frac{1}{C_F}\overline{|\mathcal{M}|^2_{q\bar{q}\to gg}}(t,s,u), \tag{2.61}$$

where the final partons in contrast to the previous case are not identical and also the averaging factors for the polarizations are different. Furthermore,

$$\overline{|\mathcal{M}|^2_{gg\to q\bar{q}}}(s,t,u) = \frac{1}{2C_F^2}\overline{|\mathcal{M}|^2_{q\bar{q}\to gg}}(s,t,u). \tag{2.62}$$

Finally, the purely gluonic process has four contributing diagrams (see Fig. 2.10 d)), whose squared sum gives

$$\overline{|\mathcal{M}|^2_{gg\to gg}}(s,t,u) = g_s^4\frac{N_C}{C_F}\left(3-\frac{tu}{s^2}-\frac{su}{t^2}-\frac{st}{u^2}\right). \tag{2.63}$$

In order to obtain the leading order cross sections, the matrix elements have to be integrated over the phase space for two-particle final states,

$$dPS^{(2)} = \int(2\pi)^4\prod_{i=1}^{2}\frac{d^4p_i\delta(p_i^2)}{(2\pi)^3}\delta^4\left(p_a+p_b-p_1-p_2\right). \tag{2.64}$$

The integrations can be performed independently of the matrix elements by exploiting the delta functions. The latter only fix momentum conservation and masslessness, which already have been taken into account while evaluating the above elements. As Eq. (2.51) requires partonic cross sections differential in $t$, we add also $\delta(t+2p_ap_1)$, which yields [33]

$$\frac{dPS^{(2)}}{dt} = \frac{1}{8\pi s} \tag{2.65}$$

as the final result. Consequently, the cross section is calculated by multiplying the matrix element with this universal factor.

## 2.5. Renormalization and running coupling

When calculating processes beyond leading order (LO) in perturbative QCD, we have to take into account diagrams with internal parton loops. Possible topologies belonging to these virtual corrections are depicted in Fig. 2.11. We distinguish between a) self-energy, b) propagator and c) vertex corrections. The particles in the loops are virtual and their momenta therefore not constrained by energy-momentum conservation. Instead, one has to integrate over all possible momenta, i.e. over the complete momentum space. The propagator of a massless particle with four-momentum $k$ will result in a factor $k^2$ in the denominator, thereby leading to an integral of the form

$$\int \frac{d^4q}{(-q^2)^\omega}, \qquad \omega = 1, 2, \ldots . \tag{2.66}$$

If $2\omega \geq 4$, the integrand becomes singular for $q^2 \to 0$, which is also called an infrared (IR) divergence, while for $2\omega \leq 4$, the expression diverges as $q^2 \to \infty$, giving rise to so-called ultraviolet (UV) divergences. In order to be able to evaluate these integrals, one has to regularize them, e.g. using the technique of dimensional regularization first presented by 't Hooft and Veltman [36]. The latter method supposes that one shifts the dimension of integration from 4 to $D = 4 - 2\varepsilon$ dimensions. The transition to physical four-dimensionality is achieved afterwards by taking the

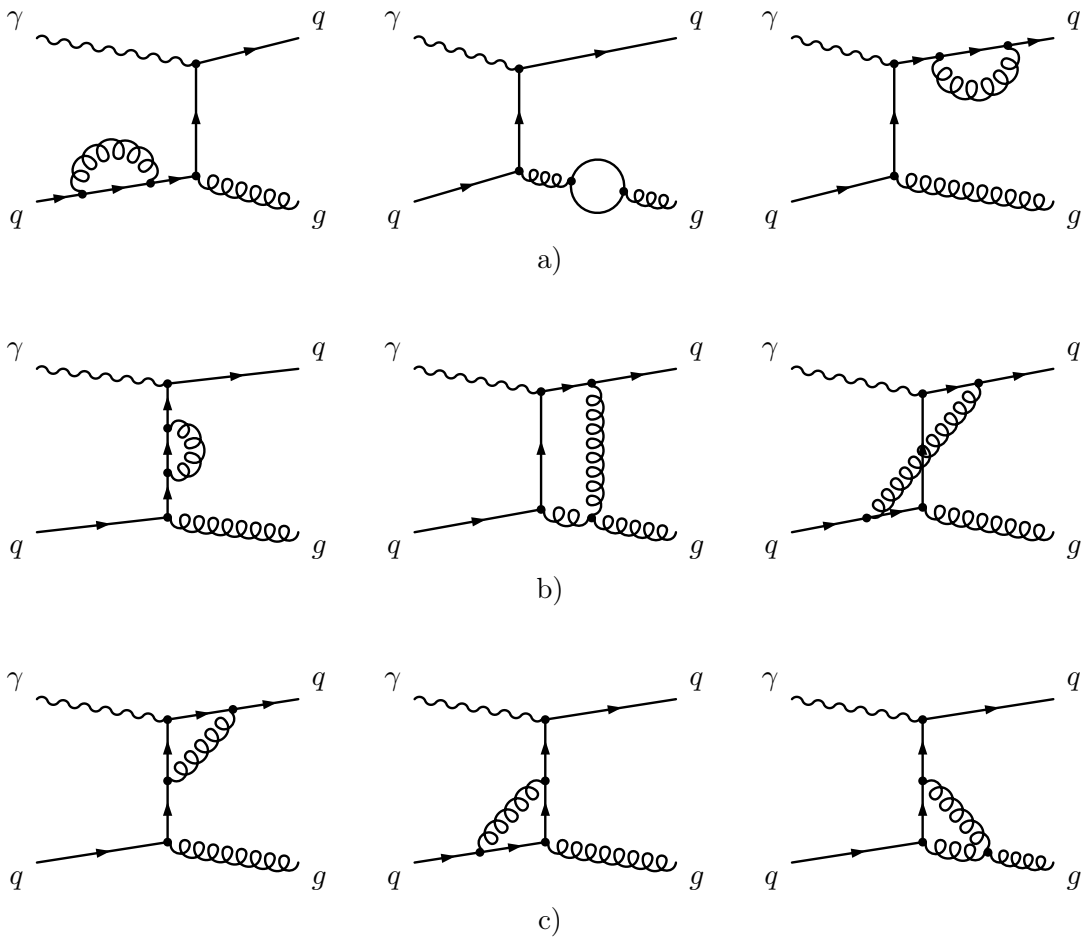


Figure 2.11: Virtual diagrams at NLO for $\gamma q \to qg$ in direct photoproduction. The circle in the first row can be either a quark, gluon or ghost loop.

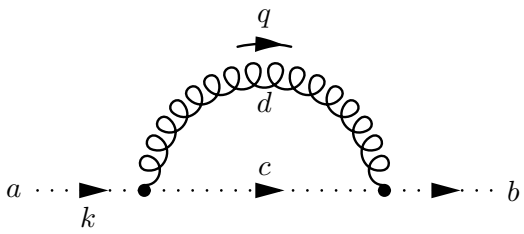


Figure 2.12: Truncated ghost self energy correction.

limit $\varepsilon \to 0$. However, the divergences present at 4 dimensions do not disappear, but they are manifest in the result at next-to-leading order (NLO) as poles $\sim \varepsilon^{-1}, \varepsilon^{-2}$. Note that in dimensional regularization, the leading order cross sections from Sec. 2.3.2 also have to be expressed in $D$ dimensions in spite of being finite, since terms of order $\varepsilon$ or even $\varepsilon^2$ might lead to additional non-vanishing contributions if they interfere with one of these poles.
All loop diagrams arising from the different topologies shown in Fig. 2.11 can be reduced to only a few basic scalar integrals, which are called $A_0$, $B_0$, $C_0$, etc.. These basic integrals can again be brought to a form proportional to [37]

$$I_n(A) = \frac{(2\pi\mu)^{4-D}}{i\pi^2} \int \frac{d^D q}{(q^2 - A + i\delta)^n}, \tag{2.67}$$

which is convergent if $D < 2n$ and $A > 0$. $\mu$ is an arbitrary mass scale introduced to keep the right mass dimensions of the integral. Finally, $I_n(A)$ is evaluated in $D$-dimensional spherical coordinates after performing a Wick rotation in the complex plane. Then, the result is

$$\begin{aligned} I_n(A) &= (-1)^n (4\pi\mu^2)^{\frac{4-D}{2}} \frac{\Gamma\left(n - \frac{D}{2}\right)}{\Gamma(n)} (A - i\delta)^{\frac{D}{2}-n} \\ &= (-1)^n (4\pi\mu^2)^{\varepsilon} \frac{\Gamma(n - 2 + \varepsilon)}{\Gamma(n)} (A - i\delta)^{2-\varepsilon-n}. \end{aligned} \tag{2.68}$$

From this expression we obtain e.g. in the case $n = 1$, $A = m^2$ and $\delta \to 0$ the scalar $A_0$ integral for a particle with mass $m$:

$$\begin{aligned} A_0(m^2) &= -(4\pi\mu^2)^{\varepsilon} \frac{\Gamma(\varepsilon - 1)}{\Gamma(1)} m^{2-2\varepsilon} \\ &= m^2 \left( \frac{1}{\varepsilon} - \gamma_E + \ln(4\pi) - \ln\left(\frac{m^2}{\mu^2}\right) + 1 \right) + \mathcal{O}(\varepsilon). \end{aligned} \tag{2.69}$$

As another example, we calculate the ghost self-energy correction as displayed in Fig. 2.12. We find for the truncated loop diagram:

$$\begin{aligned} \tilde{\Pi}(k^2) &= -iN_C \delta^{ab} g_r^2 \mu^{4-D} \int \frac{d^D q}{(2\pi)^D} \frac{k^2 + k \cdot q}{q^2 (k+q)^2} \\ &= N_C \delta^{ab} g_r^2 k^2 \frac{1}{\varepsilon} \frac{\Gamma(1+\varepsilon)}{(16\pi^2)^{1-\frac{\varepsilon}{2}}} \left(-\frac{\mu^2}{k^2}\right)^{\varepsilon} \int_0^1 dx\, x^{-\varepsilon} (1-x)^{1-\varepsilon} \\ &= N_C \delta^{ab} \frac{g_r^2}{32\pi^2} k^2 \left[ \frac{1}{\varepsilon} - \gamma_E + \ln(4\pi) + 2 + \ln\left(-\frac{\mu^2}{k^2}\right) \right] + \mathcal{O}(\varepsilon), \end{aligned} \tag{2.70}$$

with the same type of pole present. In the last expression, we arrived at the second line using the standard Feynman integral relations, which is the standard technique for solving this kind of integrals.

If we want to calculate a physical quantity, such as a cross section in QCD with higher order accuracy, we need to find a way of eliminating the poles that still remain in Eq. (2.70). For the poles stemming from UV divergences, this is done by a renormalization of fields, the coupling $g_s$, the masses and the gauge parameter $\alpha$. We introduce the renormalized fields, denoted with an index $r$, as [38]

$$G^a_\mu = \sqrt{Z_3} G^a_{r,\mu}, \qquad \phi^a = \sqrt{\tilde{Z}_3}\phi^a_r \quad \text{and} \quad \psi = \sqrt{Z_2}\psi_r, \tag{2.71}$$

as well as the renormalized parameters

$$g_s = Z_g g_r, \qquad \xi = Z_3 \xi_r \quad \text{and} \quad m = Z_m m_r. \tag{2.72}$$

The Lagrangian in Eq. (2.1) can then be rewritten as

$$\mathcal{L} = \mathcal{L}_\mathrm{r} + \mathcal{L}_\mathrm{C}, \tag{2.73}$$

where $\mathcal{L}_\mathrm{r}$ is obtained from Eq. (2.1) just by replacing the bare fields and parameters by their renormalized counterpart. $\mathcal{L}_\mathrm{C}$ denotes the so called counter-terms, which are given by [38]

$$\begin{aligned}
\mathcal{L}_\mathrm{C} = &-(Z_3-1)\frac{1}{4}\left(\partial^\mu G^\nu_{r,a} - \partial^\nu G^\mu_{r,a}\right)\left(\partial_\mu G^a_{r,\nu} - \partial_\nu G^a_{r,\mu}\right) - \left(\tilde{Z}_3 - 1\right)\left(\partial_\mu \bar{\phi}_{r,a}\right)\left(\partial^\mu \phi^a_r\right) \\
&+ (Z_2-1)\sum_f \bar{\psi}_{r,f}\left(i\gamma^\mu\partial_\mu - m_r\right)\psi_{r,f} - Z_2\left(Z_m - 1\right) m_r \sum_f \bar{\psi}_{r,f}\psi_{r,f} \\
&- \left(Z_g\sqrt{Z_3^3} - 1\right)\frac{1}{2} g_r f^{abc}\left(\partial^\mu G^\nu_{r,a} - \partial^\nu G^\mu_{r,a}\right) G^b_{r,\mu} G^c_{r,\nu} \\
&- \left(Z_g^2 Z_3^2 - 1\right)\frac{g_r^2}{4} f^{abc} f_{ade} G^\mu_b G^\nu_c G^d_\mu G^e_\nu + \left(Z_g \tilde{Z}_3 \sqrt{Z_3} - 1\right) g_r f^{abc}\left(\partial^\mu \bar{\phi}^a_r\right)\phi^b_r G^c_{r,\mu} \\
&+ \left(Z_g Z_2 \sqrt{Z_3} - 1\right) g_r \sum_f \bar{\psi}_{r,f} T^a \gamma_\mu \psi_{r,f} G^\mu_{r,a}.
\end{aligned} \tag{2.74}$$

If we define a new set of renormalization constants,

$$Z_1 \equiv Z_g\sqrt{Z_3^3}, \qquad \tilde{Z}_1 \equiv Z_g \tilde{Z}_3 \sqrt{Z}, \qquad Z_{1\mathrm{F}} \equiv Z_g Z_2 \sqrt{Z_3} \quad \text{and} \quad Z_4 \equiv Z_g^2 Z_3^2, \tag{2.75}$$

these fulfill together with the former constants the so-called *Slavnov-Taylor identity*

$$\frac{Z_1}{Z_3} = \frac{\tilde{Z}_1}{\tilde{Z}_3} = \frac{Z_{1\mathrm{F}}}{Z_2} = \frac{Z_4}{Z_1}, \tag{2.76}$$

which has to be matched if the renormalized coupling constant $g_r$ is supposed to be universal. The idea behind renormalization is the following: We take the renormalized quantities to be the physical ones, i.e. the ones we observe in experiments. The Feynman rules for $\mathcal{L}_\mathrm{r}$ in Eq. (2.73) are the same as before, and just that the bare quantities have been replaced by the renormalized ones. Therefore, we will encounter the same divergences again, with the difference that now, we also have the counter-terms, which can serve to subtract the poles which appeared e.g. in Eq. (2.69). This is achieved by combining the usual Feynman diagrams with additional diagrams that arise from $\mathcal{L}_\mathrm{C}$.
However, when defining the $Z$ constants, we are free to choose the finite terms we want to remove beside the $\varepsilon$ poles. Each choice constitutes a renormalization scheme. The scheme used throughout this thesis is the modified Minimal Subtraction ($\overline{\mathrm{MS}}$) scheme which subtracts not

only the poles, but also the universal $\ln(4\pi) - \gamma_E$ part. In this scheme, the renormalization constants at NLO are found to be [38]

$$Z_1 = 1 - \frac{g_r^2}{(4\pi)^2}\left[\left(-\frac{17}{12} + \frac{3}{4}\xi_r\right) N_C + \frac{2}{3} n_f\right]\left(\frac{1}{\varepsilon} - \gamma_E + \ln(4\pi)\right) + \mathcal{O}(g_r^4), \tag{2.77}$$

as well as

$$\tilde{Z}_1 = 1 - \frac{g_r^2}{(4\pi)^2} N_C \frac{\xi_r}{2}\left(\frac{1}{\varepsilon} - \gamma_E + \ln(4\pi)\right) + \mathcal{O}(g_r^4), \tag{2.78}$$

$$Z_{1\mathrm{F}} = 1 - \frac{g_r^2}{(4\pi)^2}\left(\frac{3+\xi_r}{4} N_C + \xi_r C_F\right)\left(\frac{1}{\varepsilon} - \gamma_E + \ln(4\pi)\right) + \mathcal{O}(g_r^4), \tag{2.79}$$

and finally

$$Z_4 = 1 - \frac{g_r^2}{(4\pi)^2}\left[N_C\left(-\frac{2}{3} + \xi_r\right) N_C + \frac{2}{3} n_f\right]\left(\frac{1}{\varepsilon} - \gamma_E + \ln(4\pi)\right) + \mathcal{O}(g_r^4). \tag{2.80}$$

It is a simple task to verify that these constants are in agreement with the Slavnov-Taylor identity in Eq. (2.76). In addition, we will soon need

$$Z_g = 1 - \frac{g_r^2}{32\pi^2}\beta_0\left(\frac{1}{\varepsilon} - \gamma_E + \ln(4\pi)\right) + \mathcal{O}(g_r^4) \tag{2.81}$$

for our upcoming discussion of the running coupling, in which we will basically follow [16]. Here, we have defined $\beta_0 = \frac{11}{3} C_F - \frac{2}{3} n_f$. Before we come to the scale dependence of the coupling constant, we will have a brief look at mass dimensions. Since the action, which is given by $\int d^D x \mathcal{L}$, has to be dimensionless, the Lagrangian density should have the dimension $[\mathcal{L}] = \mathrm{mass}^D$. This implies $[g_s] = [g_r] = \mathrm{mass}^{(4-D)/2}$ if we consider the definitions of Eq. (2.1) and (2.73). However, we have so far treated the coupling constant as dimensionless (e.g. in Eq. (2.70)), fixing the mass dimension by introducing an arbitrary mass scale $\mu$. Thus, $g_r$ and $g_s$ are scale-dependent, and should be replaced by $\tilde{g}_s(\mu_s)$ and $\tilde{g}_r(\mu_r)$, respectively. Then, we can redefine the couplings as

$$g_s \equiv \tilde{g}_s(\mu_s)\mu_s^{\frac{4-D}{2}} \qquad \text{and} \qquad g_r \equiv \tilde{g}_r(\mu_r)\mu_r^{\frac{4-D}{2}}, \tag{2.82}$$

noting that $\tilde{g}_s$ and $\tilde{g}_r$ are still dimensionless, while the bare and renormalized coupling constants $g_s$ and $g_r$ are scale-independent. Since $Z_g$ depends on $\tilde{g}_r$, it also gains a scale dependence. From $g_s = Z_g g_r$, we derive

$$\tilde{g}_r(\mu_r) = \left(\frac{\mu_s}{\mu_r}\right)^{\frac{4-D}{2}} \frac{\tilde{g}_s(\mu_s)}{Z_g(\tilde{g}_r, \mu_r)} = \left(\frac{\mu_s}{\mu_r}\right)^{\varepsilon} \frac{\tilde{g}_s(\mu_s)}{Z_g(\tilde{g}_r, \mu_r)}. \tag{2.83}$$

By simply differentiating the last equation, we find

$$\beta \equiv \mu_r \frac{d\tilde{g}_r(\mu_r)}{d\mu_r} = -\left(\varepsilon + \frac{\mu_r}{Z_g}\frac{dZ_g(\tilde{g}_r, \mu_r)}{d\mu_r}\right)\tilde{g}_r(\mu_r) = -\beta_0 \frac{\tilde{g}_r^3(\mu_r)}{16\pi^2} + \mathcal{O}(\tilde{g}_r^5, \varepsilon), \tag{2.84}$$

which we can recast using $\alpha_s = \frac{\tilde{g}_r^2}{4\pi}$ as

$$\frac{d\alpha_s(\mu_r^2)}{d\ln(\mu_r^2)} = -\frac{\beta_0}{4\pi}\alpha_s^2(\mu_r^2) + \mathcal{O}(\alpha_s^3). \tag{2.85}$$

This result is called the *renormalization group equation* (RGE) at LO. We will integrate it from a scale $\mu_0$, at which we renormalize the coupling, up to a scale $\mu_R$, at which we want to evaluate our results:

$$\alpha_s(\mu_R^2) = \frac{\alpha_s(\mu_0^2)}{1 + \alpha_s(\mu_0^2)\frac{\beta_0}{4\pi}\ln\left(\frac{\mu_R^2}{\mu_0^2}\right)} = \frac{4\pi}{\beta_0 \ln\left(\frac{\mu_R^2}{\Lambda_{\text{LO}}^2}\right)}, \tag{2.86}$$

defining

$$\Lambda_{\text{LO}}^2 \equiv \mu_0^2 \exp\left[-\frac{4\pi}{\beta_0 \alpha_s(\mu_0^2)}\right]. \tag{2.87}$$

Later on, we will basically set $\mu = \mu_R$, which will give us terms proportional to $\ln\left(\frac{\mu_R^2}{m^2}\right)$, e.g. in Eq. (2.69). In order to prevent these logarithms from becoming too large, we would have to choose $\mu_R^2 \sim m^2$ if we dealt with massive particles. A common choice for $\mu_R$ is the mass of the $Z_0$ boson. $\Lambda_{\text{LO}}^2$ as defined in Eq. (2.87) is the *QCD scale parameter*, and like the quark masses it has to be determined experimentally. The values obtained for it are typically in the range of a few hundreds of MeV.
This scale dependence of $\alpha_s$ is the reason why we speak of *running coupling*. One can see in Eq. (2.86) that as $\mu_R$ increases, $\alpha_s(\mu_R^2)$ will decreases, which means that at high scales, the use of $\alpha_s$ as an expansion parameter is justified. Also, we observe that $\alpha_s(\mu_R^2)$ tends to zero for $\mu_R^2 \to \infty$, giving rise to the property of *asymptotic freedom* of QCD.
If we also consider two loop contributions, Eq. (2.84) becomes

$$\beta \equiv \mu_r \frac{dg_r(\mu_r)}{d\mu_r} = -\beta_0 \frac{\tilde{g}_r^3(\mu_r)}{16\pi^2} - \beta_1 \frac{\tilde{g}_r^5(\mu_r)}{(16\pi^2)^2} + \mathcal{O}(\tilde{g}_r^7, \varepsilon), \tag{2.88}$$

or equivalently, the RGE at NLO:

$$\frac{d\alpha_s(\mu_r^2)}{d\ln(\mu_r^2)} = -\frac{\beta_0}{4\pi}\alpha_s^2(\mu_r^2) - \frac{\beta_1}{(4\pi)^2}\alpha_s^3(\mu_r^2) + \mathcal{O}(\alpha_s^4), \tag{2.89}$$

with $\beta_1 = 102 - \frac{38}{3}n_f$. The solution of the latter equation is somehow more involved and has to be done iteratively, leading to

$$\alpha_s(\mu_R^2) = \frac{4\pi}{\beta_0 \ln\left(\frac{\mu_R^2}{\Lambda_{\text{NLO}}^2}\right)} \left\{1 - \frac{\beta_1}{\beta_0^2} \frac{\ln\left[\ln\left(\frac{\mu_R^2}{\Lambda_{\text{NLO}}^2}\right)\right]}{\ln\left(\frac{\mu_R^2}{\Lambda_{\text{NLO}}^2}\right)} \ln\right\}, \tag{2.90}$$

while

$$\Lambda_{\text{NLO}}^2 \equiv \mu_0^2 \exp\left[-\frac{4\pi}{\beta_0 \alpha_s(\mu_0^2)}\right] \left(\frac{4\pi}{\beta_0 \alpha_s(\mu_0^2)} + \frac{\beta_1}{\beta_0^2}\right)^{\frac{\beta_1}{\beta_0^2}}. \tag{2.91}$$

At $\mu_R^2 = \Lambda^2$, the running coupling has a singularity, called the Landau pole. It is somehow unphysical, as it would probably not appear in a complete non-perturbative calculation. Still, it plays an important role when we resum the perturbative series (see Sec. 3). Although perturbation theory breaks down at low energy scales as $\alpha_s$ becomes large, and the derived equations are therefore no longer of any predictive power, one can still attribute the resulting very strong coupling to the fact that we don't see isolated quarks or gluons in nature.
As shown by 't Hooft [39], massless non-Abelian gauge theories can be renormalized to all orders, i.e. we get the same results for the renormalization constants at any order we perform the

calculation. The proof of this statement would exceed the scope of this thesis, see also [40] for a short review on the discovery of renormalizability of non-Abelian gauge theories.
So far, we have solved the problem of UV divergences, which arise when integrating over the inner loop momenta of the virtual corrections by renormalizing the fields and other parameters in the QCD Lagrangian. As a consequence of the renormalization procedure, the coupling constant $\alpha_s$ runs, which means that it depends on the energy scale at which it is evaluated.
Nevertheless, we are still left with the IR divergences that appear if particles in the loops are massless. Fortunately, these singularities cancel, if one considers also the real emission diagrams. In the case an emitted gluon becomes soft, in other words, if its energy tends to zero, the phase space integration gives rise to the same poles as occur in the virtual diagrams, but with the opposite sign. Therefore, by combining the two types of diagrams the IR divergences of the loop integration disappear. This fact is also stated in the *Kinoshita-Lee-Nauenberg theorem* [41, 42].

## 2.6. Initial state singularities and factorization

Beyond LO in perturbation theory, we have to take into account scattering processes such as in Fig. 2.13 with more than two particles in the final state. This new type of diagram unfortunately shows up with new types of divergences. If the momentum of one incoming particle and the directly connected outgoing particle become parallel, the denominator of the adjacent propagator (in the massless limit) will tend to zero, giving rise to a so-called collinear divergence. Note that this divergence is very different from the ones encountered in Sec. 2.5, since there we had to deal with singularities occurring while integrating over some unconstrained loop momentum of a virtual particle. Here, the divergence appears in the tree level amplitude while performing the phase space integration for the final states. We will come back to the collinear divergences when talking about factorization.

In certain regions of phase space, the process in Fig. 2.13 can be interpreted as an initial quark entering in a hard $\gamma q \to qg$ scattering process with the photon, after having emitted a soft gluon. If we define the emitted gluon in the center-of-mass system of the incident partons, we can assign to it the momentum fraction $1 - z_b$ of the initial quark momentum, where

$$z_b = \frac{p_1 p_2}{p_a p_b}, \qquad z_b \in [0, 1]. \tag{2.92}$$

Later, when factorization is discussed, we will see that the lower bound is actually greater than zero. After the splitting, parton $b$ enters the hard subprocess with the remaining fraction $z_b$ of its initial momentum. It is convenient, to use this momentum fraction $z_b$ also for the three particle phase space integration, which has to be performed over the squared matrix elements of amplitudes like the one depicted in Fig. 2.13. However, we encounter expressions like

$$\int_0^1 dz_b \, \frac{g(z_b)}{(1 - z_b)^{1-\varepsilon}}, \tag{2.93}$$

with a function $g(z_b)$ (including the parton distribution function) regular at $z_b = 1$, which are not finite for $\varepsilon \to 0^+$. The case in which $z_b$ becomes 1 corresponds to the situation in which the complete initial parton center-of-mass energy goes into the hard process, and the momentum of the radiated gluon vanishes. Therefore, this type of singularity is called soft divergence. As was already mentioned at the end of Sec. 2.5, the soft poles cancel against the infrared ones stemming from the virtual loop corrections due to the Kinoshita-Lee-Nauenberg theorem. In order to see how this works, we have to make the pole in Eq. (2.93) visible by expanding it in $\varepsilon$, and also get

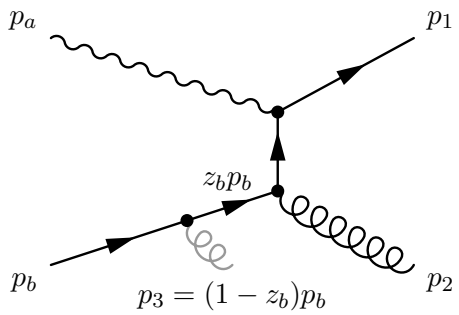


Figure 2.13: Higher order process with possible soft gluon emission.

rid of the $z_b$ integration, which is not present in the kinematics of the virtual corrections [43].

$$\begin{aligned}\int_0^1 dz_b \frac{g(z_b)}{(1-z_b)^{1-\varepsilon}} &= \int_0^1 dz_b \frac{g(1)}{(1-z_b)^{1-\varepsilon}} + \int_0^1 dz_b \frac{g(z_b)-g(1)}{(1-z_b)^{1-\varepsilon}} \\ &= \frac{1}{\varepsilon} g(1) + \int_0^1 dz_b \left[\frac{1}{1-z_b} + \varepsilon \frac{\ln(1-z_b)}{1-z_b} + \mathcal{O}(\varepsilon^2)\right] [g(z_b)-g(1)] \\ &\equiv \frac{1}{\varepsilon} g(1) + \int_0^1 dz_b \left[\left(\frac{1}{1-z_b}\right)_+ + \varepsilon \left(\frac{\ln(1-z_b)}{1-z_b}\right)_+ + \mathcal{O}(\varepsilon^2)\right] g(z_b) \end{aligned} \tag{2.94}$$

In the last step, the plus distributions were defined, which are finite quantities. The first term then is the soft pole and becomes cancelled out by the loop contributions, which in this way regularize the divergent integrand and lead to plus distributions. These distributions will play a major role in our calculations and are always a fingerprint of soft corrections.

If in one process several additional particles are emitted, terms exhibiting more than one pole will appear. These can be combinations of soft and collinear divergences, which cancel as well with their counterparts from the loop diagrams. But also collinear poles related to different kinematical variables can show up in a combined way. They are then usually separated from each other and also from other finite contributions by partial fractioning. Nevertheless, also if they are isolated, they are not cancelled out by any other contribution. Instead, they have to be treated similar as the UV divergences in Sec. 2.5: By redefining the parton distribution functions, we can absorb the remaining collinear divergences. This procedure is known as factorization and will be illustrated with an example.
Consider the process

$$\gamma(p_a) + q(p_b) \to q(p_3) + g(p_1) + g(p_2), \tag{2.95}$$

which is very suitable for our investigation on photon initial state corrections, as it only has a collinear pole and no soft one due to fact that gluons cannot couple directly to the photon. The collinear singularity will occur, if the photon ($p_a$) and one quark ($p_3$) have parallel momenta. Thus, we are only interested in terms singular in the variable

$$z' = \frac{p_a p_3}{p_a p_b}, \tag{2.96}$$

which becomes zero in the collinear limit and should not be mixed up with the hard momentum fraction

$$z_a = \frac{p_1 p_2}{p_a p_b}, \qquad z_a \in [0,1] \tag{2.97}$$

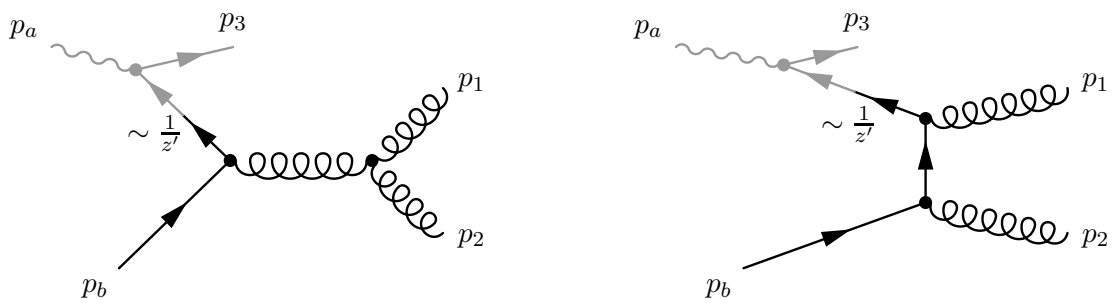


Figure 2.14: Possible tree-level graphs for the process in Eq. (2.95).

we introduce analogously to $z_b$ of the soft divergences. If $z'$ vanishes, it means that the propagator of the massless particle goes on-shell, the internal particle becomes (quasi)real. The diverging propagator can also be associated with an almost infinite propagation time of the corresponding particle. Moreover, the scattering proceeds on two very different time scales. First, we have the collinear decay of the incoming photon and the following long propagation of the quasireal anti-quark. The hard scattering process then happens on a very short time scale. Hence, in the limit $z' \to 0$, the matrix element factorizes and the born matrix element of the hard subprocess $\bar{q}q \to gg$ appears.
The singular terms are given by [7]

$$|\mathcal{M}_{\text{col}}|^2_{\gamma q \to qgg}(s',t',u') = 16\pi\alpha e_q^2 \mu_r^{2\varepsilon} N_C^2 \frac{1}{s'z'}[z_a^2 + (1-z_a)^2 - \varepsilon]\overline{|\mathcal{M}|^2}_{q\bar{q}\to gg}(s',t',u'), \tag{2.98}$$

where $\overline{|\mathcal{M}|^2}_{q\bar{q}\to gg}$ is the unpolarized born matrix element, and the kinetic variables are given as follows:

$$\begin{aligned} s' &= (z_a p_a + p_b)^2 = 2 z_a p_a p_b, \\ t' &= (z_a p_a - p_1)^2 = -2 z_a p_a p_1, \\ u' &= (z_a p_a - p_2)^2 = -2 z_a p_a p_2. \end{aligned} \tag{2.99}$$

Integration over the three final particle phase space

$$dPS^{(3)} = \int (2\pi)^D \prod_{i=1}^{3} \frac{d^D p_i \delta(p_i)}{(2\pi)^{D-1}} \delta^D\left(p_a + p_b - p_1 - p_2 - p_3\right) \tag{2.100}$$

yields

$$\begin{aligned} \int dPS^{(3)} \overline{|\mathcal{M}_{\text{col}}|^2}_{\gamma q\to qgg}(s',t',u') &= \frac{\alpha N_C^2}{4\pi^2 s'} \int_0^1 \frac{dz_a}{z_a} \left[\frac{1}{2N_C} P_{q\leftarrow\gamma}(z_a) \left(-\frac{1}{\varepsilon} + \gamma_E - \ln\left(\frac{4\pi\mu_r^2}{s}\right)\right.\right. \\ &\quad \left.\left. + \ln\left(y_{\text{cut}} \frac{1-z_a}{z_a}\right)\right) + \frac{e_q^2}{2}\right] \overline{|\mathcal{M}|^2}_{q\bar{q}\to gg}(s',t',u') \\ &= \frac{\alpha N_C^2}{4\pi^2 s'} \int_0^1 \frac{dz_a}{z_a} \left[\frac{1}{2N_C} P_{q\leftarrow\gamma}(z_a) \left(-\frac{1}{\hat{\varepsilon}} - \ln\left(\frac{\mu_a^2}{s}\right)\right.\right. \\ &\quad \left.\left. + \ln\left(y_{\text{cut}} \frac{1-z_a}{z_a}\right)\right) + \frac{e_q^2}{2}\right] \overline{|\mathcal{M}|^2}_{q\bar{q}\to gg}(s',t',u'), \end{aligned} \tag{2.101}$$

Here, we define at LO the splitting function for photons into quarks, which we already introduced in Eq. (2.23), as

$$P_{q\leftarrow\gamma}(z) = 2N_C e_q^2 P_{q\leftarrow g}(z) = N_C e_q^2 [z^2 + (1-z)^2], \tag{2.102}$$

and we add also a dependence on a new scale $\mu_a$, which will soon become clear to be the factorization scale. Furthermore, we introduce the shorthand notation

$$\frac{1}{\hat{\varepsilon}} \equiv \frac{1}{\varepsilon} - \gamma_E + \ln\left(\frac{4\pi\mu_r^2}{\mu_a^2}\right). \tag{2.103}$$

The parameter we got for using the method of *phase space slicing*, in order to separate the singular regions in phase space from the non-singular ones, is refered to as $y_{\text{cut}}$. It is actually phase space slicing, which allows us to describe the kinematics only with the help of $s'$, $t'$ and $u'$

in this $2 \to 3$ process, although they would in principle be sufficient only for the description of $2 \to 2$ kinematics.
The divergent structure in Eq. (2.101) resembles the terms we encountered in Sec. 2.5 while renormalizing the fields and coupling. In the present case, however, we have to leave perturbation theory and the purely partonic level in order to remove the $\varepsilon$ pole, a fact which is somehow related to the unobservability of single partons in a direct way.
We write the partonic cross sections in Eq. (2.101) together with leading order contributions from $\gamma q \to gq$ as

$$\begin{aligned} d\hat{\sigma}^{(1)}_{\gamma q \to qgg}(p_a, \mu_a) &= d\hat{\sigma}^{(1)}_{\gamma q \to qgg}(x_a k, \mu_a) \\ &= \sum_a \int dz_a \left[\delta_{\gamma a}\delta(1-z_a) + \frac{\alpha}{2\pi} P_{a\leftarrow\gamma}(z_a)\left(-\frac{1}{\hat{\varepsilon}} - \ln\left(\frac{\mu_a^2}{s}\right)\right)\right] d\hat{\sigma}^{(0)}_{aq}\left(z_a x_a k\right), \end{aligned} \tag{2.104}$$

where for simplicity we kept as an argument only the momentum $p_a$, which is directly related to the initial electron momentum $k$. Moreover, we omit in the following the term including $y_{\text{cut}}$ as well as $\frac{e_q^2}{2}$.
As mentioned before, we have to involve also the hadronic quantities if we want to absorb the poles in Eq. (2.104). For the moment, we keep our approach as clear as possible by simply considering an electron-quark scattering, in which we have the hadronic cross section

$$d\sigma^{(1)}_{eq}(k) = \int dx_a\, F_{\gamma/e}(x_a)\, d\hat{\sigma}^{(1)}_{\gamma q}(x_a k). \tag{2.105}$$

In the latter expression, $F_{\gamma/e}$ is the photon spectrum in the electron, given by the Weizsäcker-Williams approximation (see Sec. 2.2.1), and the index $\gamma q$ of the partonic cross section now refers to both $\gamma q \to qgg$ and $\gamma q \to qq\bar{q}$. We can also write

$$\begin{aligned} d\sigma^{(1)}_{eq}(k) = \sum_a \int_0^1 dX_a \int_0^1 dx_a \int_0^1 dz_a\, \delta\left(X_a - x_a z_a\right) F_{\gamma/e}(x_a) \left[\delta_{a\gamma}\delta(1-z_a) - \frac{\alpha}{2\pi}\frac{1}{\hat{\varepsilon}} P_{a\leftarrow\gamma}(z_a)\right] \\ \times \left[d\hat{\sigma}^{(1)}_{aq}\left(X_a k\right) + \sum_{a'} \int_0^1 dz'_a \frac{\alpha_{(s)}}{2\pi}\frac{1}{\hat{\varepsilon}} P_{a'\leftarrow a}(z'_a) d\hat{\sigma}^{(0)}_{a'q}\left(X_a z' a k\right)\right] \\ = \sum_a \int_0^1 dx_a \int_0^1 dz_a\, F_{\gamma/e}(x_a) \left[\delta_{a\gamma}\delta(1-z_a) - \frac{\alpha}{2\pi}\frac{1}{\hat{\varepsilon}} P_{a\leftarrow\gamma}(z_a)\right] \\ \times \left[d\hat{\sigma}^{(1)}_{aq}\left(x_a z_a k\right) + \sum_{a'} \int_0^1 dz'_a \frac{\alpha_{(s)}}{2\pi}\frac{1}{\hat{\varepsilon}} P_{a'\leftarrow a}(z'_a) d\hat{\sigma}^{(0)}_{a'q}\left(x_a z_a z'_a k\right)\right] \\ = \int_0^1 dx_a\, F_{\gamma/e}(x_a) \left\{d\hat{\sigma}^{(1)}_{\gamma q}(x_a k) + \sum_{a'} \int_0^1 dz'_a \frac{\alpha}{2\pi}\frac{1}{\hat{\varepsilon}} P_{a'\leftarrow\gamma}(z'_a) d\hat{\sigma}^{(0)}_{a'q}\left(x_a z'_a k\right) \right. \\ \left. - \sum_a \int_0^1 dz_a \frac{\alpha}{2\pi}\frac{1}{\hat{\varepsilon}} P_{a\leftarrow\gamma}(z_a) d\hat{\sigma}^{(0)}_{aq}\left(x_a z_a k\right)\right\} + \mathcal{O}(\alpha^2\alpha_s^2, \alpha\alpha_s^3) \\ = \int dx_a\, F_{\gamma/e}(x_a)\, d\hat{\sigma}^{(1)}_{\gamma q}(x_a k) + \mathcal{O}(\alpha^2\alpha_s^2, \alpha\alpha_s^3), \end{aligned} \tag{2.106}$$

which yields the same expression as in Eq. (2.105) if we neglect higher order terms. $X_a = x_a z_a$ describes the fraction of the electron momentum entering the hard process $2 \to 2$ subprocess. In the first line, the squared bracket includes the photonic splitting function that describes the emission of a collinear particle $a$. Within the squared brackets in the second line, the terms take into account also the collinear radiation of a further particle $a'$ off particle $a$; the latter, in

combination with the $\delta_{a\gamma}$, is a photon, and in that case contributing at NLO. If we proceeded to NNLO, we would also have to consider the product of the two splitting functions, which corresponds to the situation that two consecutive particles are emitted from the initial state. Here, we restrict ourselves to the NLO effects.
The second line of Eq. (2.106) contains what is defined as the renormalized partonic cross section in the $\overline{\text{MS}}$ factorization scheme:

$$d\tilde{\sigma}^{(1)}_{\gamma q}(x_a k, \mu_a) = d\hat{\sigma}^{(1)}_{\gamma q}(x_a k) + \sum_a \int_0^1 dz_a \, \frac{\alpha}{2\pi} \frac{1}{\hat{\varepsilon}} P_{a\leftarrow\gamma}(z_a) \, d\hat{\sigma}^{(0)}_{aq}(x_a z_a k). \tag{2.107}$$

It is a finite quantity, as the poles, e.g. from the matrix element in Eq. (2.101), are removed together with a certain choice of finite terms; the latter fixes the factorization scheme, analogously to the renormalization procedure for the fields and couplings reviewed in Sec. 2.5. Note that in Eq. (2.101) after the renormalization, a term proportional to $\ln\left(\frac{\mu_a^2}{s'}\right)$ is left over, making the renormalized cross section depend on the factorization scale $\mu_a$.
Hence, we can render finite our partonic cross section by subtracting the collinear pole. In return, we have to add the latter to the distribution function, Thereby, we define the renormalized photonic distribution function of the electron, now a distribution function for partons $a$, in the first line of Eq. (2.106) as

$$\begin{aligned}\tilde{F}_{a/e}(X_a, \mu_a^2) &= \int_0^1 dx_a \, dz_a \, \delta(X_a - x_a z_a) \left[\delta_{a\gamma}\delta(1-z_a) - \frac{\alpha}{2\pi}\frac{1}{\hat{\varepsilon}} P_{a\leftarrow\gamma}(z_a) \, d\hat{\sigma}^{(0)}_{aq}(X_a k)\right] F_{\gamma/e}(x_a) \\ &= \int_{X_a}^1 \frac{dz_a}{z_a} \left[\delta_{a\gamma}\delta(1-z_a) - \frac{\alpha}{2\pi}\frac{1}{\hat{\varepsilon}} P_{a\leftarrow\gamma}(z_a) \, d\hat{\sigma}^{(0)}_{aq}(X_a k)\right] F_{\gamma/e}\left(\frac{X_a}{z_a}\right). \end{aligned} \tag{2.108}$$

Now, the lower limit of $z_a$ becomes clear to be $X_a$, as the $z_a$ integration is convoluted with the photon density function, whose argument should not become larger than one. While the term proportional to the delta function reproduces the bare distribution function, the higher order term in some sense adds information about the possible splitting of the photon into a quark anti-quark pair, which can also take part in the hard interaction. At this point, we see the mixing of direct and resolved photon contributions to photoproduction beyond LO we already mentioned in Sec. 2.2. Although the higher order term and also the evolution equations for the parton distribution functions (see. Sec. 2.2) stem from perturbative calculations, the functions are non-perturbative quantities and have to be determined by experiment. We thus assume the renormalized parton densities like the one in Eq. (2.108) to be finite by construction and to be the physical densities subject to observation. In this way, we got rid of the last remaining divergences that arose while calculating the partonic cross section in perturbation theory. However, the price we pay for it is that in our finite order calculation we catch yet another scale dependence, which is unphysical and which only vanishes, if the perturbative series is not truncated, i.e. if it is evaluated to all orders. This factorization scale $\mu_a$ the redefined parton distribution function (2.108) as well as the partonic cross section (2.107) depend on serves to separate the soft part of the hadronic cross section, which are the distribution functions, from the hard partonic one.
In the case of the photon and proton PDFs, the factorization procedure works in a very similar way. Consequently, they also become scale-dependent:

$$\tilde{F}_{b'/p}(X_b, \mu_b^2) = \int_{X_b}^1 \frac{dz_b}{z_b} \left[\delta_{b'b}\delta(1-z_b) - \frac{\alpha_s}{2\pi}\frac{1}{\hat{\varepsilon}} P_{b'\leftarrow b}(z_b) \, d\hat{\sigma}^{(0)}_{ab'}(X_b p)\right] F_{b/p}\left(\frac{X_b}{z_b}\right), \tag{2.109}$$

with $X_b = x_b z_b$, the momentum fraction of parton $b'$ in the proton, being now the lower integration bound of the $z_b$ integral. Note that in the definition of $\hat{\varepsilon}$ in Eq. (2.103), $\mu_a$ here of course

has to be replaced by $\mu_b$. If we deal with resolved photons, we take for $F_{\gamma/e}$ the bare quantity, whereas the photon PDF is renormalized according to

$$\tilde{F}_{a'/\gamma}(y_a,\mu_a^2) = \int_{Y_a}^1 \frac{dz_a}{z_a}\left[\delta_{a'a}\delta(1-z_a) - \frac{\alpha_s}{2\pi}\frac{1}{\hat{\varepsilon}}P_{a'\leftarrow a}(z_a)\,d\hat{\sigma}^{(0)}_{a'b}(Y_a p)\right] F_{a/\gamma}\left(\frac{Y_a}{z_a}\right), \tag{2.110}$$

where $Y_a = y_a z_a$ denotes the fraction of the resolved photon momentum that is carried by parton $a'$.
For a more general description of factorization, see e.g. [16]. Just as in the case of the running coupling, one can derive evolution equations for the running parton densities. These are the DGLAP equations already given in Sec. 2.2. The evolution is governed by the Altarelli-Parisi splitting functions, which at LO are of the form

$$P^{(0)}_{q\leftarrow g}(z) = \frac{1}{2}[z^2 + (1-z)^2], \tag{2.111}$$

$$P^{(0)}_{g\leftarrow q}(z) = C_F\left[\frac{1+(1-z)^2}{z}\right], \tag{2.112}$$

$$P^{(0)}_{q\leftarrow q}(z) = C_F\left[\frac{1+z^2}{(1-z)_+} + \frac{3}{2}\delta(1-z)\right] \tag{2.113}$$

and

$$P^{(0)}_{g\leftarrow g}(z) = 2N_C\left[\frac{1}{(1-z)_+} + \frac{1}{z} + z(1-z) - 2\right] + \frac{\beta_0}{2}\delta(1-z). \tag{2.114}$$

They give the probability that (e.g. in the case of $P^{(0)}_{g\leftarrow q}(z)$) a quark emits a gluon collinearly with a momentum fraction $z$ of its longitudinal momentum. The plus distributions were defined in Eq. (2.94) as

$$\int_0^1 dz\,[f(z)]_+ g(z) = \int_0^1 dz\, f(z)[g(z) - g(1)], \tag{2.115}$$

where $f(z)$ is a function which usually has a pole at $z = 1$ and which is regularized by a regular function $g(z)$.
So far, we have settled everything we need to calculate finite cross sections in the QCD-improved parton model, and encountered the running of the coupling constant as well as the parton densities, which is not solely an unavoidable theoretical complication but also observed in nature. Nonetheless, for the finite order perturbative series to be meaningful, the omitted higher order coefficient not only have to be finite, they also should decrease as the order increases. It are precisely the latter plus distributions which cause problems at this point; these problems can be faced with the technique of resummation and will be subject of the discussion in the following section.

# 3. Threshold resummation

In the previous sections, we have seen how in the case of soft gluon emission, the infrared divergences of the real emission diagrams cancel with those of the virtual contributions, leaving behind the characteristic plus distributions in the way it was shown by Eq. (2.94). At higher orders in the perturbative series, multiple gluon emission as depicted in Fig. 3.1 will occur [14]. If we consider the consecutive emission of $n$ gluons with energy fraction $1 - z_i$, as illustrated in the graphic, the energy of the quark will gradually decrease to a final fraction $z = \prod_{i=1}^{n} z_i$ of its initial energy. In the phase space integration over all $z_i$, each gluon can become soft, giving rise to a pole in $\varepsilon$. These multiple poles produce additional finite contributions in combination with the higher order terms of the expansion in Eq. (2.94). We will then encounter a sequence of logarithms

$$\alpha_s^k \left( \frac{\ln^l(1-z)}{1-z} \right)_+, \qquad 0 \leq l \leq 2k-1, \tag{3.1}$$

where $k$ denotes the order of $\alpha_s$ beyond LO. As virtual corrections only exist at threshold, the balancing of virtual and real contribution is restricted to $z = 1$. For the real corrections, we still have to perform the $z$ integration on the full kinematically allowed interval. The expressions in Eq. (3.1) are finite, but they can grow large. In particular, If $z$ becomes equal or even larger than a value $\bar{z}$ satisfying

$$\alpha_s \ln^2(1-\bar{z}) \sim 1, \tag{3.2}$$

which is always fulfilled somewhere on the integration interval, all terms of the perturbative series are of the same order of magnitude, and any finite order truncation would be meaningless. Therefore, we have to take into account the logarithmic terms at every order of perturbation theory, in order to guarantee that we are not missing any sizeable contributions by cutting our series. This is what resummation is about. In the following, we are going to sketch the concept of resummation [44], and give an explicit calculation at leading logarithm (LL) level disregarding the running coupling effect of QCD [14]. Afterwards, we will present a more general description of the procedure at NLL, followed by the derivation of the NLO and NNLO master formulæ of N. Kidonakis [12]. We close the section with a comparison of the NLO results obtained from the said master formula to the ones from Klasen and Kramer [7], reviewing two different processes.

## 3.1. Basic concepts and a simplified example

Suppose, we have an infrared sensitive quantity, $R(M^2, m^2)$, depending on two different scales $M$ and $m$. Be $M^2$ a hard scale, and $m^2$ a scale measuring the distance to the critical region, i.e. the Landau pole. One can show (we skip the highly non-trivial proof) that for $m^2 \ll M^2$ the

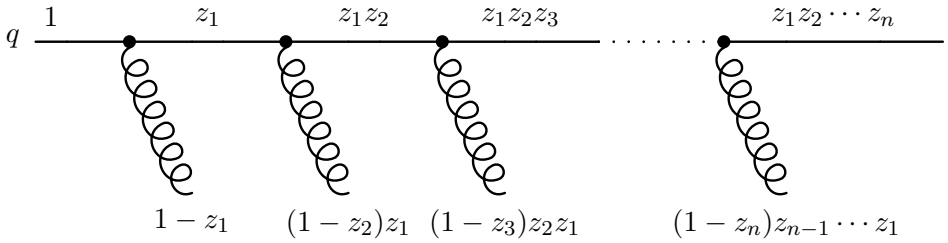


Figure 3.1: Consecutive emission of $n$ gluons from a quark parton line.

quantity factorizes into a soft and a hard part, separated by a factorization scale $\mu$ [44]:

$$R(M^2, m^2) = H\left(\frac{M^2}{\mu^2}\right) S\left(\frac{m^2}{\mu^2}\right) \tag{3.3}$$

This procedure is also called *re*factorization, in order to distinguish it from the "normal" factorization already discussed in the previous chapter. Here, it leaves the functions $S$ and $H$ with potentially large scale ratios. It is important to note that refactorization does not necessarily work out in momentum space. Usually, resummation is performed in the conjugate Mellin or moment space, defined by the transformation prescription

$$\tilde{f}(N) = \int_0^1 dz\, z^{N-1} f(z). \tag{3.4}$$

The latter transformation is a unilateral Laplace transformation

$$\tilde{f}(N) = \int_0^\infty dt\, e^{-Nt} f(t), \tag{3.5}$$

in which we choose $z = e^{-t}$. For future use, we will simply drop the tilde denoting the transformed function. Mellin transformed quantities then can be identified by their argument $N$.
If we have applied refactorization in any space whatsoever, we can exploit the factorization scale independence of $R(M^2, m^2)$ to obtain two evolution equations for $S$ and $H$, respectively. One finds

$$\frac{d\ln(H)}{d\ln(\mu^2)} = \gamma_S(\mu^2) = -\frac{d\ln(S)}{d\ln(\mu^2)}, \tag{3.6}$$

and thus, solving for $H$ and $S$,

$$H\left(\frac{M^2}{\mu^2}\right) = H(1) \exp\left[-\int_{\mu^2}^{M^2} \frac{dq^2}{q^2} \gamma_S(q^2)\right], \tag{3.7}$$

as well as

$$S\left(\frac{m^2}{\mu^2}\right) = S(1) \exp\left[-\int_{m^2}^{\mu^2} \frac{dq^2}{q^2} \gamma_S(q^2)\right]. \tag{3.8}$$

We observe that for $H$ and $S$ the large scale ratios have vanished and all scale dependence has been moved into the exponential, the so-called *Sudakov form factor*, which now allows for safe use of perturbation theory. Combining the last two equations, we obtain

$$R(M^2, m^2) = H(1)S(1) \exp\left[-\int_{m^2}^{M^2} \frac{dq^2}{q^2} \gamma_S(q^2)\right], \tag{3.9}$$

where also the final factorization scale independence becomes manifest.
As was clearly demonstrated, the key ingredients of resummation are factorization and exponentiation. We will now return to our example of the $n$ gluon emission. The first step would be to calculate the corresponding matrix element. We exploit the fact that in the soft limit we can apply the *eikonal approximation*, which means that the $n$ gluon emission matrix element $M_n$ factorizes into matrix elements $M_1$ for single emissions [14]:

$$M_n(z_1, \ldots, z_n) \simeq \frac{1}{n!} \prod_{i=1}^{n} M_1(z_i). \tag{3.10}$$

The proof especially in non-Abelian QCD is rather involved and would exceed the scope of this thesis. The $z$ phase space is proportional to

$$\prod_{i=1}^{n} dz_i, \delta\left(z - \prod_{i=1}^{n} z_i\right) \tag{3.11}$$

and does not factorize due to the delta function, whose Mellin transform is given by

$$\int_0^1 dz\, z^{N-1} \delta\left(z - \prod_{i=1}^{n} z_i\right) = \prod_{i=1}^{n} z_i^{N-1}. \tag{3.12}$$

Here, we found the $z_i^{N-1}$ that will mediate the Mellin transform with respect to each single $z_i$ and also the desired factorization.
The need for resummation arose from the potentially large logarithmic terms in Eq. (3.1), which are $z$-dependent and also have to be transformed. In Mellin space, they are of the form

$$\alpha_s^k \ln^l(N), \qquad 0 \leq l \leq 2k-1. \tag{3.13}$$

Therefore, the soft limit (threshold) in $N$ space is at large $N$. The $z$ dependence of a matrix element at order $n$ can also be written in terms of the coefficient function $C^{(n)}(z)$, which in the eikonal approximation factorizes just as the matrix element into soft order 1 coefficients. If we go to Mellin space, this is expressed as

$$C^{(n)}(N) \simeq \frac{1}{n!}\left[C^{(1)}_{\text{soft}}(N)\right]^n, \tag{3.14}$$

where the singularities are understood to have already been removed by consideration of virtual contributions. $C^{(1)}_{\text{soft}}(N)$ will in general contain terms proportional to $\ln^2(N)$ (LL) and $\ln(N)$ (NLL = next-to-leading logarithm). Taking only the LL, we have

$$C^{(1)}_{\text{soft}}(N) \simeq -A \ln^2(N) \tag{3.15}$$

with a process-dependent constant $A$, and we obtain as the resummed coefficient function

$$C^{\text{res}}(N, \alpha_s) = \sum_{n=0}^{\infty} \alpha_s^n \left[C^{(n)}(N)\right]_{\text{soft}} = \exp\left[\alpha_s C^{(1)}_{\text{soft}}(N)\right]. \tag{3.16}$$

This result is only valid at LL accuracy. Again, we achieved exponentiation, through the factorization of the single soft gluon emissions in Eq. (3.14). However, we did not consider the running of the coupling constant $\alpha_s$; hence, we miss the additional integration over the scale in the exponent.
The next step will be to discuss threshold resummation for hadronic cross sections in a more general way.

## 3.2. General approach

As we have seen, threshold resummation resums logarithmic terms which grow large in the phase space region close to threshold. For our hadronic cross section, we can distinguish between the hadronic threshold, expressed through the fraction

$$\tau = \frac{M^2}{S}, \tag{3.17}$$

where $M^2$ is the invariant mass of the hard process final state particles and $S$ the hadronic center-of-mass energy, and the partonic threshold manifested in

$$z = \frac{M^2}{s}, \tag{3.18}$$

with $s$ being the partonic equivalent to $S$. In our notation, both fractions are related through $\tau = x_a x_b z$ or $z = \frac{\tau}{x_a x_b}$, respectively. The logarithms become enhanced as $z \to 1$. This is certainly the case, if the $ep$ collision is close to threshold and $\tau \to 1$, as $x_a x_b$ will always be less than 1. But even if $\tau$ is far from threshold, which experimentally is a very common situation, we are still close to *partonic* threshold if $x_a$ and $x_b$ are small enough. The latter will happen most likely for partons whose distribution is peaked at small $x$, such as sea quarks and gluons in the case of the density function of the proton. We therefore expect that threshold resummation is important also relatively far from hadronic threshold, especially for partonic processes with gluons in the initial state.

We base our approach on [44], but provide a more general discussion taking into account also final state partons, as has been done in [45, 46, 47]. Our first goal will again be refactorization. We rewrite the cross section from Eq. (2.37) in a more general form,

$$\begin{aligned} M^2 \frac{d\sigma_{AB\to JJ}}{dM^2} = \sum_{a,b} \int_0^1 dx_a\, x_a F_{a/A}(x_a, \mu_a^2) \int_0^1 dx_b\, x_b F_{b/B}(x_b, \mu_b^2) \\ \times \int_\tau^1 dz\, z \bar{\sigma}_{ab\to cd}\left(z, M^2, \frac{M^2}{\mu_a^2}, \frac{M^2}{\mu_b^2}\right) \delta(\tau - x_a x_b z), \end{aligned} \tag{3.19}$$

in which $\bar{\sigma}_{ab\to cd}$ is rather a hard scattering function than a real cross section as the $z$ integration has not been performed, yet. Furthermore, we have made the cross section differential in $M^2$ by adding the delta function

$$\delta\left(M^2 - sz\right) = \frac{x_a x_b z}{M^2} \delta\left(\tau - x_a x_b z\right) \tag{3.20}$$

on the right-hand side. Correspondingly, we find in Mellin space after transforming $\tau$ on both sides in Eq. (3.19), which in combination with the delta function becomes a transformation of $x_a$, $x_b$ and $z$:

$$M^2 \frac{d\sigma_{AB\to JJ}}{dM^2}(N-1) = \sum_{a,b} F_{a/A}(N, \mu_a^2) F_{b/B}(N, \mu_b^2) \bar{\sigma}_{ab\to cd}\left(N, M^2, \frac{M^2}{\mu_a^2}, \frac{M^2}{\mu_b^2}\right). \tag{3.21}$$

Note that the convolution of the distribution functions in Eq. (3.19) disappears in $N$ space. The partonic cross section then factorizes in a similar way and can be written as

$$M^2 \frac{d\hat{\sigma}_{ab\to cd}}{dM^2}(N-1) = \sum_{e,f} \phi_{e/a}(N, \mu_a^2) \phi_{f/b}(N, \mu_b^2) \bar{\sigma}_{ef\to cd}\left(N, M^2, \frac{M^2}{\mu_a^2}, \frac{M^2}{\mu_b^2}\right). \tag{3.22}$$

This procedure is exactly what we discussed as factorization in Sec. 2.6, where the collinear singularities were absorbed into the parton density functions. Hence, $d\bar{\sigma}_{ef}$ is now an infrared safe quantity and can be evaluated perturbatively. $\phi_{e/a}$ and $\phi_{f/b}$ are the parton-in-parton distributions for partons $e$ and $f$ in partons $a$ and $b$ respectively. Their factorization scale evolution is also governed by the Altarelli-Parisi splitting functions, which in Mellin space at LO take the form

$$P^{(0)}_{q\leftarrow g}(N) = \frac{1}{2} \frac{2 + N + N^2}{N(N+1)(N+2)}, \tag{3.23}$$

$$P^{(0)}_{g\leftarrow q}(N) = C_F \frac{2+N+N^2}{N(N^2-1)}, \tag{3.24}$$

$$P^{(0)}_{q\leftarrow q}(N) = C_F \left[\frac{3}{2} + \frac{1}{N(N+1)} - 2\psi(N+1) - 2\gamma_E\right], \tag{3.25}$$

$$P^{(0)}_{g\leftarrow g}(N) = 2N_C \left[\frac{1}{N(N-1)} + \frac{1}{(N+1)(N+2)} - \psi(N+1) - \gamma_E\right] + \frac{\beta_0}{2}, \tag{3.26}$$

with the DiGamma function $\psi$. For threshold resummation, we are interested in the large $N$ limit, in which $\psi(N+1)$ behaves like $\ln(N)$, and therefore we find for the splitting functions

$$\begin{aligned} P^{(0)}_{q\leftarrow g}(N) &\sim \frac{1}{2N}, \qquad P^{(0)}_{q\leftarrow q}(N) = C_F\left[\frac{3}{2} - 2(\ln(N)+\gamma_E)\right] + \mathcal{O}\left(\frac{1}{N}\right), \\ P^{(0)}_{g\leftarrow q}(N) &\sim \frac{C_F}{N}, \qquad P^{(0)}_{g\leftarrow g}(N) = \frac{\beta_0}{2} - 2N_C\left[\ln(N)+\gamma_E\right] + \mathcal{O}\left(\frac{1}{N}\right). \end{aligned} \tag{3.27}$$

In this way it becomes obvious that close to threshold the parton mixing contributions are negligible, so we can recast Eq. (3.22) to

$$M^2 \frac{d\hat{\sigma}_{ab\to cd}}{dM^2}(N-1) = \phi_{a/a}(N,\mu_a^2)\phi_{b/b}(N,\mu_b^2)\bar{\sigma}_{ab\to cd}\left(N, M^2, \frac{M^2}{\mu_a^2}, \frac{M^2}{\mu_b^2}\right) + \mathcal{O}\left(\frac{1}{N}\right). \tag{3.28}$$

At this point, we are going to refactorize the cross section, and following the method of Sterman [48] we rewrite the previous expression as

$$\begin{aligned} M^2 \frac{d\hat{\sigma}_P}{dM^2}(N-1) = {} & H_P\left(M^2, \frac{M^2}{\mu_a^2}, \frac{M^2}{\mu_b^2}\right) \Psi_{a/a}\left(N, M^2, \frac{M^2}{\mu_a^2}\right) \Psi_{b/b}\left(N, M^2, \frac{M^2}{\mu_b^2}\right) \\ & \times J^{(c)}\left(N, M^2\right) J^{(d)}\left(N, M^2\right) S_P\left(N, \frac{M^2}{\mu_a^2 N^2}, \frac{M^2}{\mu_b^2 N^2}\right) + \mathcal{O}\left(\frac{1}{N}\right). \end{aligned} \tag{3.29}$$

In order to reduce clutter in the notation, $P$ replaces $ab \to cd$; as the refactorization scale $\mu$ we chose the factorization scales $\mu_a$ and $\mu_b$, which were already introduced to separate soft and hard part of the cross section. Infrared safe contributions are pooled in the hard function $H_P$, which can therefore be expanded in a perturbative series:

$$H_P\left(M^2, \frac{M^2}{\mu_a^2}, \frac{M^2}{\mu_b^2}\right) = \alpha^k \alpha_s^m \sum_{n=0}^{\infty} \left(\frac{\alpha_s}{2\pi}\right)^n H_P^{(n)}\left(M^2, \frac{M^2}{\mu_a^2}, \frac{M^2}{\mu_b^2}\right), \tag{3.30}$$

setting $k = m = 1$ for direct and $k = 0$, $m = 2$ for resolved photoproduction. Its renormalization is determined by

$$H_{P,\text{bare}} = \prod_{i=a,b} Z_i Z_S^{-1} H_P (Z_S^*)^{-1}, \tag{3.31}$$

introducing the renormalization constants $Z_S$ of the soft function $S_P$, and $Z_i$ of the incoming parton field $i$, $i = a, b$.

In contrast to $\phi_{a/a}$ and $\phi_{b/b}$ in Eq. (3.28), which measure the momentum fraction of partons in partons, $\Psi_{a/a}$ and $\Psi_{b/b}$ in Eq. (3.29) are defined in terms of energy fractions. Both densities are described by different evolution equations. On the one hand, we have

$$\frac{d\Psi_{i/i}}{d\ln(\mu_i^2)} = \gamma_i \Psi_{i/i}\left(N, M, \frac{M^2}{\mu_i^2}\right), \tag{3.32}$$

with $\gamma_i$ being the anomalous dimension of the parton field $i$, given in the axial gauge by the virtual part (the part proportional to $\delta(1-z)$ in $z$ space and thus the $N$-independent terms in Mellin space except the Euler gamma) of the splitting functions. That is, at LO one finds $\gamma_g^{(0)} = \frac{\beta_0}{2}$ for gluons and $\gamma_q^{(0)} = \frac{3}{2}C_F$ for quarks. On the other hand,

$$\frac{d\phi_{i/i}}{d\ln(\mu_i^2)} = \gamma_{i/i}(N)\phi_{i/i}\left(N, M, \frac{M^2}{\mu_i^2}\right),, \tag{3.33}$$

which uses the anomalous dimension $\gamma_{i/i}$ of the operator whose matrix element represents the density $\phi_{i/i}$ [49]. It is given in the axial gauge by

$$\begin{aligned}\gamma_{q/q} = &-\frac{\alpha_s}{2\pi}\left[2C_F\ln(N) - \frac{3}{2}C_F\right] + \left(\frac{\alpha_s}{2\pi}\right)^2\left[2KC_F\ln(N) + C_F^2\left(\frac{3}{8} - 3\zeta_2 + 6\zeta_3\right)\right.\\ &\left.+C_FC_A\left(\frac{17}{24} + \frac{11}{3}\zeta_2 - 3\zeta_3\right) - n_fC_F\left(\frac{1}{12} + \frac{2}{3}\zeta_2\right)\right] + \mathcal{O}\left(\frac{1}{N}\right)\end{aligned} \tag{3.34}$$

and

$$\begin{aligned}\gamma_{g/g} = &-\frac{\alpha_s}{2\pi}\left[2C_A\ln(N) - \frac{\beta_0}{2}\right] + \left(\frac{\alpha_s}{2\pi}\right)^2\left[2KC_A\ln(N) + C_A^2\left(\frac{8}{3} + 3\zeta_3\right)\right.\\ &\left.-n_f\left(\frac{C_F}{2} + \frac{2C_A}{3}\right)\right] + \mathcal{O}\left(\frac{1}{N}\right)\end{aligned} \tag{3.35}$$

for initial state quarks and gluons, respectively. The occurring values of the Riemann zeta function are $\zeta_2 = \frac{\pi^2}{6}$ and $\zeta_3 = 1.2020569\ldots$; also, we defined in both expressions

$$K = C_A\left(\frac{67}{18} - \frac{\pi^2}{6}\right) - \frac{5}{9}n_f. \tag{3.36}$$

$J^{(c)}$ and $J^{(d)}$ are jet functions that organize the fragmentation of the massless final state partons $c$ and $d$. Lastly, we encounter again the eikonal approximation in the calculation of $S_P$, which describes the soft gluon emission. The associated evolution equation is given by

$$S_{P,\text{bare}} = Z_S^* S_P Z_S, \tag{3.37}$$

leading to the following RGE:

$$\left(\mu_r\frac{\partial}{\partial\mu_r} + \beta\left(\tilde{g}_r\right)\frac{\partial}{\partial\tilde{g}_r}\right)S_P = -2\text{Re}\left(\Gamma_S\right)S_P, \tag{3.38}$$

where $\beta$ is defined in Eq. (2.84) and

$$\Gamma_S = \lim_{\varepsilon\to 0}\frac{\tilde{g}_r}{2}\frac{\partial}{\partial\tilde{g}_r}\text{Res}\left[Z_S\left(\tilde{g}_r, \varepsilon\right)\right] \tag{3.39}$$

is the soft anomalous dimension.
By comparison of Eqs. (3.28) and (3.29), we conclude

$$\begin{aligned}\bar{\sigma}_P\left(N, M^2, \frac{M^2}{\mu_a^2}, \frac{M^2}{\mu_b^2}\right) = &H_P\left(M^2, \frac{M^2}{\mu_a^2}, \frac{M^2}{\mu_b^2}\right)\frac{\Psi_{a/a}\left(N, M^2, \frac{M^2}{\mu_a^2}\right)\Psi_{b/b}\left(N, M^2, \frac{M^2}{\mu_b^2}\right)}{\phi_{a/a}(N, \mu_a^2)\phi_{b/b}(N, \mu_b^2)}\\ &\times J^{(c)}\left(N, M^2\right)J^{(d)}\left(N, M^2\right)S_P\left(N, \frac{M^2}{\mu_a^2N^2}, \frac{M^2}{\mu_b^2N^2}\right) + \mathcal{O}\left(\frac{1}{N}\right).\end{aligned} \tag{3.40}$$

The factors $\frac{\Psi_i}{\phi_i}$ are universal between electroweak and hard QCD processes, and together with the jet functions they provide the LL corrections.
We proceed to the exponentiation of the eikonal function $S_P$. For this purpose, one has to solve Eq. (3.38) in order to evolve the soft function to the common refactorization scales:

$$S_P\left(N, \frac{M^2}{\mu_a^2 N^2}, \frac{M^2}{\mu_b^2 N^2}\right) = S_P(N,1,1) \exp\left[\sum_{i=a,b} \int_{\mu_i^2}^{\frac{M^2}{N^2}} \frac{dq^2}{q^2} \mathrm{Re}\left[\Gamma_{S,i}\left(\alpha_s(q^2)\right)\right]\right] \tag{3.41}$$

Here, $\Gamma_S$ has been split up into two parts $\Gamma_{S,a} + \Gamma_{S,b}$, which correspond to the two different factorization scales $\mu_a$ and $\mu_b$. The exponentiation of the parton densities and the jet functions is achieved in a similar way, i.e. through solving Eq. (3.32).
Finally, we find for the resummed scattering function:

$$\begin{aligned}\bar{\sigma}_{P,\mathrm{res}}\left(N, M^2, \frac{M^2}{\mu_a^2}, \frac{M^2}{\mu_b^2}\right) &= \mathcal{H}_P\left(M^2, \frac{M^2}{\mu_a^2}, \frac{M^2}{\mu_b^2}\right) \exp\left[G_P\left(N, \frac{M^2}{\mu_a^2}, \frac{M^2}{\mu_b^2}\right)\right] \\ &\times S_P(N,1,1) \exp\left[\sum_{i=a,b} \int_{\mu_i^2}^{\frac{M^2}{N^2}} \frac{dq^2}{q^2} \mathrm{Re}\left[\Gamma_{S,i}\left(\alpha_s(q^2)\right)\right]\right] + \mathcal{O}\left(\frac{1}{N}\right),\end{aligned} \tag{3.42}$$

where $H_P$ has been redefined after the absorption of $N$-independent terms, and where the function

$$G_P\left(N, \frac{M^2}{\mu_a^2}, \frac{M^2}{\mu_b^2}\right) = \sum_i E_i(N) + \sum_j E'_j(N) \tag{3.43}$$

consists of

$$E_i(N) = \int_0^1 dz\, \frac{z^{N-1}-1}{1-z} \left\{ \int_{\mu_i^2}^{(1-z)^2 M^2} \frac{dq^2}{q^2} A_i\left(\alpha_s(q^2)\right) - \nu_i\left(\alpha_s\left((1-z)^2 M^2\right)\right) \right\} \tag{3.44}$$

and

$$E'_j(N) = \left\{ \int_{(1-z)^2 M^2}^{(1-z) M^2} \frac{dq^2}{q^2} A_j\left(\alpha_s(q^2)\right) - B_j\left(\alpha_s\left((1-z) M^2\right)\right) - \nu_j\left(\alpha_s\left((1-z)^2 M^2\right)\right) \right\}. \tag{3.45}$$

These functions arise from the scale evolution of the parton densities and the jet functions. They correspond to the logarithms of so-called radiation factors. $i$ in the first expression runs over the initial partons $a$ and $b$, and the $A_i$ collect initial state contributions from soft gluons which are collinearly radiated off the parton $a$ and $b$, respectively. $A_i$ is given by the coefficient of the plus distribution in the $P_{ii}(z)$ splitting function. The sum over $j$ in Eq. (3.45) is related to the final state partons $c$ and $d$, and it only appears if the latter are massless quarks or gluons. Consequently, $A_j$ and $B_j$ take into account collinear final-state emission. $\nu_i$ and $\nu_j$ collect large-angle radiation effects. The difference in the scale dependences in the arguments of $B$ and $D$ as well as in the integration bounds is due to hard scattering kinematics, which affect in a different way initial- or final-state radiation and soft or collinear emission. Note that all radiative factors are renormalization-group-invariant quantities. An explicit $\mu_R$-dependence only appears, if the expressions are truncated to a certain logarithmic degree, as will become visible below [50]. However, the expressions of Eqs. (3.44) and (3.45) are ill-defined, as the outer integrations make $z$ to take any value between 0 and 1; the latter means that the scale $q^2$ in the second integral is forced to reach zero and thereby passes the Landau pole of $\alpha_s(q^2)$. One can avoid this problem in actual calculations by expanding the inner integral in powers of $\alpha_s$ and evaluating the Mellin

transform separately at each order. Taking the large $N$ limit and resumming the power series then leads to a finite result.
For all functions $A$, $B$ and $\nu$, we can now likewise perform a power series expansion in $\alpha_s$, finding

$$A_{i/j} = \sum_{n=0}^{\infty} \left(\frac{\alpha_s}{2\pi}\right)^n A_{i/j}^{(n)}, \qquad B_j = \sum_{n=0}^{\infty} \left(\frac{\alpha_s}{2\pi}\right)^n B_j^{(n)}, \qquad \text{and} \qquad \nu_{i/j} = \sum_{n=0}^{\infty} \left(\frac{\alpha_s}{2\pi}\right)^n \nu_{i/j}^{(n)}. \quad (3.46)$$

$i$ and $j$ can stand for a quark or a gluon, respectively. The $A^{(n)}$ are obtained from the coefficients of the plus distributions in the $n$-loop splitting functions as mentioned before. They are calculated to be [51]

$$A_f^{(1)} = 2C_f \qquad \text{and} \qquad A_f^{(2)} = 2C_f K, \quad (3.47)$$

with $C_f = C_F$ if $f = q$ for quarks and anti-quarks, and $C_f = C_A = N_C = 3$ if $f = g$ for gluons. Analogously, we find

$$B_q^{(1)} = \frac{3}{2} C_F, \qquad B_g^{(1)} = \frac{\beta_0}{2}, \quad (3.48)$$

whereas the $\nu_i$ and $\nu_j$, which are used in [12] and correspond to the function $D$ in [50], at lowest order are given by

$$\nu_f^{(1)} = 2C_f. \quad (3.49)$$

After the integrations in Eqs. (3.44) and (3.45) have been performed, $G_P$ is rewritten as [52]

$$G_P\left(N, \frac{M^2}{\mu_a^2}, \frac{M^2}{\mu_b^2}\right) = \ln(N) g_P^{(1)}(\lambda) + g_P^{(2)}\left(\lambda, \frac{M^2}{\mu_a^2}, \frac{M^2}{\mu_b^2}\right) + \frac{\alpha_s}{2\pi} g_P^{(3)}\left(\lambda, \frac{M^2}{\mu_a^2}, \frac{M^2}{\mu_b^2}\right) + \mathcal{O}\left(\alpha_s^2\right), \quad (3.50)$$

with $\lambda = \frac{\alpha_s}{2\pi}\frac{\beta_0}{2}\ln(N)$ and

$$g_P^{(l)}(\lambda, \dots) = \sum_{k=1}^{\infty} \left(\frac{\alpha_s}{2\pi}\ln(N)\right)^k g_{P,k}^{(l)}(\lambda, \dots). \quad (3.51)$$

For LL accuracy, we only need the first term in Eq. (3.50), which is given by [50]

$$g_{ab\to cd}^{(1)}(\lambda) = \frac{1}{2}\left(\sum_i A_i^{(1)} - \sum_j A_j^{(1)}\right) h^{(1)}(\lambda) + \frac{1}{2}\sum_j A_j^{(1)} h^{(1)}\left(\frac{\lambda}{2}\right), \quad (3.52)$$

where

$$h^{(1)}(\lambda) = \frac{2}{\beta_0 \lambda}\left[2\lambda + (1-2\lambda)\ln(1-2\lambda)\right]. \quad (3.53)$$

If NLL accuracy is desired, we also have to evaluate

$$\begin{aligned} g_{ab\to cd}^{(2)}\left(N, \frac{M^2}{\mu_a^2}, \frac{M^2}{\mu_b^2}\right) = {} & \frac{1}{2}\left(\sum_i A_i^{(1)} - \sum_j A_j^{(1)}\right) h^{(2)}(\lambda) + \sum_j A_j^{(1)} h^{(2)}\left(\frac{\lambda}{2}\right) \\ & - \frac{\sum_i \nu_i^{(1)} + \sum_j \nu_j^{(1)}}{\beta_0}\ln(1-2\lambda) + 2\frac{\sum_j \left(\gamma_E A_j^{(1)} - B_j^{(1)}\right)}{\beta_0}\ln(1-\lambda) \\ & - 2\lambda \sum_i A_i^{(1)} \ln\left(\frac{M^2}{\mu_i^2}\right) + \left\{\frac{\sum_i A_i^{(1)}}{\beta_0}\left[2\lambda + \ln(1-2\lambda)\right]\right. \\ & \left. + \frac{\sum_j A_j^{(1)}}{\beta_0}\left[2\ln(1-\lambda) + \ln(1-2\lambda)\right]\right\} \ln\left(\frac{M^2}{\mu_R^2}\right), \end{aligned} \quad (3.54)$$

with the auxiliary function

$$h^{(2)}(\lambda) = 2\frac{\beta_1}{\beta_0^3}\left[2\lambda + \ln(1-2\lambda) + \frac{1}{2}\ln^2(1-2\lambda)\right] - \frac{4\gamma_E}{\beta_0}\ln(1-2\lambda) - \frac{4K}{\beta_0^2}\left[2\lambda + \ln(1-2\lambda)\right]. \tag{3.55}$$

Note that although the factorization scale dependence only showed up in Eq. (3.54) and otherwise has been omitted so far, it has always been present in the running of $\alpha_s$. Its explicit appearance is due to the truncation of the logarithmic series in Eq. (3.50).
The comparison of Eq. (3.42) (after the replacement $H_P \leftrightarrow \mathcal{H}_P$) and the power series expansion of $S_P$ with the one of the hard scattering function $\bar{\sigma}$,

$$\bar{\sigma}_{P,\mathrm{res}}\left(N, M^2, \frac{M^2}{\mu_a^2}, \frac{M^2}{\mu_b^2}\right) = \alpha^k \alpha_s^m \sum_{n=0}^{\infty}\left(\frac{\alpha_s}{2\pi}\right)^n \bar{\sigma}^{(n)}_{P,\mathrm{res}}\left(N, M^2, \frac{M^2}{\mu_a^2}, \frac{M^2}{\mu_b^2}\right), \tag{3.56}$$

yields, as the expansion of the exponential in Eq. (3.42) is 1 at zeroth order:

$$\mathcal{H}_P^{(0)}\left(M^2, \frac{M^2}{\mu_a^2}, \frac{M^2}{\mu_b^2}\right) S_P^{(0)} = \bar{\sigma}^{(0)}_{P,\mathrm{res}}\left(M^2, \frac{M^2}{\mu_a^2}, \frac{M^2}{\mu_b^2}\right), \tag{3.57}$$

where $\alpha^k \alpha_s^m \bar{\sigma}^{(0)}_{P,\mathrm{res}}$ represents the Born cross section, which is just as $S_P^{(0)}$ and $\mathcal{H}_P$ $N$-independent. Consequently, $\mathcal{H}_P$ will be $z$-independent in physical space. Thus, the next higher order coefficient $\mathcal{H}_P^{(1)}$ will correspond to the virtual NLO corrections, but also to the contributions of the NLO real corrections which are proportional to $\delta(1-z)$. The latter can be found e.g. in the splitting functions (2.113) and (2.114).
If we write Eq. (3.42) as a series in $\alpha_s$ and use $G_P$ at LL accuracy, we obtain, suppressing any scale dependence in the arguments:

$$\begin{aligned}\frac{\bar{\sigma}_P^{LL}}{\alpha^k \alpha_s^m}(N) = {} & \mathcal{H}_P^{(0)} S_P^{(0)} + \frac{\alpha_s}{2\pi}\left\{\mathcal{H}_P^{(0)} S_P^{(0)}\left(\sum_i A_i + \frac{1}{2}\sum_j A_j\right)\ln^2(N)\right. \\ & \left. + \mathcal{H}_P^{(1)} S_P^{(0)} + \mathcal{H}_P^{(0)} S_P^{(1)} + \mathcal{O}\left(\ln(N)\right)\right\} + \mathcal{O}\left(\alpha_s^2\right).\end{aligned} \tag{3.58}$$

Here, only the coefficients of the highest powers of $\ln(N)$ are exact, i.e. the contributions of $\ln^2(N)$ at order $\alpha_s$ and those of $\ln^4(N)$ at order $\alpha_s^2$. All other contributions will change if we proceed to NLL accuracy, that is, if we take into account also $g_P^{(2)}$:

$$\begin{aligned}\frac{\bar{\sigma}_P^{NLL}}{\alpha^k \alpha_s^m}(N) = {} & \mathcal{H}_P^{(0)} S_P^{(0)} + \frac{\alpha_s}{2\pi}\left\{\mathcal{H}_P^{(0)} S_P^{(0)}\left[\left(\sum_i A_i + \frac{1}{2}\sum_j A_j\right)\ln^2(N)\right.\right. \\ & + \left[\sum_i A_i\left(2\gamma_E - \beta_0 \ln\left(\frac{M^2}{\mu_i^2}\right)\right) + \sum_j\left(B_j - 3\gamma_E A_j - 2A_j \ln\left(\frac{M^2}{\mu_R^2}\right)\right)\right. \\ & \left.\left. \left. + \sum_i \nu_i^{(1)} + \sum_j \nu_j^{(1)} + 2\gamma_E\right]\ln(N)\right] + \mathcal{H}_P^{(1)} S_P^{(0)} + \mathcal{H}_P^{(0)} S_P^{(1)}\right\} + \mathcal{O}\left(\alpha_s^2\right).\end{aligned} \tag{3.59}$$

With the latter expression, we have found the complete resummed partonic cross section in the soft limit up to NLO. In general, one can obtain all logarithmically enhanced contributions of

| Log. approx. | $g_P^{(k)}$ up to | $(\mathcal{H}_P S_P)^{(m)}$ up to | accuracy: $\alpha_s^n \ln^l(N)$ |
|---|---|---|---|
| LL | $k = 1$ | $m = 0$ | $l = 2n$ |
| NLL | $k = 2$ | $m = 1$ | $2(n-1) \leq l \leq 2n$ |
| NNLL | $k = 3$ | $m = 2$ | $2(n-2) \leq l \leq 2n$ |

Table 3: Orders of logarithmic approximations and accurately predicted contributions.

order $\ln^l(N)$ with $2(n-p) \leq l \leq 2n$ to a fixed order calculation at $\alpha_s^n$ with the expansion of the resummed cross section at N$^{\text{p}}$LL level up to the same order in $\alpha_s$, as is also shown in Tab. 3 for the first few orders.
After resumming the cross section in Mellin space, we need to transform the result back to physical $z$ space. However, the inverse Mellin transform of Eq. (3.42) is not defined because of singularities arising in the exponent at $\lambda = 1$ and $\lambda = 0$. The former is reached at

$$N_L = \exp\left(\frac{4\pi}{\alpha_s \beta_0}\right), \tag{3.60}$$

which represents the Landau pole in $N$ space. In order to perform the necessary integration, one has to find a prescription that avoids the divergence and that allows to construct a resummed expression to which the divergent series is asymptotic. In the *minimal prescription* [53, 14, 54],

$$\bar{\sigma}_{P,\text{res}}\left(z, M^2, \frac{M^2}{\mu_a^2}, \frac{M^2}{\mu_b^2}\right) = \frac{1}{2\pi i}\int_{C_{\text{MP}}-i\infty}^{C_{\text{MP}}+i\infty} dN\, z^{-N} \bar{\sigma}_{P,\text{res}}\left(N, M^2, \frac{M^2}{\mu_a^2}, \frac{M^2}{\mu_b^2}\right), \tag{3.61}$$

one opts for an integration path in the complex $N$ plane, chosen such that it passes to the left of the Landau pole and to the right of all other singularities of the integrand (see Fig. 3.2). Then, the Mellin inversion can be realized order by order in $\alpha_s(M^2)$. The slope of the path exhibited in the graphic can be varied in order to achieve numerical stability of the calculation. Of course, the final result has to be independent of the choice of slope, which has been shown in [53].
If an integration prescription has been found, one has to match the resummed hard scattering function to the fixed order calculation of interest. Usually, the NLL resummed result is matched to the NLO cross section, whereas NNLL contributions are added to a NNLO calculation in such a way that double-counting of logarithmic terms is avoided. Thus, one subtracts from the full resummed result its first orders in $\alpha_s$ up to the fixed calculation order:

$$\begin{aligned}\bar{\sigma}^{\text{N}^{\text{n}}\text{LO}}_{\text{N}^{\text{p}}\text{LL}}(z,\dots) = \alpha^k \alpha_s^m \Bigg[ &\sum_{j=0}^{n} \left(\frac{\alpha_s}{2\pi}\right)^j \bar{\sigma}_P^{(j)}(z,\dots) \\ &+ \frac{1}{2\pi i}\int_{C_{\text{MP}}-i\infty}^{C_{\text{MP}}+i\infty} dN\, z^{-N} \left[\bar{\sigma}_{\text{N}^{\text{p}}\text{LL}}(N,\dots) - \sum_{j=0}^{n}\left(\frac{\alpha_s}{2\pi}\right)^j \bar{\sigma}^{(j)}_{\text{N}^{\text{p}}\text{LL}}(N,\dots)\right]\Bigg].\end{aligned} \tag{3.62}$$

## 3.3. NNLO master formula for soft and virtual corrections

Expressions like Eq. (3.59), if kept general throughout the evaluation, can be used to find master formulæ for soft and virtual corrections at desired order for any hard $2 \to 2$ process. In the following, we will sketch the derivation of such a formula for NNLO corrections stemming from threshold resummation, as it was done in [12, 46, 55].

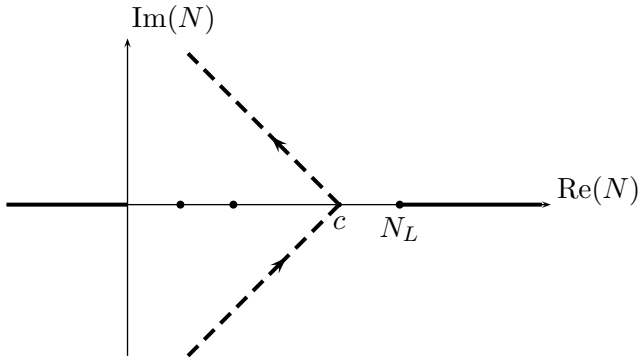


Figure 3.2: Integration path for the minimal prescription; the dots on the real axis indicate singularities, thick lines are evidence of a branch cut.

As we are interested in one-jet inclusive cross sections, we introduce a new threshold variable which is very suitable to describe this kind of kinematics:

$$s_4 = s + t + u, \tag{3.63}$$

where $t$ and $u$ are defined with respect to the momentum $p_J$ of the observed jet, measures the invariant mass of the system recoiling against the jet and thus becomes zero at threshold if all particle involved are massless. Analogously, we define its hadronic counterpart,

$$S_4 = S + T + U, \tag{3.64}$$

with the hadronic Mandelstam variables

$$S = \frac{s}{x_a x_b}, \qquad T = \frac{t}{x_a} \qquad \text{and} \qquad U = \frac{u}{x_b}, \tag{3.65}$$

which lead us directly to the relation

$$\begin{aligned} \frac{S_4}{S} &= -(1-x_a)\frac{u}{s} - (1-x_b)\frac{t}{s} + \frac{s_4}{s} \\ &\equiv w_a\left(\frac{-u}{M^2}\right) + w_b\left(\frac{-t}{M^2}\right) + (w_J + w_S)\,\frac{s}{M^2}. \end{aligned} \tag{3.66}$$

In the second line, we defined the weights $w_a$, $w_b$, $w_J$ and $w_S$ for later use, with $M^2$ being any hard scale of the process under consideration, e.g. the jet transverse momentum $p_T$. The plus distributions that have to be resummed then take the form

$$\mathcal{D}_l(s_4) = \left[\frac{\ln\left(\frac{s_4}{M^2}\right)}{s_4}\right]_+. \tag{3.67}$$

Their definition is

$$\int_0^{M^2} ds_4 \left[f(s_4)\right]_+ g(s_4) = \int_0^{M^2} ds_4 f(s_4)\left[g(s_4) - g(0)\right], \tag{3.68}$$

requiring a smooth function $g(s_4)$. Also, the transformation to moment space will change:

$$\tilde{f}(N) = \int_0^\infty \frac{ds_4}{s} e^{-N\frac{s_4}{s}} f(s_4). \tag{3.69}$$

With these ingredients, we can perform the transformation of the factorized partonic cross section with respect to the hadronic threshold variable $S_4$; using also the first line of Eq. (3.66), we obtain [45]

$$\begin{aligned}\int \frac{dS_4}{S} e^{N\frac{S_4}{S}} E_J \frac{d^3\hat{\sigma}_{ab\to cd}}{d^3p_J} = &\int dx_a e^{-N_a(1-x_a)\frac{M^2}{s}} \phi_{a/a}\left(x_a,\mu_a^2\right) \int dx_b e^{-N_b(1-x_b)\frac{M^2}{s}} \phi_{b/b}\left(x_b,\mu_b^2\right) \\ &\int \frac{ds_4}{s} e^{-N_j\frac{s_4}{s}\frac{M^2}{s}} E_J \frac{d^3\bar{\sigma}_{ab\to cd}}{d^3p_J}\left(s_4,s,\frac{s}{\mu_a^2},\frac{s}{\mu_b^2}\right) \\ \equiv &\,\phi_{a/a}\left(N_a,\mu_a^2\right)\phi_{b/b}\left(N_b,\mu_b^2\right) E_J \frac{d^3\bar{\sigma}_{ab\to cd}}{d^3p_J}\left(N_j,s,\frac{s}{\mu_a^2},\frac{s}{\mu_b^2}\right). \end{aligned} \tag{3.70}$$

Here, the $\phi_{i/i}$ are the parton-in-parton distributions analogous to Eq. (3.22), and we neglect again the parton mixing contributions which will become small in the large-$N$ limit for the reasons discussed in the previous section. Furthermore, we used $s$ as the hard scattering scale, and we introduced the moments

$$N_a \equiv \frac{-t_a}{M^2}N, \qquad N_b \equiv \frac{-t_b}{M^2}N, \qquad \text{and} \qquad N_j \equiv \frac{s}{M^2}N \tag{3.71}$$

with $t_a = u$ and $t_b = t$, which are characteristic for the underlying one-jet inclusive kinematics. The jet energy is refered to as $E_J$.
Alternatively, before performing the Mellin transform, one can refactorize the partonic cross section according to the weights we specified in Eq. (3.66). At fixed $S_4$, we find

$$\begin{aligned} E_J\frac{d^3\hat{\sigma}_{ab\to cd}}{d^3p_J} = &H\left(s,\frac{s}{\mu_a^2},\frac{s}{\mu_b^2}\right)\int dw_a dw_b dw_J dw_S\, \Psi_{a/a}\left(w_a,\frac{s}{\mu_a^2}\right)\Psi_{b/b}\left(w_b,\frac{s}{\mu_b^2}\right) \\ &\times\, J^{(c)}\left(w_J,s\right) J^{(d)}\left(w_J,s\right) S\left(\frac{w_S^2 s}{\mu_a^2},\frac{w_S^2 s}{\mu_b^2}\right) \\ &\times\, \delta\left(\frac{S_4}{S} - w_a\left(\frac{-u}{s}\right) - w_b\left(\frac{-t}{s}\right) - w_J - w_S\right). \end{aligned} \tag{3.72}$$

Note that from now on, we will omit the process-dependent index of $H$ and $S$ for the sake of clarity. The transition to Mellin space for the last expression is realized as follows:

$$\begin{aligned} \int \frac{dS_4}{S} e^{N\frac{S_4}{S}} E_J \frac{d^3\hat{\sigma}_{ab\to cd}}{d^3p_J} = &H\left(s,\frac{s}{\mu_a^2},\frac{s}{\mu_b^2}\right)\int dw_a e^{-w_a N_a}\Psi_{a/a}\left(w_a,\frac{s}{\mu_a^2}\right) \\ &\times \int dw_b e^{-w_b N_b}\Psi_{b/b}\left(w_b,\frac{s}{\mu_b^2}\right)\int dw_J e^{-w_J N_j} J^{(c)}\left(w_J,s\right) \\ &\times J^{(d)}\left(w_J,s\right)\int dw_S e^{-w_S N_j} S\left(\frac{w_S^2 s}{\mu_a^2},\frac{w_S^2 s}{\mu_b^2}\right) \\ \equiv &H\left(s,\frac{s}{\mu_a^2},\frac{s}{\mu_b^2}\right)\Psi_{a/a}\left(N_a,\frac{s}{\mu_a^2}\right)\Psi_{b/b}\left(N_b,\frac{s}{\mu_b^2}\right) \\ &\times J^{(c)}\left(N_j,s\right) J^{(d)}\left(N_j,s\right) S\left(\frac{s}{\tilde{N}_j^2\mu_a^2},\frac{s}{\tilde{N}_j^2\mu_b^2}\right), \end{aligned} \tag{3.73}$$

using $\tilde{N}_j = N_j e^{\gamma_E}$ as shorthand notation. The combination of Eqs. (3.70) and (3.73) then yields

$$E_J\frac{d^3\bar{\sigma}_{ab\to cd}}{d^3p_J}\left(N\right) = \frac{\Psi_{a/a}\left(N_a\right)\Psi_{b/b}\left(N_b\right)}{\phi_{a/a}\left(N_a\right)\phi_{b/b}\left(N_b\right)} J^{(c)}\left(N_j\right) J^{(d)}\left(N_j\right) H\, S\left(\frac{s}{\tilde{N}_j^2\mu_a^2},\frac{s}{\tilde{N}_j^2\mu_b^2}\right), \tag{3.74}$$

where we hid the factorization scale dependence in the arguments of all functions besides $S$. Exponentiation now works just as in the previous section. The parton distribution function are evaluated at the common scale $s$:

$$\frac{\Psi_{i/i}\left(N_i,1\right)}{\phi_{i/i}\left(N_i,s\right)} = R_i\left(\alpha_s\left(s\right)\right)\exp\left[\tilde{E}_i(N_i)\right] \tag{3.75}$$

and

$$\tilde{E}_i(N_i) = \int_0^1 dz\,\frac{z^{N_i-1}-1}{1-z}\left\{\int_s^{(1-z)^2 s}\frac{dq^2}{q^2}A_i\left(\alpha_s(q^2)\right) - \nu_i\left(\alpha_s\left((1-z)^2 s\right)\right)\right\} \tag{3.76}$$

in the $\overline{\text{MS}}$ scheme. $R_i$ is an $N$-independent function of the coupling and can at lowest order considered to be unity through normalization. Eq. (3.76) has to be evoluted to the factorization scale unless we want to set $\mu_i = s$ everywhere. The evolution of $\Psi_{i/i}$ and $\phi_{i/i}$ has already been specified in Eq. (3.32) and (3.33) and leads us to

$$\tilde{E}_i(N_i) = E_i(N_i) + \int_{\mu_i^2}^{s}\frac{dq^2}{q^2}\left[\frac{\alpha_s\left(q^2\right)}{2\pi}\gamma_i^{(1)} + \gamma'^{(2)}_{i/i}\left(\alpha_s\left(q^2\right)\right)\right] \tag{3.77}$$

$E_i(N_i)$ is obtained from Eq. (3.44) by replacing $M^2$ by $s$, whereas $\gamma'^{(2)}_{i/i}$ denotes the $N$-independent two-loop contributions of $\gamma_{i/i}$, which are given by Eqs. (3.34) and (3.35), respectively. The fact that we need only a part of both $\gamma_i$ and $\gamma_{i/i}$ is due to the specific form in which we cast our resummed cross sections. Since this leaves the integration in Eq. (3.77) independent of $N$, the corresponding term has been included in the hard function in Eq. (3.42) and did not show up explicitly there.

In [12], hard and soft function $H$ and $S$ are considered to be matrices in the space of colour exchanges, whose components in the following will be indicated by capital roman letters. The dimension of the matrices depends on the colour flow of the hard scattering process. We distinguish simple colour flow as in the direct photoproduction processes, in which at least one colourless particle is involved, and complex flow if the Born process is purely partonic. In the simple case, $H$, $S$ and $\Gamma_S$ reduce to $1\times 1$ matrices; the most complex case is $gg\to gg$, providing 8 colour dimensions.

The evolution of the soft matrix $S$ is fixed by the RGE [49]

$$\mu_R\frac{d}{d\mu_R}S_{KL} = -\Gamma^{\dagger}_{S,KM}S_{ML} - S_{KM}\Gamma_{S,ML}, \tag{3.78}$$

with $\Gamma_S$ now being the soft anomalous dimension matrix, which is calculated at one-loop order for all hard scattering processes of our interest in [56]. For the evolution of the soft matrix $S$ from $\frac{s}{N^2}$ to $s$ we find

$$\begin{aligned} S\left(\frac{s}{\tilde{N}_j^2\mu_a^2},\frac{s}{\tilde{N}_j^2\mu_b^2}\right) = \bar{P}\exp\left[\frac{1}{2}\int_s^{s/\tilde{N}_j^2}\frac{dq^2}{q^2}\,\Gamma_S'^{\,\dagger}\left(\alpha_s\left(q^2\right)\right)\right]\,\tilde{S}\left(\alpha_s\left(\frac{s}{\tilde{N}_j^2}\right)\right) \\ \times P\exp\left[\frac{1}{2}\int_s^{s/\tilde{N}_j}\frac{dq^2}{q^2}\,\Gamma'_S\left(\alpha_s\left(q^2\right)\right)\right]. \end{aligned} \tag{3.79}$$

We get $\Gamma'_S$ from $\Gamma_S$ by dropping gauge-dependent terms. This is allowed, since the gauge dependence has shown to cancel out in the final result. The symbol $P$ refers to path-ordering in the sense of the integration variable $q^2$ in the following exponential, i.e. $\Gamma'_S(s)$ is ordered to

the far right, whereas $\Gamma'_S\left(s/\tilde{N}_j^2\right)$ will end up on the far left. As one would expect, $\bar{P}$ denotes path-ordering in the opposite sense. Path-ordering can be omitted if the $\Gamma'_S$ are diagonalized, which, however, in the case of complex colour flow can be very complicated.
If we rewrite the hard matrix according to its renormalization properties as

$$H\left(\alpha_s\left(s\right)\right) = H\left(\alpha_s(\mu_R^2)\right) \exp\left[d_{\alpha_s} \int_{\mu_R^2}^{s} \frac{dq^2}{q^2} \beta\left(\alpha_s(q^2)\right)\right], \tag{3.80}$$

where $d_{\alpha_s}$ counts the number of QCD vertices in the underlying hard scattering process and is equal to $m$ in Eq. (3.30), we can unite our previous results to [12]

$$\begin{aligned}
\bar{\sigma}^{\mathrm{res}}(N) = &\exp\left[\sum_i E_i(N_i)\right] \exp\left[\sum_j E'_j(N_j)\right] \\
&\times \exp\left[\sum_i \int_{\mu_i^2}^{s} \frac{dq^2}{q^2}\left(\frac{\alpha_s(q^2)}{2\pi}\gamma_i^{(1)} + \gamma'_{i/i}\left(\alpha_s(q^2)\right)\right)\right] \exp\left[d_{\alpha_s}\int_{\mu_R^2}^{s}\frac{q^2}{q^2}\beta\left(\alpha_s(q^2)\right)\right] \\
&\times \mathrm{Tr}\left\{\mathrm{H}\left(\alpha_{\mathrm{s}}(\mu_{\mathrm{R}}^2)\right)\, \bar{\mathrm{P}} \exp\left[\int_{\mathrm{s}}^{\mathrm{s}/\tilde{\mathrm{N}}_{\mathrm{j}}^2} \frac{\mathrm{dq}^2}{\mathrm{q}^2}\, \Gamma_{\mathrm{S}}'^{\,\dagger}\left(\alpha_{\mathrm{s}}(\mathrm{q}^2)\right)\right] \tilde{\mathrm{S}}\left(\alpha_{\mathrm{s}}\left(\frac{\mathrm{s}}{\tilde{\mathrm{N}}_{\mathrm{j}}^2}\right)\right)\right. \\
&\left.\times P\exp\left[\int_s^{s/\tilde{N}_j} \frac{dq^2}{q^2}\,\Gamma'_S\left(\alpha_s(q^2)\right)\right]\right\},
\end{aligned} \tag{3.81}$$

which is the complete expression for the resummed cross section. Here, $E'_j(N_j)$ is the same as in Eq. (3.45) after exchanging $M^2$ for $s$, and the trace is supposed to be taken in colour space.
The expansion of Eq. (3.81) finally yields the desired master formulæ. At NLO, the soft and virtual corrections from threshold resummation are given by

$$\bar{\sigma}^{(1)}_{ab\to cd} = \sigma^B_{ab\to cd} \frac{\alpha_s\left(\mu_R^2\right)}{\pi}\left\{c_3\mathcal{D}_1\left(s_4\right) + c_2\mathcal{D}_0\left(s_4\right) + c_1\delta\left(s_4\right)\right\} \tag{3.82}$$

and

$$\bar{\sigma}^{(1)}_{ab\to cd} = \sigma^B_{ab\to cd} \frac{\alpha_s\left(\mu_R^2\right)}{\pi}\left\{c_3\mathcal{D}_1\left(s_4\right) + c_2\mathcal{D}_0\left(s_4\right) + c_1\delta\left(s_4\right)\right\} + \frac{\alpha_s^{d_{\alpha_s}+1}\left(\mu_R^2\right)}{\pi} A^c \mathcal{D}_0\left(s_4\right) \tag{3.83}$$

for simple and complex colour flow, respectively. While the $\mathcal{D}_l$ distributions have already been defined in Eq. (3.67), the newly introduced abbreviations are

$$c_3 = 2\sum_i C_{f,i} - \sum_j C_{f,j}, \tag{3.84}$$

where as always $i$ runs over initial and $j$ over final state massless partons,

$$\begin{aligned}
c_2 = 2\mathrm{Re}\left(\Gamma'^{(1)}_S\right) &- \sum_i \left[C_{f,i} + 2C_{f,i}\ln\left(\frac{-t_i}{M^2}\right) + C_{f,i}\ln\left(\frac{\mu_i^2}{s}\right)\right] \\
&- \sum_j \left[C_{f,j} + \frac{1}{2}B_j^{(1)} + C_{f,j}\ln\left(\frac{M^2}{s}\right)\right],
\end{aligned} \tag{3.85}$$

of which the first term is only needed for simple colour flow, in which $A^c$ is absent, and

$$c_1^\mu = \sum_i \left[C_{f,i}\ln\left(\frac{-t_i}{M^2}\right) - \frac{1}{2}\gamma_i^{(1)}\right] + d_{\alpha_s}\frac{\beta_0}{4}\ln\left(\frac{\mu_R^2}{s}\right). \tag{3.86}$$

Note that $c_1 = c_1^{\mu} + T_1$, with $T_1$ collecting all renormalization- and factorization-scale-independent terms from the full NLO virtual corrections, divided of course by the corresponding Born cross section; the latter is given by

$$\sigma^B = \mathrm{Tr}\left(H^{(0)} S^{(0)}\right), \tag{3.87}$$

analogous to Eq. (3.57). Lastly, we specify

$$A^c = \mathrm{Tr}\left(H^{(0)} {\Gamma'}_S^{(1)\dagger} S^{(0)} + H^{(0)} S^{(0)} {\Gamma'}_S^{(1)}\right). \tag{3.88}$$

These results are compared to the ones in [7] in the following section. For now, we will proceed to the NNLO formula, which is obtained from the expansion of Eq. (3.81) to order $\alpha_s^{d_{\alpha_s}+2}$ and matching to the full NLO soft plus virtual result. For simple colour flow, we find

$$\begin{aligned}
\bar{\sigma}^{(2)}_{ab\to cd} = {} & \frac{1}{2}c_3^2\,\mathcal{D}_3(s_4) + \left[\frac{3}{2}c_3\,c_2 - \frac{\beta_0}{4}c_3 + \sum_j C_{f_j}\frac{\beta_0}{8}\right]\mathcal{D}_2(s_4) \\
& + \Bigg\{ c_3\,c_1 + c_2^2 - \zeta_2\,c_3^2 - \frac{\beta_0}{2}T_2 + \frac{\beta_0}{4}c_3 \ln\left(\frac{\mu_R^2}{s}\right) + \sum_i C_{f,i}\,K \\
& \quad + \sum_j C_{f,j}\left[-\frac{K}{2} + \frac{\beta_0}{4}\ln\left(\frac{M^2}{s}\right)\right] - \sum_j \frac{\beta_0}{8}B_j^{(1)} \Bigg\}\mathcal{D}_1(s_4) \\
& + \Bigg\{ c_2\,c_1 - \zeta_2\,c_2\,c_3 + \zeta_3\,c_3^2 - \frac{\beta_0}{2}T_1 + \frac{\beta_0}{4}\,c_2 \ln\left(\frac{\mu_R^2}{s}\right) + 2\,\mathrm{Re}{\Gamma'}_S^{(2)} - \frac{1}{4}\sum_i \nu_i^{(2)} \\
& \quad + \sum_i C_{f,i}\left[\frac{\beta_0}{8}\ln^2\left(\frac{\mu_i^2}{s}\right) - \frac{K}{2}\ln\left(\frac{\mu_i^2}{s}\right) - K\,\ln\left(\frac{-t_i}{M^2}\right)\right] - \frac{1}{4}\sum_j\left(B_j^{(2)} + \nu_j^{(2)}\right) \\
& \quad + \sum_j C_{f,j}\left[\frac{\beta_0}{8}\ln^2\left(\frac{M^2}{s}\right) - \frac{K}{2}\ln\left(\frac{M^2}{s}\right)\right] - \sum_j \frac{\beta_0}{8}B_j^{(1)}\ln\left(\frac{M^2}{s}\right) \Bigg\}\mathcal{D}_0(s_4) \\
& + \Bigg\{ \frac{1}{2}c_1^2 - \frac{\zeta_2}{2}\,c_2^2 + \frac{1}{4}\zeta_2^2\,c_3^2 + \zeta_3\,c_3\,c_2 - \frac{3}{4}\zeta_4\,c_3^2 + \frac{\beta_0}{4}c_1\ln\left(\frac{\mu_R^2}{s}\right) + 2\,\mathrm{Re}{\Gamma'}_S^{(2)}\ln\left(\frac{M^2}{s}\right) \\
& \quad - \frac{\beta_0}{2}T_1\ln\left(\frac{M^2}{s}\right) + \frac{\beta_0}{4}T_2\ln^2\left(\frac{M^2}{s}\right) + \frac{d_{\alpha_s}}{16}\left[-\frac{\beta_0^2}{2}\ln^2\left(\frac{\mu_R^2}{s}\right) + \beta_1\ln\left(\frac{\mu_R^2}{s}\right)\right] \\
& \quad + \sum_i \frac{\beta_0}{16}\left[\gamma_i^{(1)} - 2C_{f,i}\ln\left(\frac{-t_i}{M^2}\right)\right]\ln^2\left(\frac{\mu_i^2}{s}\right) + \sum_i C_{f,i}\frac{K}{2}\ln\left(\frac{-t_i}{M^2}\right)\ln\left(\frac{\mu_i^2}{s}\right) \\
& \quad - \sum_i {\gamma'}_{i/i}^{(2)}\ln\left(\frac{\mu_i^2}{s}\right) + \sum_i C_{f,i}\left[\frac{\beta_0}{6}\ln^3\left(\frac{-t_i}{M^2}\right) + \left(\frac{\beta_0}{4} + \frac{K}{2}\right)\ln^2\left(\frac{-t_i}{M^2}\right)\right] \\
& \quad + \sum_i C_{f,i}\frac{\beta_0}{2}\ln\left(\frac{M^2}{s}\right)\left[\ln^2\left(\frac{-t_i}{M^2}\right) - \ln\left(\frac{-t_i}{M^2}\right)\ln\left(\frac{M^2}{s}\right) - \frac{1}{2}\ln\left(\frac{M^2}{s}\right) + \ln\left(\frac{-t_i}{M^2}\right)\right] \\
& \quad + \frac{1}{4}\sum_i \nu_i^{(2)}\ln\left(\frac{-t_i}{M^2}\right) - \frac{1}{4}\sum_j\left(B_j^{(2)} + \nu_j^{(2)}\right)\ln\left(\frac{M^2}{s}\right) \\
& \quad + \sum_j\left[\frac{\beta_0}{8}C_{f,j}\ln\left(\frac{M^2}{s}\right) - \frac{K}{4}C_{f,j} - \frac{\beta_0}{16}B_j^{(1)}\right]\ln^2\left(\frac{M^2}{s}\right) + R \Bigg\}\delta(s_4),
\end{aligned} \tag{3.89}$$

with $\zeta_4 = \frac{\pi^4}{96}$. The other two-loop functions are partly derived in [12].
In the case of complex color flow, we have

$$\begin{aligned}\bar{\sigma}^{(2)}_{ab\to cd} =& \bar{\sigma}^{(2)}_{\text{simple}} + \frac{\alpha_s^{d_{\alpha_s}+2}(\mu_R^2)}{\pi^2}\left\{\frac{3}{2}c_3\,A^c\,\mathcal{D}_2\left(s_4\right) + \left[\left(2c_2 - \frac{\beta_0}{2}\right)A^c + F\right]\mathcal{D}_1\left(s_4\right)\right.\\ &+ \left[\left(c_1 - \zeta_2 c_3 + \frac{\beta_0}{4}\ln\left(\frac{\mu_R^2}{s}\right)\right)A^c + F\ln\left(\frac{M^2}{s}\right) + G\right]\mathcal{D}_0\left(s_4\right)\\ &+ \left[(\zeta_3 c_3 - \zeta_2 c_2)A^c + \frac{1}{2}\left(\ln^2\left(\frac{M^2}{s}\right) - \zeta_2\right)F + \frac{\beta_0}{4}A^c\ln^2\left(\frac{M^2}{s}\right)\right.\\ &\left.\left.+ G\ln\left(\frac{M^2}{s}\right) + R^c\right]\delta\left(s_4\right)\right\},\end{aligned} \tag{3.90}$$

where we defined

$$F = \text{Tr}\left[H^{(0)}\left(\Gamma_S'^{(1)\,\dagger}\right)^2 S^{(0)} + H^{(0)}S^{(0)}\left(\Gamma_S'^{(1)}\right)^2 + 2H^{(0)}\Gamma_S'^{(1)\,\dagger}S^{(0)}\Gamma_S'^{(1)}\right], \tag{3.91}$$

$$\begin{aligned}G =& \text{Tr}\left(H^{(1)}\Gamma_S'^{(1)\,\dagger}S^{(0)} + H^{(1)}S^{(0)}\Gamma_S'^{(1)} + H^{(0)}\Gamma_S'^{(1)\,\dagger}S^{(1)} + H^{(0)}S^{(1)}\Gamma_S'^{(1)}\right.\\ &\left.+ H^{(0)}\Gamma_S'^{(2)\,\dagger}S^{(0)} + H^{(0)}S^{(0)}\Gamma_S'^{(2)}\right)\end{aligned} \tag{3.92}$$

and

$$R^c = \text{Tr}\left(H^{(2)}S^{(0)} + H^{(0)}S^{(2)} + H^{(1)}S^{(1)}\right) - \frac{1}{2}T_1^2. \tag{3.93}$$

After dropping all $\Gamma_S'$-dependent terms and $R$, $\bar{\sigma}^{(2)}_{\text{simple}}$ is obtained from Eq. (3.89). As mentioned before, the one-loop anomalous dimension matrices can be found in [56], the two-loop functions for $2 \to n$ processes then are simply related to these results by [57]

$$\Gamma_S'^{(2)} = \frac{K}{2}\Gamma_S'^{(1)}. \tag{3.94}$$

The higher order matrices of $H$ and $S$, however, are more difficult to find.
With the master formula whose derivation we sketched above, we can in principle calculate soft and virtual corrections at NNLO to any process of interest, and therefore also improve the calculations that have been done in [7]. As far as we know, these will be the first results on photoproduction beyond NLO. But before passing the border to NNLO, we compare in the last section of this chapter the outcome of Eqs. (3.82) and (3.83) with the corresponding terms in [7], in order to see if the different approaches applied lead to the same results.

## 3.4. Comparison of NLO results

The first step towards a reasonable comparison of the NLO corrections calculated by Klasen and Kramer [7] and the results obtained by the NLO master formula from the previous section is to perform a variable transformation, since the threshold variables to be integrated over are not the same in both cases. Whereas Kidonakis [12] uses $s_4$ as defined in Eq. (3.63), which becomes zero at threshold, the corresponding variable implemented in [7] is $z$ and closely related to the threshold variable in Secs. 3.1 and 3.2. However, if we want to stay in one-particle inclusive kinematics, we have to introduce two independent threshold variables $z_a$ and $z_b$ corresponding to the initial partons $a$ and $b$, as was done in Sec. 2.6. Therefore, the occurring plus distributions

will have a slightly different shape, which will also depend on to which initial particle they are assigned to.
We have in the prescription of Klasen and Kramer [7]

$$s_4 = s + t + u = 2p_a p_b - 2p_a p_1 - 2p_b p_1 = 2p_2 p_3 = -\frac{s'}{z_i}\frac{t_i'}{s'}(1 - z_i), \tag{3.95}$$

where the $t_i'$ for $i = a, b$ are specified below Eq. (3.71), and thus

$$ds_4 = t_i' \frac{dz_i}{z_i^2}. \tag{3.96}$$

Note that the Mandelstam variables $s'$, $t'$ and $u'$ are used here in the sense of [7] and also Sec. 2.3.2, where they are calculated "backwards", i.e. from jet transverse momenta and rapidities; for this reason, they are always defined within the hard $2 \to 2$ subprocess. They fulfill $s' + t' + u' = 0$ by definition, which is why we do not have $s_4 = s' + t' + u'$ in the present case. Nonetheless, at NLO at least one of $z_a$ and $z_b$ is equal to one, and it happens that the $t_i'$ here are just the same as the $t_i$ in the previous section. In general, we have

$$s = \frac{s'}{z_a z_b}, \qquad t = \frac{t'}{z_a} \qquad \text{and} \qquad u = \frac{u'}{z_b}, \tag{3.97}$$

whereas at threshold of course both variable sets match. At this point it should be mentioned that the Born cross section $\sigma_B$, whenever it appears in the formulæ of Sec. 3.3, should be evaluated at threshold or using the primed variables, even if the terms it is multiplied with are integrated.
If we introduce

$$u_a \equiv t = \frac{u_a'}{z_a}, \qquad u_b \equiv u = \frac{u_b'}{z_b} \tag{3.98}$$

the transformation of the $\mathcal{D}_l(s_4)$ can be written as follows:

$$\begin{aligned}
\int_0^{s_4^{\max}} ds_4\, \mathcal{D}_l(s_4) &\equiv \int_0^{s_4^{\max}} ds_4 \left[\frac{\ln^l\left(\frac{s_4}{p_T^2}\right)}{s_4}\right]_+ = \int_1^{x_i} t_i \frac{dz_i}{z_i^2}\left[\frac{z_i}{t_i(z_i-1)}\ln^l\left(\frac{-s}{u_i}\frac{1-z_i}{z_i}\right)\right]_+ \\
&= \int_{x_i}^1 \frac{dz_i}{z_i^2}\left[\frac{z_i}{(1-z_i)}\ln^l\left(\frac{-s}{u_i}\frac{1-z_i}{z_i}\right)\right]_+ \\
&= \int_{x_i}^1 \frac{dz_i}{z_i^2}\left\{\left[\frac{\ln^l\left(\frac{-s}{u_i}\frac{1-z_i}{z_i}\right)}{(1-z_i)}\right]_+ - \ln^l\left(\frac{-s}{u_i}\frac{1-z_i}{z_i}\right)\right\}.
\end{aligned} \tag{3.99}$$

Here, we took the definition of Eq. (3.67) and inserted $M^2 = p_T^2 = \frac{tu}{s} = \frac{t'u'}{s'}$, as is common for jet cross sections. Next, the delta function is rewritten as

$$\int_0^{s_4^{\max}} ds_4\, \delta(s_4) = \int_1^{x_i} t_i \frac{dz_i}{z_i^2}\frac{1}{|t_i|}\delta(1-z_i) = \int_{x_i}^1 \frac{dz_i}{z_i^2}\delta(1-z_i). \tag{3.100}$$

The upper integration bound $s_4^{\max}$ in principle should be $p_T^2$. For our purposes, we chose

$$s_4^{\max} \equiv t_i \frac{x_i - 1}{x_i}, \tag{3.101}$$

reproducing thereby the lower bound $x_i$ in [7], where it arises due to the fact that in the occurring integrals we have the convoluted particle distribution functions with argument $\frac{x_i}{z_i}$, which cannot become larger than 1 (see also the discussion in Sec. 2.6). This restriction, however, only affects the part of the distribution, in which the regularizing function is $z_i$-dependent. In particular, we have

$$\int_0^1 dz_i \, [f(z_i)]_+ g(z_i) = \int_{x_i}^1 dz \, f(z) F\left(\frac{x_i}{z_i}\right) - \int_0^1 dz \, f(z_i) F(x_i). \tag{3.102}$$

For numerical integration it is convenient to use $x_i$ and 1 as boundaries for both integrals in Eq. (3.102). The remaining part of the second integral,

$$\int_0^{x_i} dz \, f(z) F(x_i), \tag{3.103}$$

can be calculated analytically (e.g., using `Mathematica`) and is therefore treated separately. The explicit results for these extra-terms can be found in Appx. B.

### 3.4.1. Simple colour flow

Now, that we have fixed the transformation prescription, we can juxtapose the different results. We restrict ourselves at first to the case of direct photoproduction, where the expressions are less lengthy due to the fact that the colour factors $C_f$ in Eqs. (3.84)-(3.86) vanish for the colourless photon. Thus, Eq. (3.82) does not take into account contributions from the collinear splitting of a photon into a quark anti-quark pair, and the corresponding factorization scale $\mu_a$ will not appear in the formulæ. For the QCD Compton scattering process, the virtual corrections given by Klasen and Kramer [7] are

$$\bar{V}_{\gamma q \to g q}(s,t,u) = \sigma^B \frac{\alpha_S}{\pi} \left\{ C_F \left[ \frac{\pi^2}{3} - \frac{7}{2} + \frac{1}{2} \ln^2\left(\frac{t}{u}\right) \right] - N_C \left[ \frac{\pi^2}{12} + \frac{1}{4} \ln^2\left(\frac{t}{u}\right) \right] + \frac{\beta_0}{4} \ln\left(\frac{\mu_R^2}{s}\right) \right\} + \ldots, \tag{3.104}$$

stating here only the terms proportional to $\sigma^B$ (see Eq. (2.52)). In the NLO master formula, the virtual corrections correspond to the coefficient $c_1$, whose scale-dependent part for this specific process takes the form

$$c_{1,\gamma q}^{\mu} = -\left[ C_F \ln\left(\frac{-u}{s}\right) + \frac{3}{4} C_F \right] \ln\left(\frac{\mu_b^2}{s}\right) + \frac{\beta_0}{4} \ln\left(\frac{\mu_R^2}{s}\right). \tag{3.105}$$

$c_3$, $c_2$, $c_1^{\mu}$ and $A^c$ are given for all relevant processes in Appx. A. The scale-independent terms in Eq. (3.105), which are grouped in $T_1$, are not specified in [12] and have to be taken from an external full NLO calculation anyway. We see that the renormalization-scale-dependent term in Eq. (3.104) is reproduced, whereas the additional terms would be assigned to $T_1$ and therefore do not appear in Eq. (3.105). In the latter expression, also factorization-scale-dependent terms occur. They can partly be identified with delta contributions from the splitting functions, which

in [7] are included in the initial state corrections for the proton,

$$\begin{aligned}\bar{J}_{\gamma q\to gq}(s',t',u') = \int_{X_b}^1 \frac{dz_b}{z_b}\frac{\alpha_S}{\pi}\Bigg\{C_F\Bigg[2\left(\frac{\ln(1-z_b)}{1-z_b}\right)_+ + \left(\ln\left(\frac{-t'}{s'}\right) - \frac{1+z_b^2}{2}\ln\left(\frac{\mu_b^2}{s'}\right)\right)\\ \times\left(\frac{1}{1-z_b}\right)_+ - 2\left(\frac{\ln(z_b)}{1-z_b}\right)_+ + \delta(1-z_b)\left(\frac{1}{4}\ln^2\left(\frac{-t'}{s'}\right) + \frac{\pi^2}{2} - \frac{3}{4}\ln\left(\frac{\mu_b^2}{s'}\right)\right)\\ \frac{1-z_b}{2} - \frac{1}{2}\ln\left(\frac{-t'}{s'}\left(\frac{1-z_b}{z_b}\right)^2\right)\Bigg] - N_C\Bigg[\frac{1}{2}\ln\left(\frac{u'}{t'}\right) + \frac{1}{2}\ln\left(\frac{t'}{u'}\right)\left(\frac{1}{1-z_b}\right)_+\\ +\delta(1-z_b)\left(\frac{1}{8}\ln^2\left(\frac{-t'}{s'}\right) - \frac{1}{8}\ln^2\left(\frac{-u'}{s'}\right)\right)\Bigg]\Bigg\}\sigma^B + \dots. \end{aligned} \tag{3.106}$$

Here, only terms not including the phase space slicing cut parameter have been taken into account. Furthermore, parton mixing contributions have been neglected, as has been done for the derivation of the master formula. In the second line, at least one of the two factorization-scale-dependent terms of Eq. (3.105) is found. However, the missing part, which according to Kidonakis [12] is exclusively for one-particle-inclusive kinematics, is absent for all processes in [7].

By Eq. (3.106), we also gave all terms from QCD Compton scattering in [7] which are proportional to plus distributions. They should be compared to the expressions arising from the $c_3$ and $c_2$ coefficients in Eq. (3.82). For the process under consideration, we find

$$\begin{aligned}\int ds_4\, c_{3,\gamma q}\,\mathcal{D}_1(s_4) = \int_{X_b}^1 \frac{dz_b}{z_b^2}(C_F - N_C)\Bigg\{\left(\frac{\ln(1-z_b)}{1-z_b}\right)_+ - \left(\frac{\ln(z_b)}{1-z_b}\right)_+\\ - \ln\left(\frac{-u'}{s'}\right)\left(\frac{1}{1-z_b}\right)_+ - \ln\left(\frac{-u'}{s'}\frac{1-z_b}{z_b}\right)\Bigg\}\end{aligned} \tag{3.107}$$

and

$$\begin{aligned}\int ds_4\, c_{2,\gamma q}\,\mathcal{D}_0(s_4) = \int_{X_b}^1 \frac{dz_b}{z_b^2}\Bigg[-C_F\ln\left(\frac{\mu_b^2}{s'}\right) + 4C_F\ln\left(\frac{-u'}{s'}\right) - \frac{3}{4}C_F - \frac{\beta_0}{4}\\ +N_C\ln\left(\frac{t'}{u'}\right) - (C_F+N_C)\ln\left(\frac{t'u'}{s'^2}\right) - 2C_F\ln(z_b)\Bigg]\left\{\left(\frac{1}{1-z_b}\right)_+ - 1\right\}.\end{aligned} \tag{3.108}$$

As becomes obvious in this form, the leading logarithms do not coincide. If we exchange $t'$ and $u'$ in Eq. (3.107) and (3.108), several of the subleading distribution terms in Eq. (3.106) are reproduced apart from a factor $\frac{1}{2}$. Interestingly, all (quasi)matching contributions in Eq. (3.108) stem from the $2\mathrm{Re}(\Gamma'_S)$ part in Eq. (3.85). Note that in our numerical calculations we will not distinguish between the primed and unprimed Mandelstam variables so that the final $\ln(z_i)$ term in $c_2$ will be omitted.

The observations made while comparing the different results for the boson gluon fusion process are basically the same: At LL level the different outcomes do not match, at subleading level a part of the terms can be identified, which again are linked to $\Gamma'_S$ and miss a factor of $\frac{1}{2}$. Also, $c_1^\mu$ is reproduced in parts just as in the previous example. Nevertheless, it stays unclear how to treat the different powers of $z_b$ that stick to the differential.

### 3.4.2. Complex colour flow

Before closing this chapter, we will extend our comparison on the resolved processes. In particular, we will consider the scattering of two quarks which have different flavour. The fact that all partons involved are quarks, makes $c_3$, $c_2$ and $c_1$ symmetric in $a$ and $b$; an exception form the $t_i$,

which of course are different for $a$ and $b$, but which do not have an equivalent in the results of [7] anyway. There, correspondingly, the initial state corrections for the the resolved photon and the proton are the same functions in $z_a$ and $z_b$, respectively. Thus, we give the following expressions only for parton $a$, starting with

$$c^{\mu,a}_{1,qq'} = -C_F \left[\ln\left(\frac{-t}{s}\right) + \frac{3}{4}\right] \ln\left(\frac{\mu_a^2}{s}\right) + \frac{\beta_0}{4} \ln\left(\frac{\mu_R^2}{s}\right), \tag{3.109}$$

which again can be found in the virtual corrections (in the case of the last term) and as a delta term in the initial state corrections of [7]:

$$\begin{aligned}\bar{J}_{qq'\to qq'}(s',t',u') = \int_{X_a}^1 \frac{dz_a}{z_a}\frac{\alpha_S}{\pi} \Bigg\{ &(2C_F - N_C)\left[\frac{z_a}{2}\ln\left(\frac{t'u'}{s'^2}\right)\left(\frac{1}{1-z_a}\right)_+ + \frac{1}{8}\left(\ln^2\left(\frac{-t'}{s'}\right)\right.\right. \\ &\left.\left. + \ln^2\left(\frac{-u'}{s'}\right)\right)\delta(1-z_a)\right] + C_F\left[2\left(\frac{\ln(1-z_a)}{1-z_a}\right)_+ - 2\left(\frac{\ln(z_a)}{1-z_a}\right)_+ \right. \\ &+ \left(\ln\left(\frac{-u'}{s'}\right) - \frac{1+z_a^2}{2}\ln\left(\frac{\mu_a^2}{s'}\right)\right)\left(\frac{1}{1-z_a}\right)_+ + \left(-\frac{3}{4}\ln\left(\frac{\mu_a^2}{s'}\right)\right. \\ &\left.\left. + \frac{1}{4}\ln^2\left(\frac{-u'}{s'}\right) + \frac{\pi^2}{2}\right)\delta(1-z_a) - \ln\left(\frac{-u'}{s'}\left(\frac{1-z_a}{z_a}\right)^2\right) + 1 - z_a\right]\Bigg\}\sigma^B + \ldots,\end{aligned} \tag{3.110}$$

where cut-parameter-dependent contributions and those related to parton mixing have been omitted. The plus distributions in this equation are compared to

$$\begin{aligned}\int ds_4\, c^a_{3,qq'}\, \mathcal{D}_1(s_4) = \int_{X_a}^1 \frac{dz_a}{z_a^2} C_F \Bigg\{ &\left(\frac{\ln(1-z_a)}{1-z_a}\right)_+ - \left(\frac{\ln(z_a)}{1-z_a}\right)_+ \\ &- \ln\left(\frac{-t'}{s'}\right)\left(\frac{1}{1-z_a}\right)_+ - \ln\left(\frac{-t'}{s'}\frac{1-z_a}{z_a}\right)\Bigg\}\end{aligned} \tag{3.111}$$

and

$$\begin{aligned}\int ds_4 \left(c^a_{2,qq'} + \frac{A^c}{\sigma^B}\right)\mathcal{D}_0(s_4) = \int_{X_a}^1 \frac{dz_a}{z_a^2}\Bigg[&-C_F \ln\left(\frac{\mu_a^2}{s'}\right) - \frac{11}{4}C_F + 2C_F \ln\left(\frac{-u'}{s'}\right) \\ &- \frac{1}{N_C}\ln\left(\frac{t'u'}{s'^2}\right) + \left(C_F - \frac{1}{N_C}\right)\ln(z_a)\Bigg]\left\{\left(\frac{1}{1-z_a}\right)_+ - 1\right\}.\end{aligned} \tag{3.112}$$

Just as before, the expressions in Eqs. (3.110) and (3.111) do not coincide at LL level, although the difference in this case is merely a factor 2. The analogy to $2\mathrm{Re}(\Gamma'_S)$ in the simple colour flow is $A^c$ for the complex flow, as it provides additional $\mathcal{D}_0$ contributions. Since for this process, $A^c$ is also completely proportional to the Born cross section, it has been included in Eq. (3.112). Again, it are these terms, which can also be identified in Eq. (3.110) apart from the usual factor of $\frac{1}{2}$. This becomes visible after replacing $2C_F - N_C$ in latter equation by $-\frac{1}{N_C}$.
In spite of some open questions this comparison leaves us with, we used the expressions given through the NNLO master formulæ in Eqs. (3.89) and (3.90) to complement the NLO calculations from [7]. The results are presented in the following section.

# 4. Numerical implementation of the NNLO corrections

In this section, we will present the results of our NNLO calculations for direct and resolved photoproduction, compare them to experimental data and see how the higher order contributions affect the scale dependence of the calculated cross sections. First, we will comment on the approach we have chosen for implementing the expressions from the previous section.

## 4.1. Matching the master formula with the NLO code

The basis for our calculation was the `FORTRAN` code by Klasen and Kramer [7], which already provides a full fixed order NLO calculation for electron-proton as well as for proton-proton collisions. It uses Monte Carlo integrations, which are realized with a `VEGAS` routine.
In order to extend the code with NNLO contributions, the following tasks had to be accomplished:

- All quantities appearing in Eqs. (3.89) and (3.90) had to be identified for each process of Sec. 2.3.2.
- The integration variables had to be aligned in order to be able to incorporate the additional contributions into the existing integrations.
- The NNLO corrections had to be separated according to their relation to one of the initial state particles, so each contribution could be integrated separately.

The first task could be solved only partly. Whereas a lot of the different coefficients and functions are already given in [12], the two-loop functions $B_j^{(2)}$ and $\nu_i^{(2)}$ in particular are not completely specified and not easy to find in literature. In the case of complex colour flow, we also lack the knowledge of the higher order matrices of $H$, $S$ and $\Gamma'_S$, which are merely available at lowest order in [56] and allow only for the calculation of $A^c$ and $F$ in Eqs. (3.88) and (3.91). Especially the functions $G$ and $R^c$ as defined in Eqs. (3.92) and (3.93), respectively, could therefore not be evaluated. We have avoided this problem by only considering the scale-dependent terms of the master formula (i.e. those proportional to $\ln\left(\frac{\mu^2}{p_T}\right)$ with $\mu$ being either the factorization or the renormalization scale), all of which we can doubtlessly derive. More precisely, we have implemented the full contributions for the three highest logarithmic powers, since they are known entirely, and we have restricted ourselves to the scale-dependent part of the terms going with $\mathcal{D}_0(s_4)$ and $\delta(s_4)$. Although the delta terms had already been reduced and are in any case easy to treat when it comes to integration, they turned out to spoil the results by contributions which were far too large and which of course only appeared if the scales were set different from $p_T$. Although we are rather sure to have reproduced the terms correctly in the code and also compared our analytical results to the closely related case of photon production discussed in [58], the problem could not be fixed, which is why we are neglecting in our calculations also all expressions including $\delta(s_4)$. Unfortunately, this means that we are missing all NNLO virtual corrections.
The second and the third task to some degree refer to the same difficulty. In [12] we just have one threshold variable, $s_4$, which is not explicitly related to any of the particles involved in the process. Originally, there is only one factorization scale $\mu_F$ commonly defined for the initial partons $a$ and $b$. Klasen and Kramer, on the contrary, distinguish two different integration variables $z_a$ and $z_b$, as well as two different factorization scales $\mu_a$ and $\mu_b$. Concerning the scales, this problem is easily fixed; it has already been solved in the way we have stated the formula in the previous section. Whenever the factorization scale appears in Eqs. (3.89) and (3.90) it can uniquely be assigned to one of the particles $a$ and $b$. However, the issues with the integration variables are somewhat more involved. Their transformation into each other has been discussed in

Sec. 3.4. Yet the question remains, in which of the two $z$ $s_4$ should be transformed. It would not be right to integrate the entire corrections using just one of $z_a$ and $z_b$, as due to convolution both appear in the arguments of the corresponding and in general different parton densities. Hence, we have to split up the NNLO contributions and perform at least two separate integrations. The terms can be grouped into four different classes: First, we have the contributions that can be clearly assigned to either $a$ or $b$. They can easily be identified and stem from the sums with index $i$ in the master formula. In these cases, it is also very clear how the integration should be performed, and especially which integration should be carried out. The terms which are related to both or none of the two particles constitute the third and fourth class, respectively. Here, the matter becomes complicated. Physically, the situation is quite clear: At NNLO, in contrast to NLO, the emission of two gluons, possibly one from each initial particle, is allowed. Thus, we should actually assume that both $z_a$ and $z_b$ can simultaneously be different from unity, and both integrations should be carried out, which is not possible at NLO. From Eq. (3.97), we deduce

$$s_4 = \frac{s' + z_b t' + z_a u'}{z_a z_b} \tag{4.1}$$

for this general case. We see from this expression that it is no longer feasible to derive a reasonable transformation prescription for the integration over $s_4$. In particular, it remains unclear how the single integration can be replaced by a two-fold one.
In our search for a reasonable way to handle this problem we have tried several ways to distribute the new terms to the existing integrations. The simplest solution was to divide the complete NNLO contributions by two in order to integrate symmetrically over $z_a$ for one half and over $z_b$ for the other. The two factorization scales had to be distinguished within each integration.
Another possibility we have tested was to divide the different processes into two similar groups according to the different orders of the initial particles. For example, the contributions resulting from $qg \to qg$ would be integrated over $z_a$ using solely the factorization scale $\mu_a$, whereas $gq \to gq$ would be assigned to $z_b$ and $\mu_b$. The idea behind this is sketched in the following. For $qg \to qg$, at NLO, the initial state corrections to the s-channel diagram, neglecting parton mixing contributions, would be the ones depicted in Fig. 4.1 a) and b), whereas for $gq \to gq$, we would correspondingly have the diagrams c) and d). Diagram b) exhibits a gluon radiated

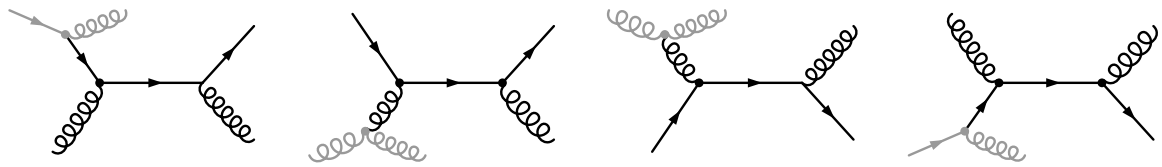

a) b) c) d)

Figure 4.1: Flavour-diagonal initial state corrections.

off initial particle $b$ and thus should be integrated over $z_b$ at the scale $\mu_b$. However, if we flip it over vertically, it equals diagram c), for which the reverse argument applies. If the flipping does not affect the calculation of the amplitude, which is definitely correct for the underlying Born amplitude, one could exchange the diagrams b) and c). Consequently, one would integrate $qg \to qg$ over $z_a$ and $gq \to gq$ over $z_b$, just as stated above. Of course, when trying to transfer this concept to NNLO amplitudes, we are faced with the old problem if we have radiation off both initial states.
The way we have finally dealt with these issues has been to really carry out the division of the contributions into the four classes and to assign one half of class three and four to the integrations

of each $z_a$ and $z_b$. For the direct photoproduction part, the purely photon-related terms vanish. Because here, the assignment of any terms of class three and four to the $z_a$ integration, and the consequent convolution of these terms with the photon density have led to absurdly high cross sections, we have finally used the $z_b$ integration for the complete direct contributions.
This whole approach is certainly not entirely correct, but we may take the reasonable results we are about to present as a justification for it. Further technical comments on the way of implementation are given in Appx. C.

## 4.2. Numerical results

As a first step, we demonstrate the reliability of our calculations by reproducing existing results. In [56], the threshold resummation formalism as presented in Sec. 3.3 has been applied to jet production and has been tested for $p\bar{p}$ collisions, which are investigated in the Tevatron storage ring at Fermilab in Chicago. The differential cross section has been evaluated at pure NLO and also in consideration of NNLO corrections for $\mu_R = \mu_a = \mu_b = \frac{1}{2}E_T$ and for all scales equal to $2E_T$. For our code, this task has been a check only of the part treating the resolved processes, since in this case both incoming particles are hadrons and no photons have to be taken into account. Our calculations using the NLO code of [7] and the new NNLO contributions have led to the results shown in Fig. 4.2, where we use the NLO curve at $\mu = \frac{1}{2}p_T$ as a reference and give the relative difference to that curve for the remaining outcomes. Note that we obtain a plot similar to the corresponding graphic in [56], in particular, that the corrections we have determined are of the same size, and that a similar sensitivity to scale variation can be observed at both orders.

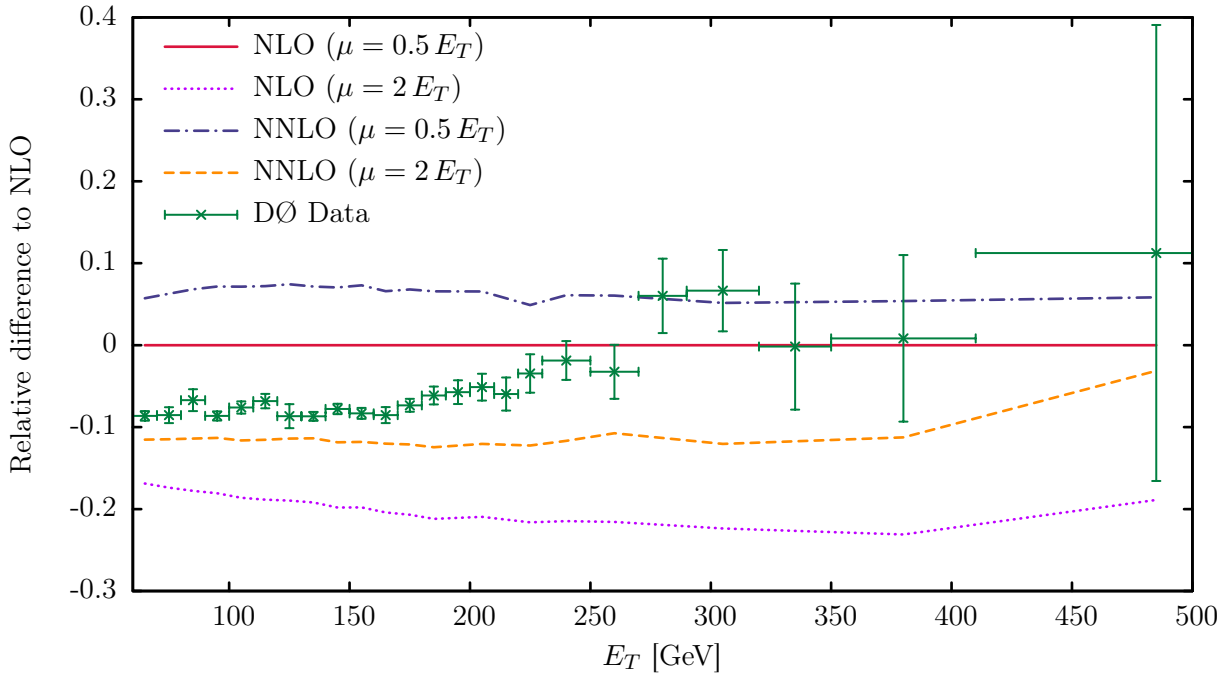


Figure 4.2: NLO and NNLO calculations for inclusive jet production in $p\bar{p}$ collisions at $\sqrt{S} = 1.8\,\text{TeV}$, $|\eta_{\text{jet}}| \leq 0.5$, compared to data from the DØ Collaboration [59].

As a further test, we have used our code to replicate the theoretical curves in an old publication on photoproduction of the H1 Collaboration at HERA [6], testing for a first time the direct photon part of the code. Here, we have restricted ourselves to the calculation of the differential cross section $\frac{d\sigma}{dE_T}$ in only one of the different kinematical ranges. In Fig. 4.3, we see that our LO and NLO results coincide with the ones in [6]. The NNLO contributions are new and yield a slight correction towards higher values for each data bin; thereby they amplify the tendency of the NLO curve, which already lies above the experimental data points throughout the considered transverse energy range. Thus, the agreement of data and theory has not been improved, but the corrections brought by our calculations are reasonably small and, as can be seen in Fig. 4.4, the scale dependence of the theoretical result has been reduced.

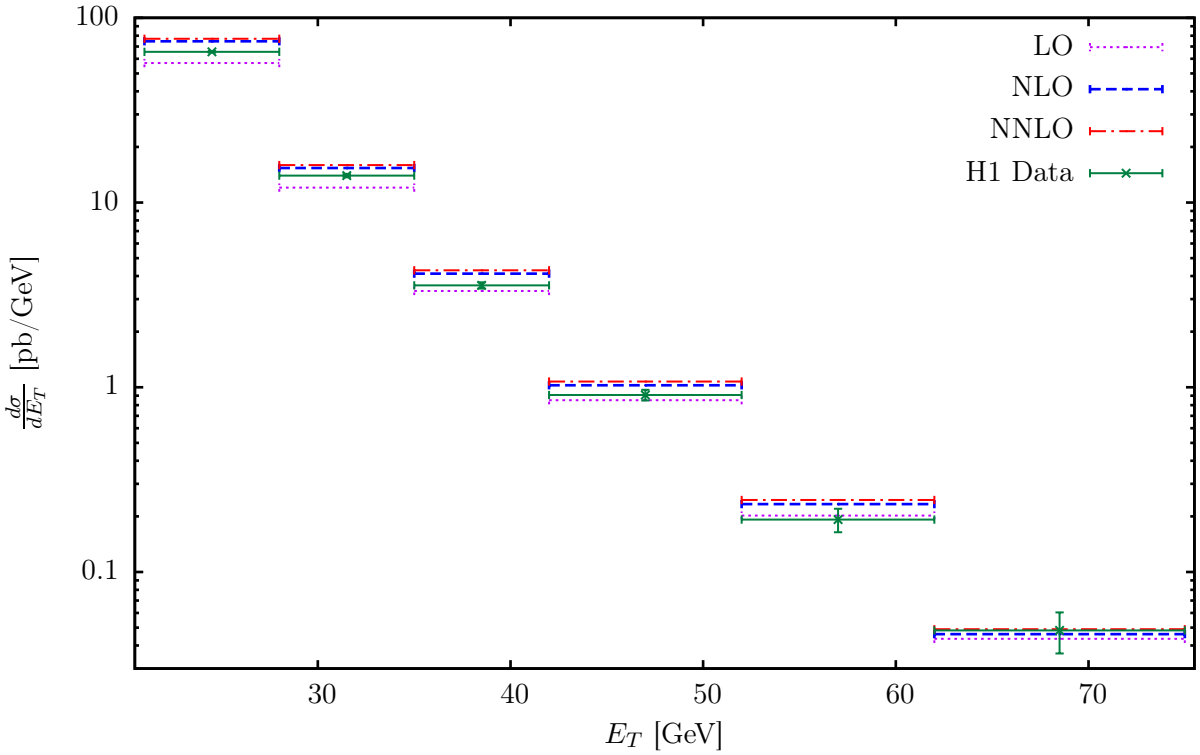


Figure 4.3: LO, NLO and NNLO calculations for the differential inclusive jet cross sections $\frac{d\sigma}{dE_T}$, with $\sqrt{S} = 300\,\text{GeV}$, $-1 \leq \eta_{\text{jet}} \leq 2.5$ and $95 \leq W_{\gamma p} \leq 285\,\text{GeV}$, compared to H1 results [6].

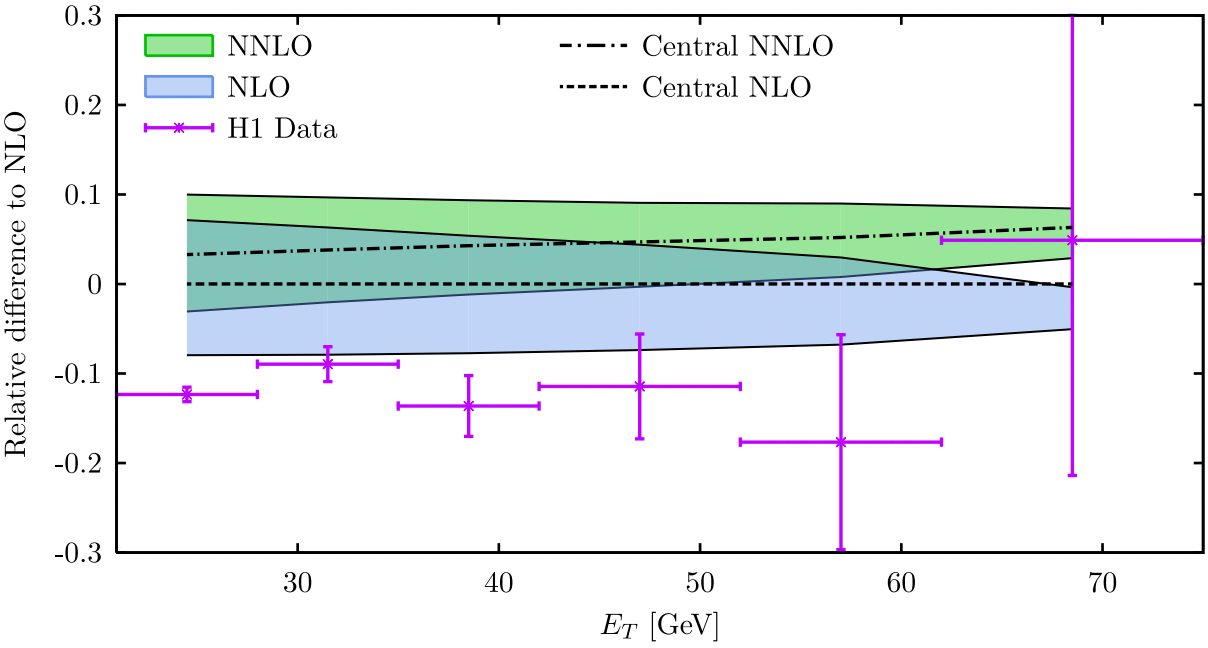


Figure 4.4: Relative difference of data points and NNLO calculations to the central NLO result for the cross section in Fig. 4.3. The bands display the theoretical uncertainty due to variation of both factorization scales and the renormalization scale.

This is expected to be so, since the scale dependence in our expressions is always a consequence of the truncation of the perturbative series at some finite order, i.e. it is an unphysical artefact. Thus, if we collected *all* scale-dependent terms up to infinite order, they ought to cancel out completely. At NNLO, we are already considering more of these scale-dependent contributions, so that the sensitivity of the result to scale variations should be reduced. Consequently, we expect the error band, which is spanned by the relative curves stemming from calculations at $\mu = \frac{1}{2}p_T$ for the upper bound and $\mu = 2p_T$ for the lower one, to be slenderer at NNLO. In Fig. 4.4, both error bands have about the same width, but note that the NNLO band would be narrower, if its two outer curves would be related to the central NNLO instead of the central NLO result. The central curve is evaluated at $\mu = p_T$, which sets all $\ln\left(\frac{\mu^2}{p_T^2}\right)$ equal to zero. One observes that the new terms change the NLO result constantly by around 5 percent.

Encouraged by these beginnings, we moved the focus of our interest on more recent photoproduction data published by the ZEUS collaboration only one year ago [3]. The theoretical NLO curves presented there have likewise been obtained using the code of Klasen and Kramer. Starting to replicate these results (see Fig. 4.5), we have encountered problems with the last data bin, where the theoretical prediction turned out to significantly underestimate the experimental value. In particular, the direct photon part of the cross section became negative in the high $p_T$ regime. This problem has been fixed by increasing the phase space slicing cut parameter, which we have finally set to 0.01. Nonetheless, the sum of direct and resolved contributions still lies well below the data point.
An improvement of these outcomes has been achieved by adding the NNLO contributions, which are depicted in Fig. 4.5 by the dash-dotted markers. The latter universally correct the NLO points to higher values of the differential cross section, thereby approaching the experimental results.
In Fig. 4.6, the scale dependences of the NLO and NNLO calculations are compared. For this plot, just as described for Fig. 4.4, we have set all scales to a common value, which has again been $\frac{1}{2}p_T$, $p_T$ and $2p_T$. While the NNLO error band displays is only slightly narrower at low transverse energies, this trend becomes clearer towards higher $p_T$. Furthermore, the data point in the lowest $p_T$ bin lies within the NNLO uncertainty. The size of the relative difference between the two central higher order results is about 3 percent in the low $p_T$ range and increases steadily up to about 6 percent for high tranverse momenta.
Having compared the differential cross section, we also take a look at the total photoproduction cross section, which is obtained after integrating over all bins in Fig. 4.5. Its value at different orders of perturbation theory is given in Fig. 4.7, where we have additionally tested the scale dependence by changing all scales from $\mu = \frac{1}{8}p_T$ up to $\mu = 8p_T$. As in the previous plots, it can be seen here that the NNLO corrections are considerably smaller than the NLO corrections. At the central scale, NLO and NNLO line are rather close together. If the scale-dependence is reduced, the NNLO curve should exhibit a flatter trend than its lower-order counterpart, eventually cutting it at lower values of $\mu$. However, such behaviour is not displayed by our results. In fact, the NNLO result appears to be more sensitive to scale variations for small $\mu$, whereas we observe at least a faint improvement at high scales, as the curves drift apart a little.
So far, we have modified the three different scales $\mu_R$, $\mu_a$ and $\mu_b$ simultaneously when evaluating the sensitivity of our results to scale variation, although in general they can be chosen independently. In order to gain a deeper insight into the behaviour of certain parts of the new corrections, and to discover possible errors in the code, it is interesting to do the same calculations as in Figs. 4.6 and 4.7 varying only one of the scales. The remaining two scales are set equal to $p_T$, which makes the corresponding logarithms vanish. The fact that the results presented earlier are not as insensitive to scale variation as expected can be related to either of the three different scales;

in the following we will check which terms are possibly spoiling the scale dependence.

The first dependence to be checked independently is the one on the renormalization scale, which finds its way into the calculation of $\alpha_s$ and is also present e.g. in the coefficient $c_1$. Its variation leads to the results depicted in Fig. 4.8. Obviously, the theoretical error increases once we move to NNLO, especially in the lower $p_T$ regime. This may to some extent reflect the problem we have discussed in Sec. 4, where we have stated that some of the NNLO terms are difficult to integrate within the framework provided by the code of [7]. The $\mu_R$-dependent contributions are part of the terms not directly related to any of the initial state particles, which we have heuristically divided into two equal halves. It seems that at this point, the latter simplification gets back on us. Therefore, it may be advisable to search for a better solution to handle the integration issues, which we have not been able to realize in the context of this project due to a lack of time. Interestingly, the scale-dependence of the total cross section shown in Fig. 4.9 does exhibit an improvement at lower scale by even cutting the NLO curve. However, at high scales, we observe a worsening in the trend of the curve at NNLO compared to the trend at NLO, which is probably owing to the reasons mentioned above.

Next, we have analyzed the performance of our calculations under the variation of the proton factorization scale. Fig. 4.10 displays the corresponding results for the differential cross sections. The central curves, needless to say, are the same as in Figs. 4.6 and 4.8, whereas the error bands in this case were obtained by changing only $\mu_b$. Here, we really achieved an improvement of the scale dependence. Also, more experimental data points are located inside the NNLO band than in the NLO error range. For small transverse momenta, however, both calculations fail to describe the increase exhibited by the data. Nevertheless, we take this result as evidence for the correctness of our calculations regarding the terms related to the proton initial state. Consequently, we also note in Fig. 4.11 an improved behaviour of the total photoproduction cross section under variation of $\mu_b$. The expected cutting of the NNLO and the NLO curve is indeed observed at low scales, and towards higher scales the trend of the NNLO line is also flattened. Note that the overall dependence on the proton factorization scale is considerably weaker than the dependence on the renormalization scale.

After these satisfactory results, the last scale dependence to be investigated separately is the one on $\mu_a$. For this case, the relative corrections to the differential cross section are given in Fig. 4.12. The error band embracing the central NNLO curve turns out to be significantly wider than the corresponding band at lower order; evidently, this is contrary to the effect we were hoping for, although the NNLO band covers most of the data points thanks to its larger extension. Having seen the results for the proton factorization scale, one might expect to see similarly good results for the photon scale, since according to the discussion on our approach in Sec. 4 both initial states have also been treated symmetrically when distributing the unrelated terms. But note that the symmetry only holds in the case of resolved photoproduction, and that in either case we have different parton distribution functions for the proton and the photon. From the direct photon part, we do not get any new contributions containing the photon factorization scale because all these terms vanish due to the colorlessness of the QED gauge boson. In the calculations of [7], there is a photon scale dependence caused by the $P_{\gamma\leftarrow q}$ in connection with collinear poles, which lead to contributions that are proportional to other Born matrix elements than the initial LO process. On the other hand, in the derivation of the NNLO master formula these cases are ruled out by dropping the flavour mixing contributions. This means that unlike the full NLO part, in which resolved and direct contributions complement each other, at NNLO we miss the direct photon part, which might cause a certain mismatch and spoil the photon scale

dependence as seen in the corresponding plots.
Consequently, we cannot observe the balancing of direct and resolved contributions, as it is demonstrated in Fig. 28 of [60] for NLO direct and LO resolved photoproduction, at a higher level. The NNLO direct corrections are $\mu_b$-independent, and also have turned out to be very small, so that after adding the NNLO contributions, the direct NLO curve in the graphic of [60] remains basically.

Having seen the influence of the different scales, we can conclude that in Figs. 4.6 and 4.7, where all the discussed effects are superposed due to the simultaneous variation of all scales, the slight improvements which can be seen are mainly related to the proton factorization scale, and are weakened by the negative influence of the other two scales.

Fig. 4.14 shows the cross section differential in the jet rapidity $\eta_{\text{jet}}$ for LO, NLO and NNLO calculations. The $W_{\gamma p}$ range is the same as in Fig. 4.5, and all jets with $E_T > 17\,\text{GeV}$ are taken into account. We observe that the NLO curve from [3] is again reproduced correctly, but fails to describe the experimental data especially in the higher rapidity range, i.e. in the forward direction, where the calculation predicts a considerably smaller cross section. The accordance of theory and experiment at high rapidities is significantly improved by adding the NNLO contributions, which account for comparatively large corrections especially in the high $\eta_{\text{jet}}$ regime. This is also true for the last two data bins in the backward direction, where the NNLO contributions shift the NLO result towards lower values. However, it still seems that the proton-related terms are implemented more accurately. The general discrepancy between theory and experiment in this low rapidity region emphasizes the need for an update of the photon structure function. It is also in these outer rapidity regions, where the sensitivity to scale variation is largest. Fig. 4.15 displays the theoretical error bands which were calculated with equal values for all scales. In contrast to the previous plots of this kind, the central NNLO curve does not exhibit the universal positive sign of the corrections, but reduces the NLO result in the low $\eta_{\text{jet}}$ region. Moreover, the absolute value of the NNLO corrections becomes highest where the differential cross section has its lowest values. On the contrary, the corrections become small in the rapidity range around $\eta_{\text{jet}} = 0$, where the differential cross section takes its maximum.
Comparing the width of the two error bands, we state that perpendicular to the beam axis the NNLO calculations are less scale-dependent, whereas in the forward direction, the NNLO band exceeds the NLO band in its broadness, as already mentioned. Nevertheless, one should keep in mind that in this outer region the central NNLO value for the cross section is about 8 percent higher than the result from the NLO calculation, so that the variation relative to the NNLO result will be a lot smaller.

The next graphic (Fig. 4.16) shows the differential cross section $\frac{d\sigma}{d\eta_{\text{jet}}}$ in the same rapidity range as the previous plots, but this time with a transverse energy cut at $E_T = 21\,\text{GeV}$. Since the majority of the jets has low transverse energy, a significant number of events is not detected. Consequently, the differential cross section we arrive at is much smaller. Apart from this fact, the observation we make regarding the trends of the curves in the $\eta_{\text{jet}}$ extremes, the size of the corrections, and the comparison of the scale dependence are mainly the same for Figs. 4.14 and 4.16 as well as for Figs. 4.15 and 4.17.

As a last application we have used our program to determine the best fitting value of the strong coupling constant $\alpha_s$. For this purpose, we have run our calculation with 13 different NNLO proton PDF sets by the CT10 collaboration [13] for values of $\alpha_s(M_Z)$ from 0.112 to 0.124. The corresponding results have been compared to the same ZEUS data mentioned above; for each

| $\alpha_s$ | $\mu = 0.125\,p_T$ | $\mu = 0.25\,p_T$ | $\mu = 0.5\,p_T$ | $\mu = p_T$ |
|---|---|---|---|---|
| 0.112 | 535 | 660 | 1527 | 2629 |
| 0.113 | 437 | 423 | 1171 | 2207 |
| 0.114 | 384 | 254 | 873 | 1834 |
| 0.115 | 394 | 135 | 606 | 1475 |
| 0.116 | 431 | 83 | 380 | 1132 |
| 0.117 | 513 | 107 | 222 | 850 |
| 0.118 | 629 | 203 | 125 | 615 |
| 0.119 | 782 | 382 | 87 | 420 |
| 0.120 | 965 | 656 | 120 | 263 |
| 0.121 | 1164 | 1009 | 224 | 166 |
| 0.122 | 1393 | 1440 | 401 | 123 |
| 0.123 | 1619 | 1960 | 654 | 133 |
| 0.124 | 1920 | 2612 | 1017 | 209 |

Table 4: Reduced $\chi^2$ for the fitting of NNLO calculations at different scales and values of $\alpha_s$ to recent ZEUS data [3].

PDF set we have evaluated the reduced $\chi^2$ at different scales $\mu = \mu_a = \mu_b = \mu_R$ and have obtained the values given in Tab. 4. According to these results, the best fitting is reached by setting all scales equal to $\frac{1}{4}p_T$, although the goodness achieved by choosing $\mu = \frac{1}{2}p_T$ is similar. We determine the value of the coupling constant to be

$$\alpha_s(M_Z) = 0.116 \pm 0.001\,{}^{+0.003}_{-0.002}.$$

The first uncertainty given here is the experimental one including the statistical and the systematic error, whereas the second error describes the theoretical uncertainty obtained from scale variation. Consequently, the world average of 0.118 lies within our uncertainty range. In [3], the determination of $\alpha_s$ has led to $\alpha_s(M_Z) = 0.1206\,{}^{+0.0023}_{-0.0022}(\text{exp.}){}^{+0.0042}_{-0.0035}(\text{th.})$, which does not match our result. Note that at least the error ranges overlap, and that the uncertainty of our result is smaller compared to the result of the ZEUS analysis.

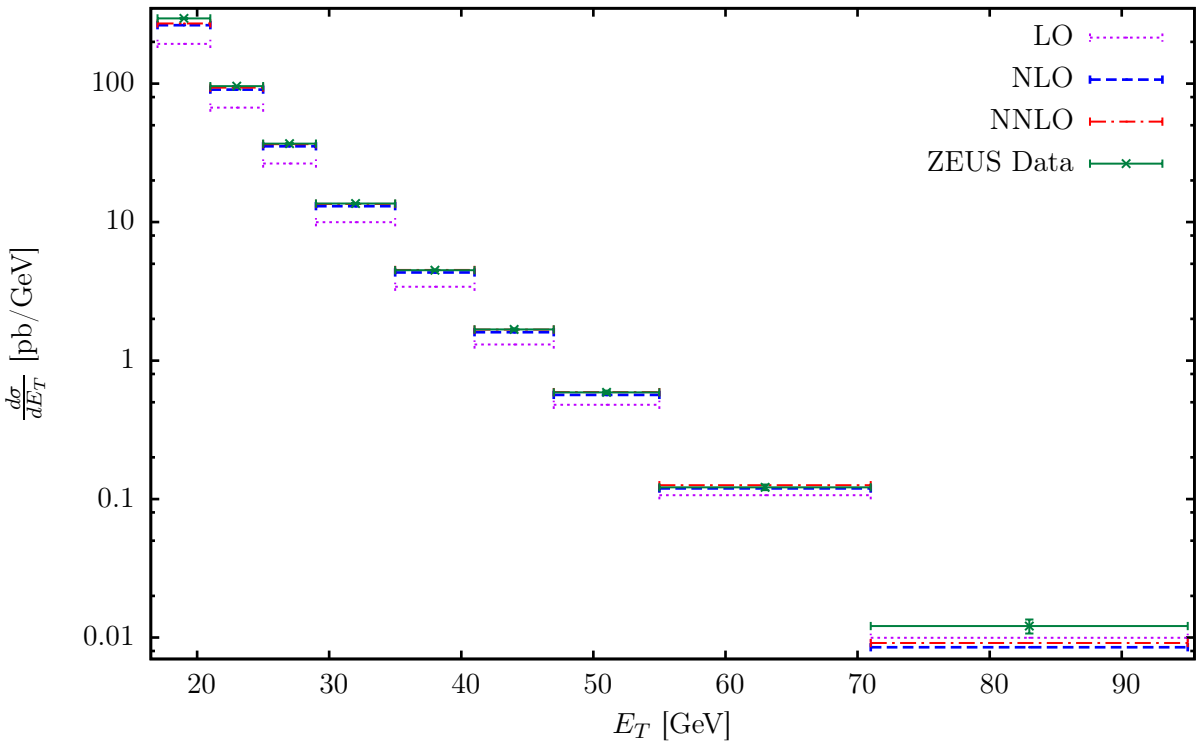


Figure 4.5: LO, NLO and NNLO calculations for the differential inclusive jet cross section $\frac{d\sigma}{dE_T}$, with $\sqrt{S} = 318\,\text{GeV}$, $-1 \leq \eta_{\text{jet}} \leq 2.5$ and $142 \leq W_{\gamma p} \leq 293\,\text{GeV}$, compared to the ZEUS results in [3].

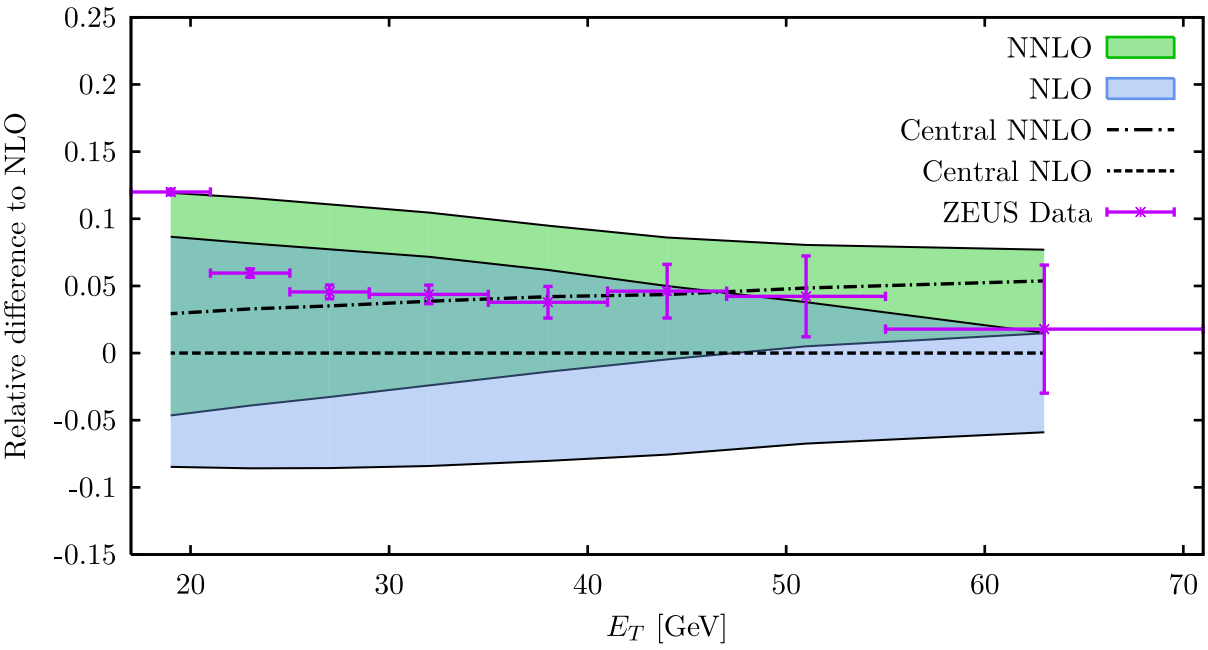


Figure 4.6: Relative difference of data points and NNLO calculations to the central NLO result for the cross section in Fig. 4.5. The bands display the theoretical uncertainty due to variation of both factorization scales and the renormalization scale.

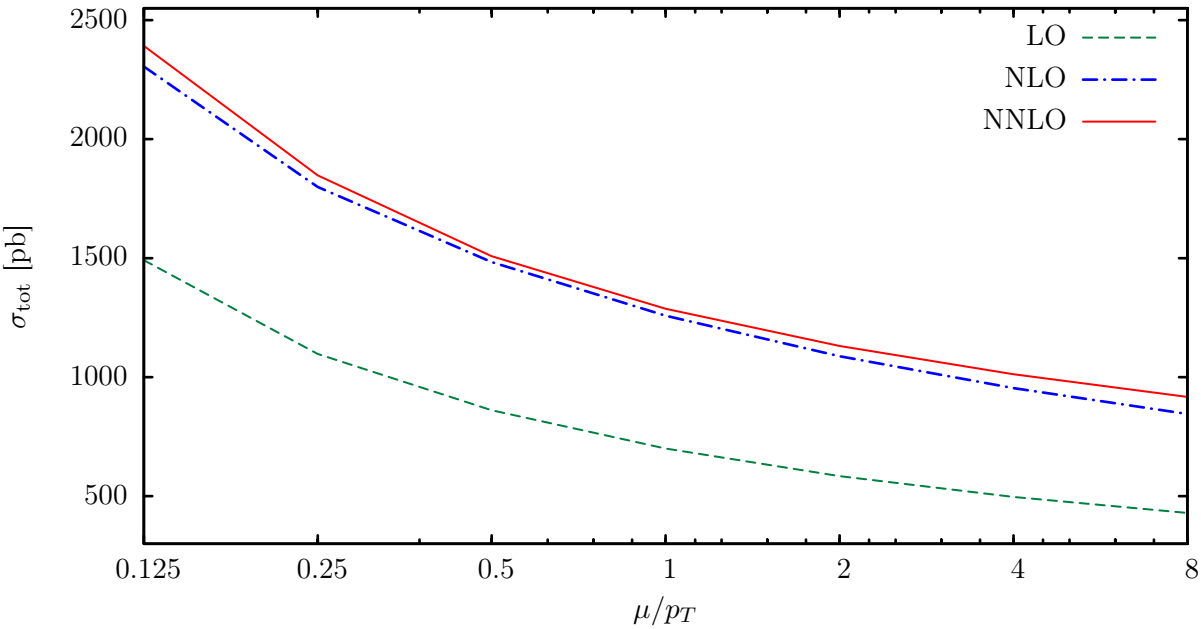


Figure 4.7: LO, NLO and NNLO calculations for the total inclusive jet cross section $\sigma_{\mathrm{tot}}$ with all kinematical parameters given in Fig. 4.5. Both factorization scales and the renormalization scale were set equal to $\mu$.

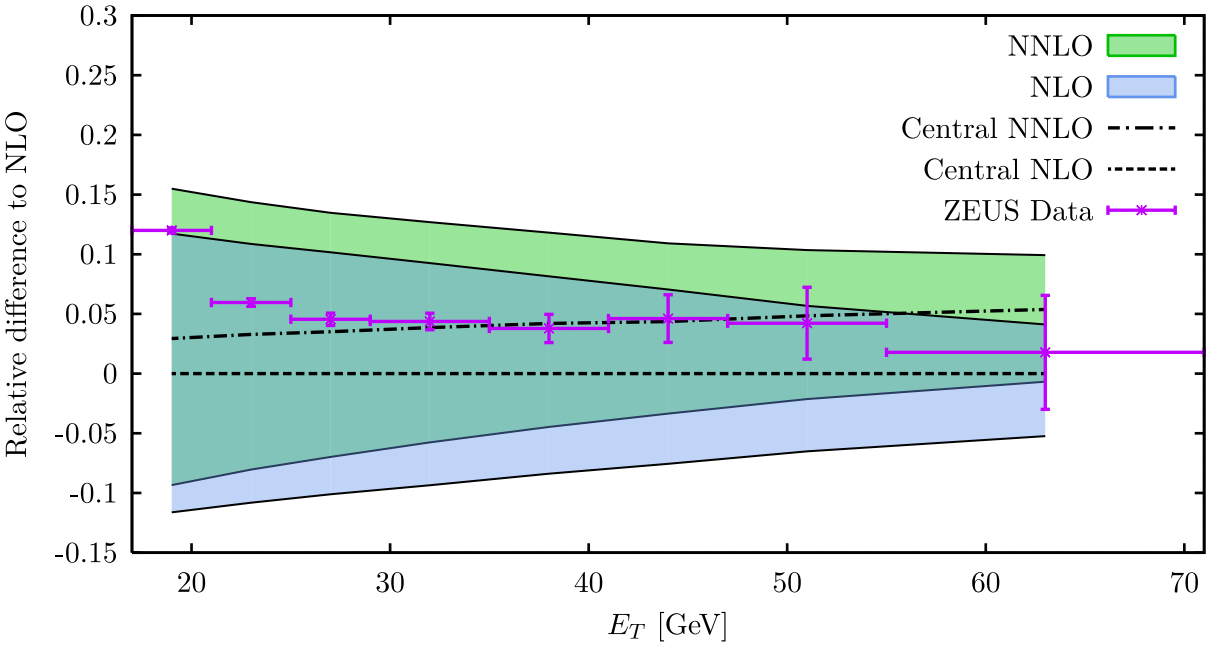


Figure 4.8: Relative difference of data points and NNLO calculations to the central NLO result for the cross section in Fig. 4.5. The bands display the theoretical uncertainty due to variation of the renormalization scale.

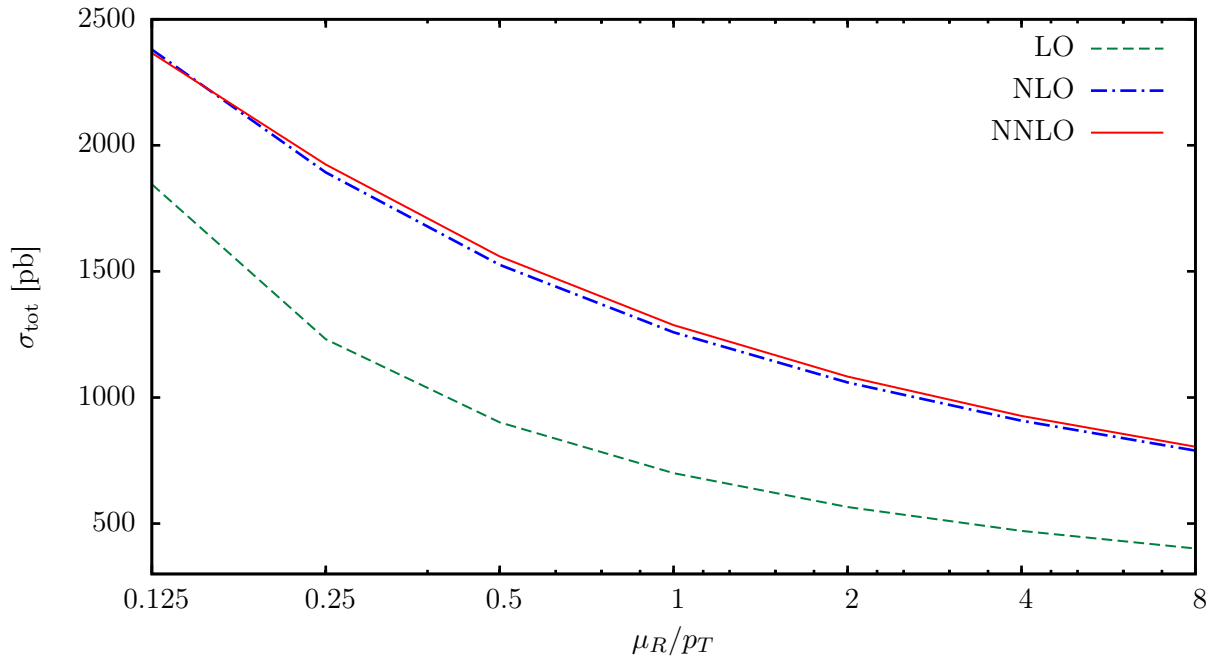


Figure 4.9: LO, NLO and NNLO calculations for the total inclusive jet cross section $\sigma_{\text{tot}}$ for different values of the renormalization scale. All kinematical parameters are given in Fig. 4.5.

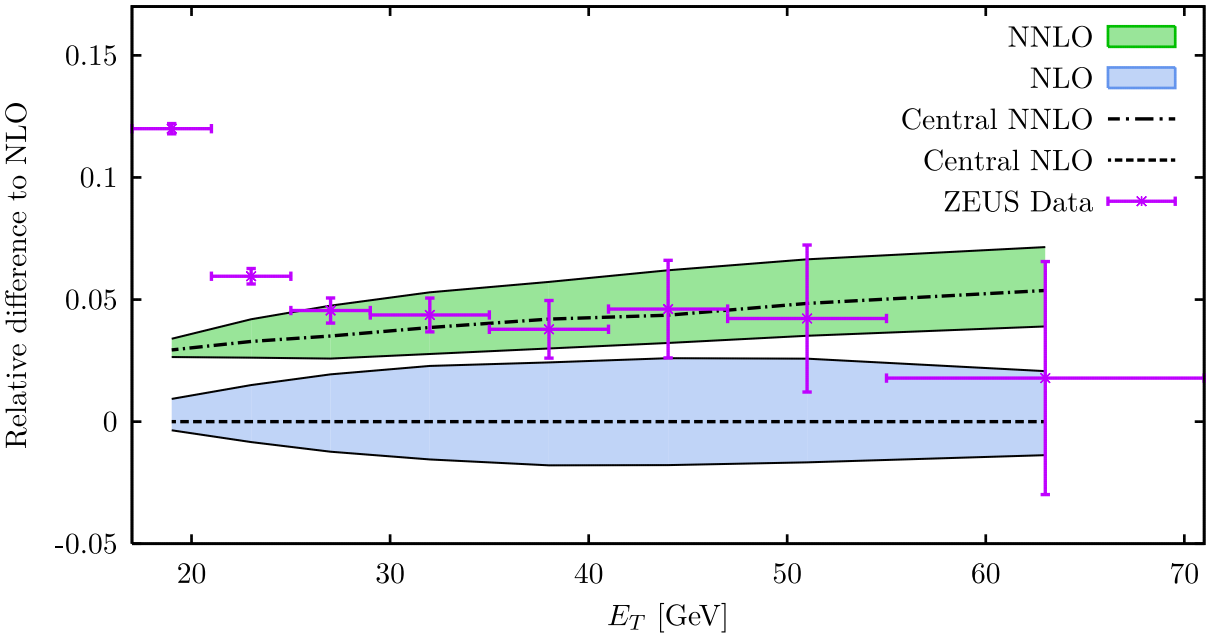


Figure 4.10: Relative difference of data points and NNLO calculations to the central NLO result for the cross section in Fig. 4.5. The theoretical error band was obtained by varying the proton factorization scale.

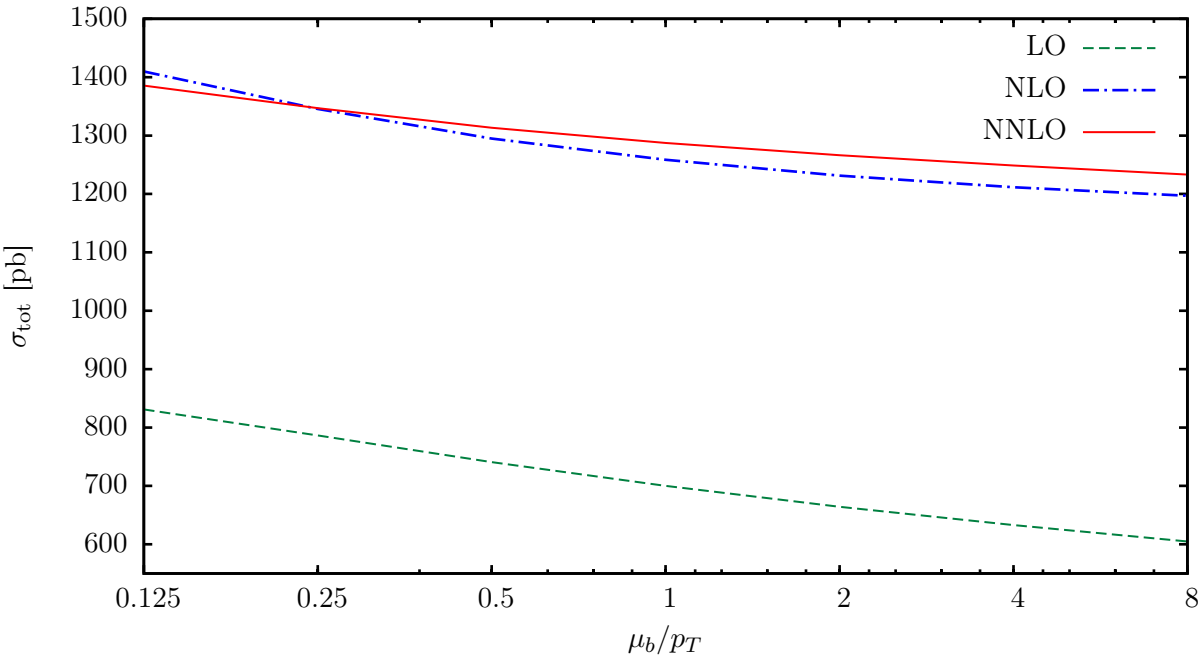


Figure 4.11: LO, NLO and NNLO calculations for the total inclusive jet cross section $\sigma_{\text{tot}}$ for different values of the proton factorization scale. All kinematical parameters are given in Fig. 4.5.

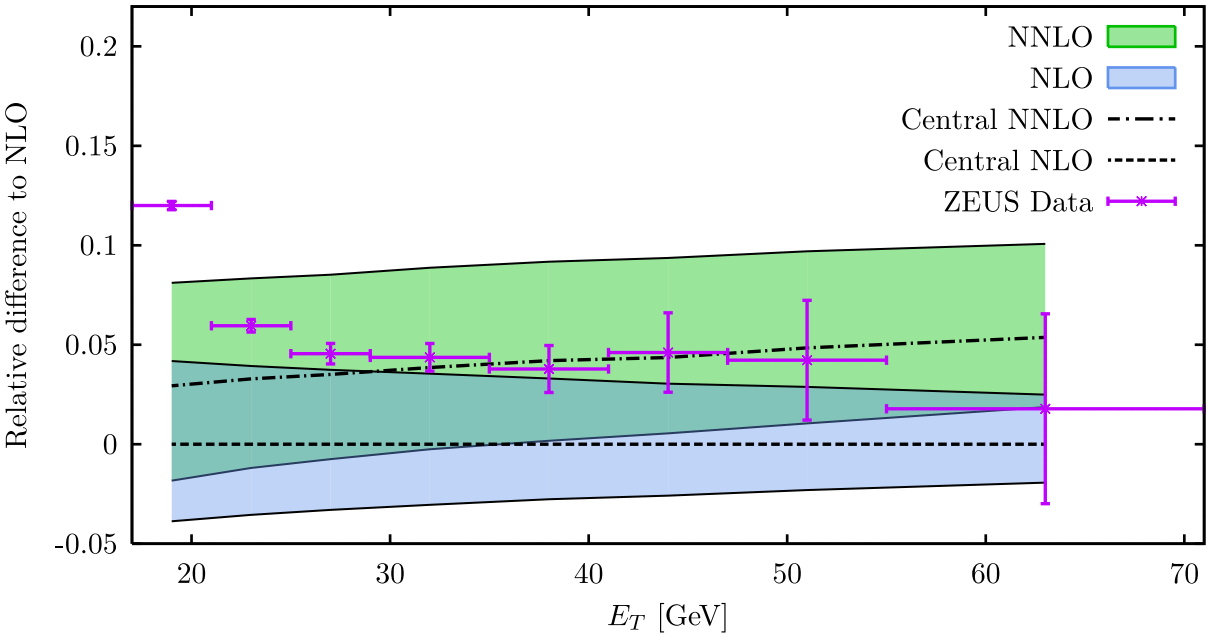


Figure 4.12: Relative difference of data points and NNLO calculations to the central NLO result for the cross section in Fig. 4.5. The theoretical error band was obtained by varying the photon factorization scale.

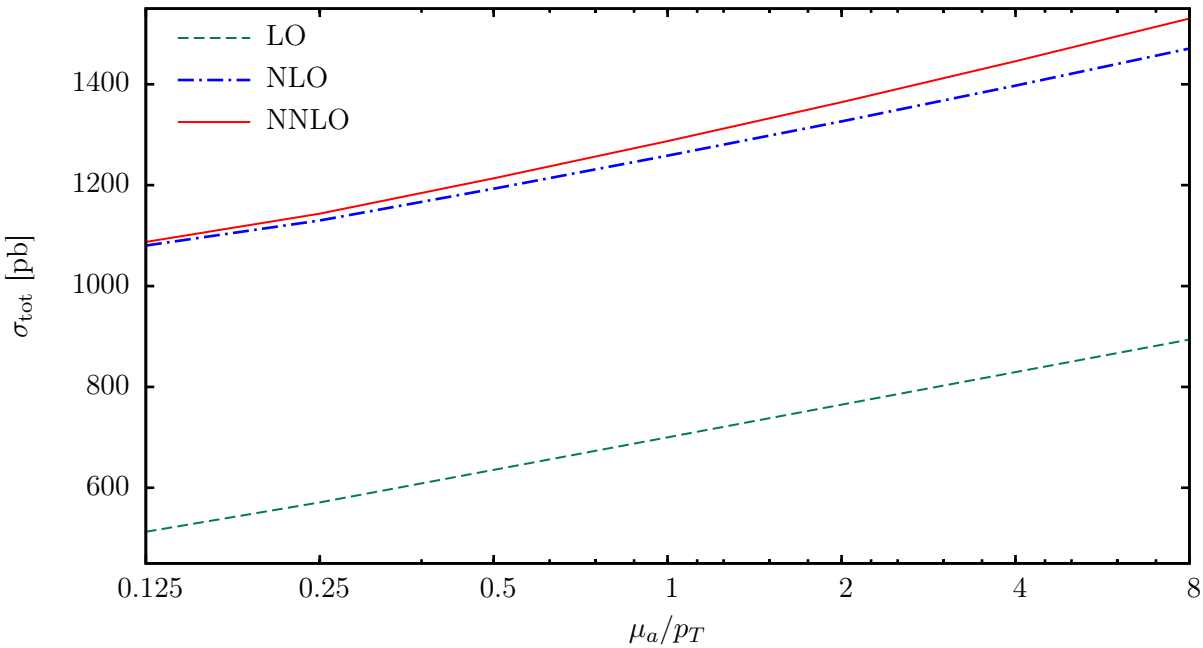


Figure 4.13: LO, NLO and NNLO calculations for the total inclusive jet cross section $\sigma_{\text{tot}}$ for different values of the photon factorization scale. All kinematical parameters are given in Fig. 4.5.

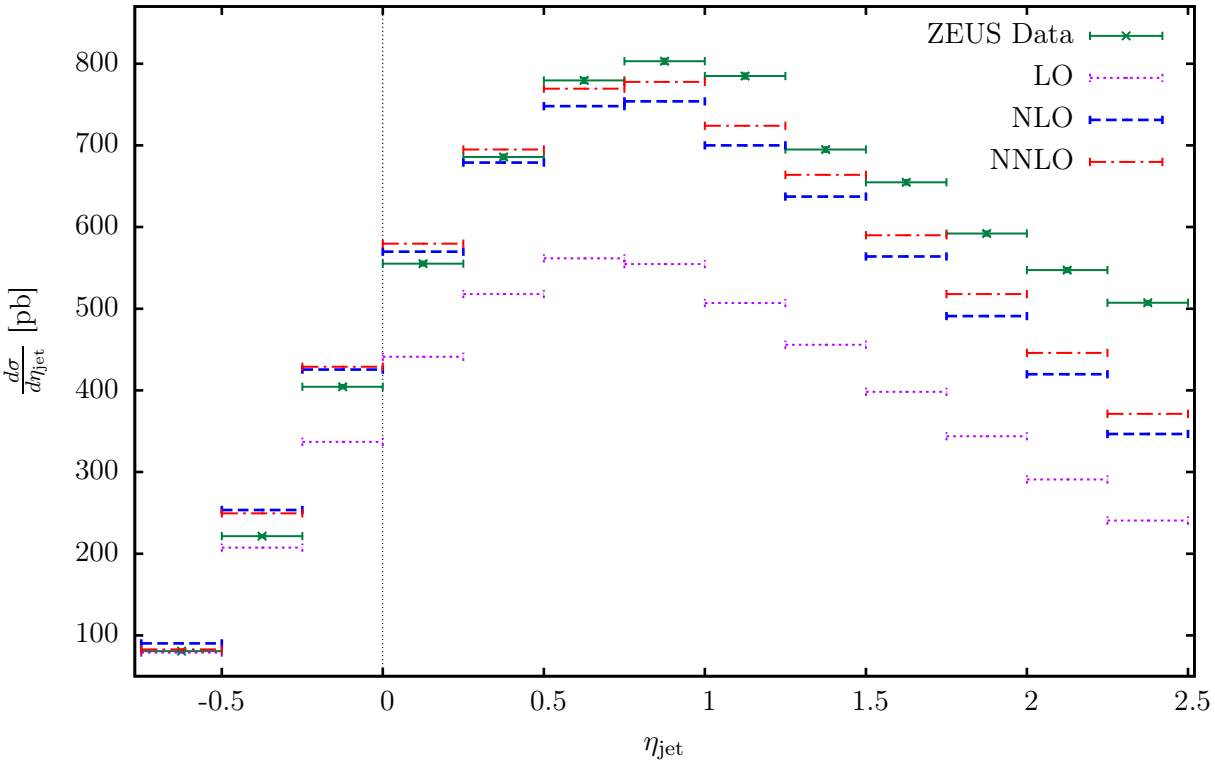


Figure 4.14: LO, NLO and NNLO calculations for the differential inclusive jet cross section $\frac{d\sigma}{d\eta_{\text{jet}}}$ with $\sqrt{S} = 318\,\text{GeV}$, $E_T > 17\,\text{GeV}$ and $142 \leq W_{\gamma p} \leq 293\,\text{GeV}$, compared to the ZEUS results in [3].

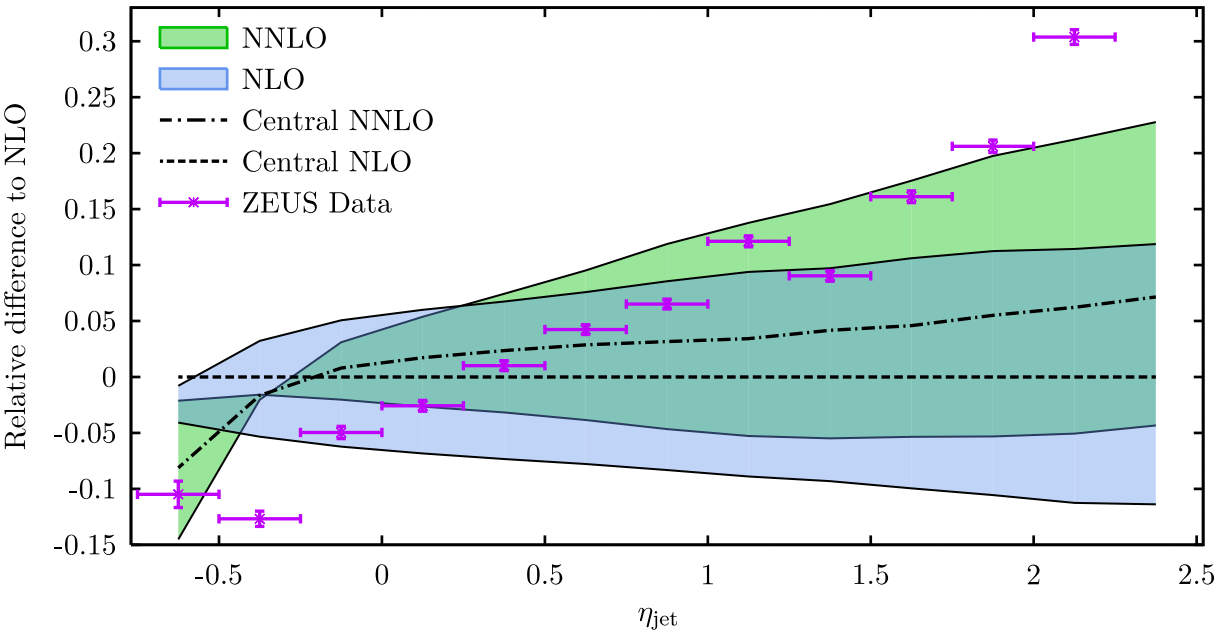


Figure 4.15: Relative difference of data points and NNLO calculations to the central NLO result for the cross section in Fig. 4.14. The bands display the theoretical uncertainty due to the variation of both factorization scales and the renormalization scale.

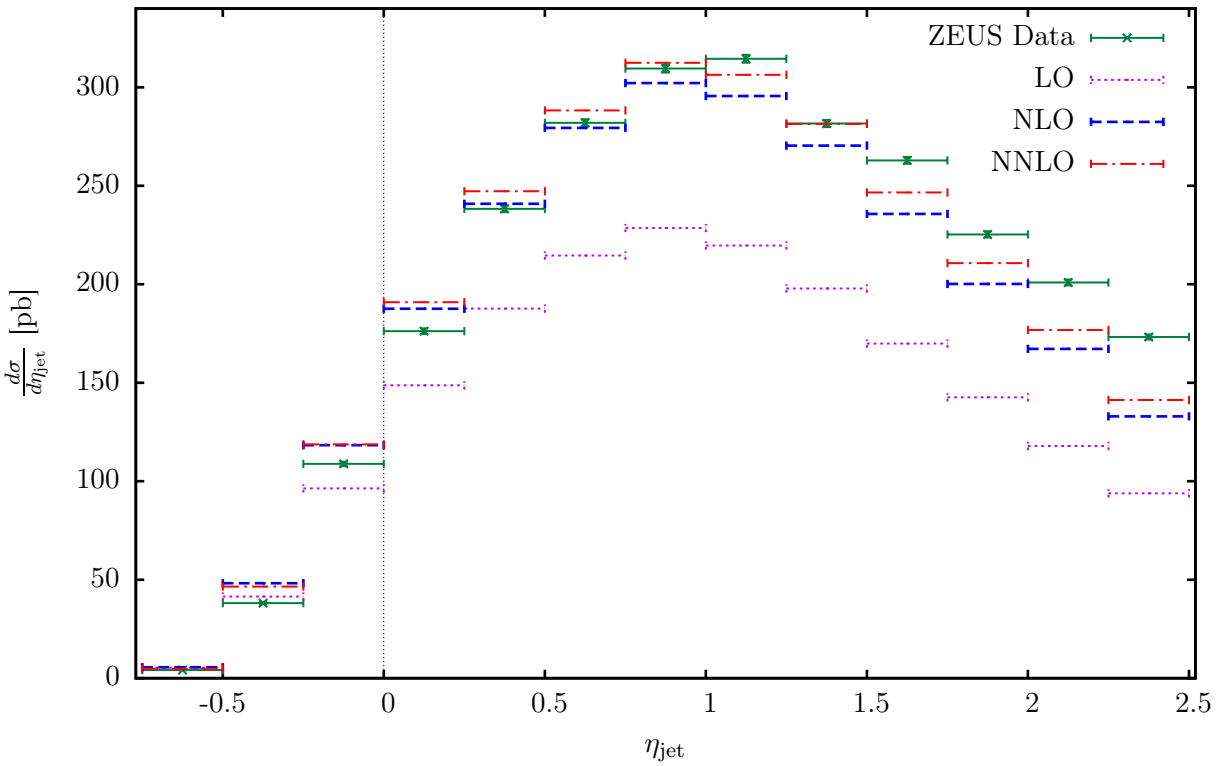


Figure 4.16: LO, NLO and NNLO results for the total jet cross section $\sigma_{\rm tot}$ with $\sqrt{S} = 318\,\text{GeV}$, $E_T > 21\,\text{GeV}$ and $142 \leq W_{\gamma p} \leq 293\,\text{GeV}$, compared to the ZEUS results in [3].

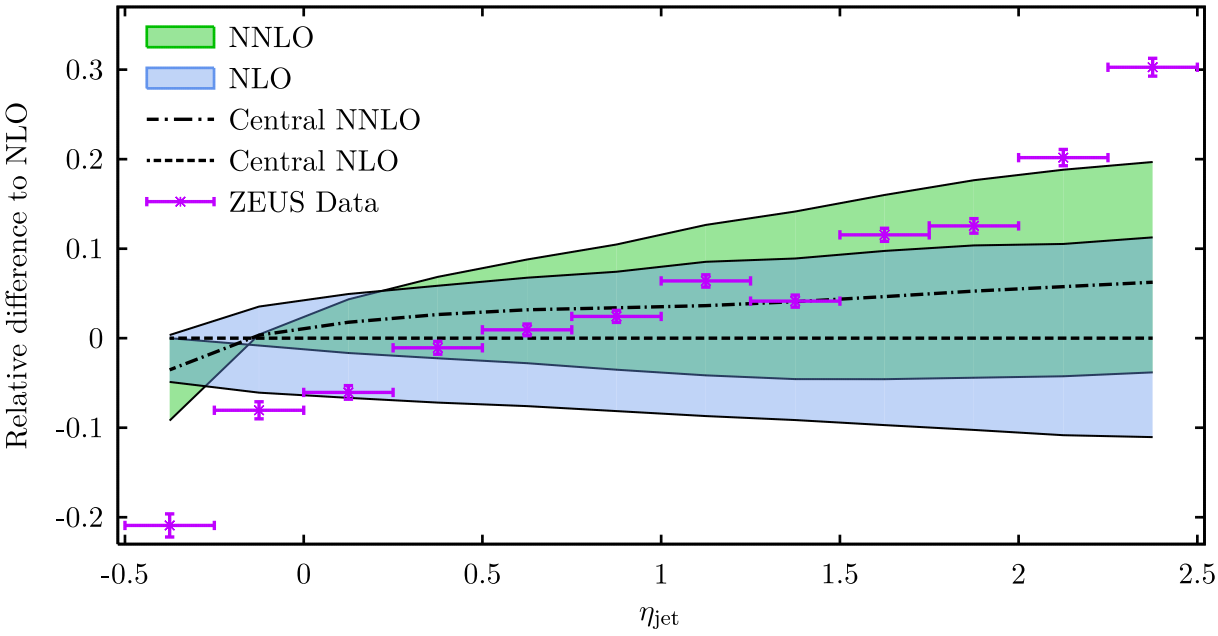


Figure 4.17: Relative difference of data points and NNLO calculations to the central NLO result for the cross section in Fig. 4.16. The bands display the theoretical uncertainty due to the variation of both factorization scales and the renormalization scale.

# 5. Summary and outlook

In Secs. 2 and 3, we have provided the essential theoretical background by shortly presenting the main features of photoproduction cross sections, renormalization, factorization and threshold resummation. We have derived the expressions for the NLO and NNLO master formulæ by N. Kidonakis [12], which arise from the perturbative expansion of a general resummed cross section. As a next step, we have adapted the NLO formula to the processes relevant for photoproduction and compared the analytic results to the corresponding NLO corrections in [7]. For this purpose, we had to transform the threshold variable $s_4$ used in the master formula to $z_a$ and $z_b$, which are defined in the work of Klasen and Kramer. The full NLO calculation should generally contain all of the soft and virtual corrections predicted by the master formula. However, at leading logarithmic level the coefficients of both results do not match, although they have a particularly simple form. Several of the terms proportional to the subleading NLL terms are missing in the expressions of [7], among which we also find those that are supposed to be exclusively connected to one-particle inclusive kinematics. At least we have been able to identify most of the scale-dependent terms, as well as the terms related to the soft anomalous dimension matrix $\Gamma'_S$, except for a constant factor. Sec. 3.4 actually leaves us with some open questions. If neglect the use of different threshold variables and possible errors, which might be caused by the transformation, the results are still quite different. As we use the virtual corrections from [7] for the scale-independent coefficient $T_1$, we gain almost full agreement for $c_1$. If we went on and dropped the terms assigned to one-particle inclusive kinematics, which are basically the $t_i$-dependent parts of the master formulæ, the scale-dependent terms would also coincide in both formulæ. In our calculations, however, we have not given up this $t_i$-dependence.
A further approach we have not taken could be to use the full NLO result of Klasen and Kramer to redefine $c_1$, $c_2$, $c_3$, and also $A^c$ in the case of resolved photoproduction; this would create a common base for the NNLO calculations, as the NLO would then match by definition.

The comparison of the NLO results have been followed by the description the method we have used to implement the new NNLO contributions into the `FORTRAN` code provided by Klasen and Kramer. Because in [12] one threshold variable is confronted with two different variables in [7], exact treatment of the NNLO corrections is only possible for those terms that could be assigned uniquely to initial parton $a$ or $b$. Contributions connected to both $a$ and $b$ represent initial state radiation off both of the incoming partons. For these terms, as well as for those not related to any initial particle, we have not been able to establish an accurate integration prescription. We have dealt with this problem by incorporating equal halves of the problematic terms in each of the $z$ integrations. In the case of direct processes, all non-vanishing terms have been integrated over $z_b$, which is related to the proton.
The results we have presented exhibit a relative size of the NNLO corrections between about 3 and 6 percent for the inclusive jet cross section differential in $E_T$, which is steadily increasing towards higher transverse energies in both kinematical regions probed by H1 and ZEUS (4.4, 4.6). For the pure hadronic $p\bar{p}$ collision we observe a more or less constant correction around 5 percent (see Fig. 4.2). In the case of the ZEUS data, which the originial NLO calculation tends to underestimate, the NNLO corrections lead to an improved agreement of theoretical and experimental values. All the previous statements refer to the central choice $\mu = p_T$, which causes a major part of the new terms to vanish due to the logarithmic form $\ln\left(\frac{\mu^2}{p_T^2}\right)$ of the scale-dependent terms. Hence, the performance of the results under variation of the scales has been another important aspect to be checked. In general, the inclusion of higher order scale-dependent terms should reduce the sensitivity of the overall result. We have tested the dependence of the NLO and NNLO differential cross section on the renormalization scale (Fig. 4.8), the proton

factorization scale (Fig. 4.10) and the photon factorization scale (Fig. 4.12). While the proton factorization scale dependence is significantly reduced by the new contributions as expected, the sensitivity to the variation of the renormalization scale is even slightly increased at NNLO. Most likely, this can be attributed to our treatment of the terms which are neither associated with parton $a$ nor with $b$, since a great part of the $\mu_R$-dependent contributions belong to this class. Therefore, in order to improve the renormalization scale dependence of the result, the problem related to the integration has to be solved. A proper integration of the new terms using $z_a$ and $z_b$ does not seem to be possible. Thus, the only solution we can propose is to set up an independent integration over the original $s_4$ within the existing NLO program. However, special attention has to be paid to the proper use of the Mandelstam variables as well as the parton distribution functions. Especially for the latter, the way in which they enter in the calculation is not completely specified in [12].
In the case of the photon factorization scale, the scale dependence at NNLO is considerably worse compared to the NLO calculation. This can be explained by pointing out that for direct photoproduction no $\mu_b$ dependence is added; the NNLO formula provides no explicitly $\mu_b$-dependent terms for this class of processes. As discussed in the first chapters of this thesis, the factorization scale dependence for the photon in photoproduction is governed by an interplay of direct and resolved contributions at different orders in perturbation theory. In our calculations, the NNLO corrections stemming from the resolved processes have no counterpart within the group of the direct ones. Still, the $\mu_b$ dependence of the jet cross sections should be improved, when the integration issues are fixed.
For the cross section differential in the jet rapidity, both agreement with experimental data and sensitivity to scale variation have changed for the better, concerning the directions perpendicular to the beam axis and also in forward direction, which is the direction of the proton. The different cuts in the transverse energy (17 GeV, Fig. 4.14 and 21 GeV, Fig. 4.16) have led to results that are qualitatively very similar. There is a greater scale uncertainty for both energy cuts in the outer rapidity ranges, in which a certain excess of the data with respect to the theoretical calculations at NLO and NNLO can also be observed. These discrepancies are assumed to be caused by the underlying event, i.e. by beam remnants or initial- and final-state radiation, which are non-perturbative effects and are therefore not taken into account in the calculation. In [3], the implementation of different photon PDFs have led to the discovery of a great influence of the photon density function in the high and low rapidity regime. Here, it would be a great advantage to have an updated photon PDF, since the newest available set, the GRV set [30] used in our calculations is based exclusively on the old $\gamma^*\gamma$ and $e^+e^-$ scattering data.
The determination of the strong coupling constant has yielded $\alpha_s(M_Z) = 0.116 \pm 0.001\,^{+0.003}_{-0.002}$ using the ZEUS data from [3] and the NNLO proton PDFs for different values of $\alpha_s(M_Z)$ by the CT10 collaboration. Whereas the world average of 0.118 is included in our uncertainty range, the value obtained in [3] using the same experimental data lies outside of this range.

As soon as the problems concerning the different notations and integrations have been solved, it would probably be a diligent but routine piece of work to go beyond NNLO. In [61], Kidonakis has published master formulæ for soft and virtual NNNLO corrections, derived from the same general resummed cross section which we have quoted in Eq. (3.81). The prescriptions which are used, are therefore equal; however, as expected, the terms which have to be implemented are considerably lengthier. Although the number of expressions to be implemented is higher, the corrections they provide will be even smaller than those from NNLO. Hence, NNNLO contributions will mainly serve to further reduce the scale dependence of the result. The mismatch of data points and theory, as e.g. in Fig. 4.14, will only slightly change for the better. Concerning this problem, further efforts have to be made to an improve the non-perturbative parts of the calculation.

## Acknowledgements

I wish to thank

- Prof. Dr. Michael Klasen for his support during the last month, for entrusting me with the continuation of the work of his Ph.D. thesis, for many explanations, advice, and patience.
- Prof. em. Dr. Gustav Kramer for the idea of this interesting project, for coming to Münster several times, and for taking the time to support me during my stay in Hamburg.
- my officemate Michael Topp for helping me many times, for useful discussions and also for livening up from time to time the hours of hard work.
- my brother Johannes for hours of careful reading of the manuscript and a lot of linguistic advice.
- Anja, Carlos, Carolin, Christoph, David, Florian, Manuel, Marcel, Marcel, Matthias, Moritz, Peter, Patrick, Sonja, Steffi, and Vincent for interesting and cheerful discussions and conversations during and outside lunch breaks.
- all my friends, physicists and non-physicists, for providing the right counterbalance especially in stressful moments.
- particularly my family for supporting me in every moment, even more in the last weeks of writing this thesis, and also with my future plans.

# A. Explicit expressions for the NNLO coefficients

## A.1. Direct contributions

Here, we give the c coefficients according to Eqs. (3.84), (3.85) and (3.86) for the two partonic processes involving direct photons. For the scale-independent part $T_1$ we use (also in the case of the resolved processes) the virtual corrections of [7].

### A.1.1. $\gamma g \to q\bar{q}$

In the case of the boson gluon fusion, the coefficients are given by

$$c_3 = 2(C_A - C_F), \tag{A.1}$$

$$c_2 = -C_A \ln\left(\frac{\mu_b^2}{s}\right) - \frac{3}{2}C_F + 2C_A \ln\left(\frac{-u}{s}\right) + C_A \ln\left(\frac{tu}{s^2}\right) - 2C_F \ln\left(\frac{p_T^2}{s}\right), \tag{A.2}$$

with $2\mathrm{Re}\left(\Gamma'_S\right) = 2C_F + C_A \ln\left(\frac{tu}{s^2}\right) + C_A$ [12] and $t_\gamma = u$, $t_g = t$. From that, we deduce

$$T_2 = -2C_A \ln\left(\frac{-u}{p_T^2}\right) - \frac{3}{2}C_F + (N_C - 2C_F) \ln\left(\frac{p_T^2}{s}\right). \tag{A.3}$$

Lastly, we find

$$c_1^\mu = \left[-C_A \ln\left(\frac{-u}{s}\right) - \frac{\beta_0}{4}\right] \ln\left(\frac{\mu_b^2}{s}\right) + \frac{\beta_0}{4} \ln\left(\frac{\mu_R^2}{s}\right). \tag{A.4}$$

### A.1.2. $\gamma q \to gq$

The coefficients for QCD Compton scattering are

$$c_3 = C_F - C_A, \tag{A.5}$$

$$c_2 = -C_F \ln\left(\frac{\mu_b^2}{s}\right) + 4C_F \ln\left(\frac{-u}{s}\right) - \frac{3}{4}C_F - \frac{\beta_0}{4} + C_A \ln\left(\frac{t}{u}\right) - (C_F + C_A) \ln\left(\frac{p_T^2}{s}\right), \tag{A.6}$$

where we assumed $t_\gamma = u$, $t_q = t$ and used $2\mathrm{Re}\left(\Gamma'_S\right) = 2C_F \ln\left(\frac{-u}{s}\right) + 2C_F + C_A \ln\left(\frac{t}{u}\right) + C_A$ [12]. Consequently, we have

$$T_2 = 4C_F \ln\left(\frac{-u}{s}\right) - \frac{3}{4}C_F - \frac{\beta_0}{4} + C_A \ln\left(\frac{t}{u}\right) - (C_F + C_A) \ln\left(\frac{p_T^2}{s}\right), \tag{A.7}$$

and also

$$c_1^\mu = -C_F \left[\ln\left(\frac{-u}{s}\right) + \frac{3}{4}\right] \ln\left(\frac{\mu_b^2}{s}\right) + \frac{\beta_0}{4} \ln\left(\frac{\mu_R^2}{s}\right). \tag{A.8}$$

## A.2. Resolved contributions

Dealing with the resolved processes, one more quantity has to be calculated, which is $A^c$ as defined in Eq. (3.88). Expressions for the soft, hard and anomalous dimension matrices can be found in [56]. While at leading order all resolved processes can be calculated from only four different born matrix elements (see Sec. 2.4), at next-to-next-to-leading order the crossing relations do not simply hold. We will therefore treat each of the ten processes listed in Sec. 3.3 of [7] separately.

### A.2.1. $qq' \to qq'$

The first process is the scattering of two quarks of different flavours. We find (see Sec. 4.3.1 of [12])

$$c_3 = 2C_F, \tag{A.9}$$

$$c_2 = -C_F \left[\ln\left(\frac{\mu_a^2}{s}\right) + \ln\left(\frac{\mu_b^2}{s}\right)\right] - \frac{11}{2}C_F, \tag{A.10}$$

where we are setting $T_2 = -\frac{11}{2}C_F$, and

$$c_1^\mu = -C_F \left[\ln\left(\frac{-t}{s}\right) + \frac{3}{4}\right] \ln\left(\frac{\mu_a^2}{s}\right) - C_F \left[\ln\left(\frac{-u}{s}\right) + \frac{3}{4}\right] \ln\left(\frac{\mu_b^2}{s}\right) + \frac{\beta_0}{2} \ln\left(\frac{\mu_R^2}{s}\right). \tag{A.11}$$

The scale-independent part $T_1$ again is taken to be the virtual corrections of [7] after subtracting the terms depending on the the renormalization scale. Finally, we have

$$A^c = \frac{\alpha_S^3}{\pi} 2\frac{C_F}{N_C^2} \frac{s^2+u^2}{t^2} \left[2C_F N_C \ln\left(\frac{-u}{s}\right) - \ln\left(\frac{tu}{s^2}\right)\right]. \tag{A.12}$$

### A.2.2. $q\bar{q}' \to q\bar{q}'$

In this case the $c$-coefficients are just the same as in the previous section as all partons are of quark type. Thus, we are only left with

$$A^c = -\frac{\alpha_S^3}{\pi} 2\frac{C_F}{N_C^2} \frac{s^2+u^2}{t^2} \ln\left|\frac{st}{u^2}\right|. \tag{A.13}$$

### A.2.3. $q\bar{q} \to q'\bar{q}'$

Again, the $c$-coefficients are given by Eq. (A.9) - (A.11). For $A^c$ we find

$$A^c = \frac{\alpha_S^3}{\pi} 2\frac{C_F}{N_C^2} \frac{t^2+u^2}{s^2} \left[2C_F N_C \ln\left(\frac{-t}{s}\right) - \ln\left|\frac{st}{u^2}\right|\right]. \tag{A.14}$$

### A.2.4. $qq \to qq$

In addition to Eq. (A.9) - (A.11), we calculate

$$\begin{aligned} A^c = \frac{\alpha_S^3}{\pi} 2\frac{C_F}{N_C} \Bigg\{ & \frac{t^2+s^2}{u^2} \left[-\frac{1}{N_C^3} \ln\left(\frac{tu}{s^2}\right) + 4\frac{C_F^2}{N_C} \ln\left(\frac{-t}{s}\right) - 2\frac{C_F}{N_C^2} \ln\left(\frac{-u}{s}\right)\right] \\ & + \frac{s^2+u^2}{t^2} \left[-\frac{1}{N_C} \ln\left(\frac{tu}{s^2}\right) + 2C_F \ln\left(\frac{-u}{s}\right)\right] + \frac{2}{N_C^2}\frac{s^2}{tu} \ln\left(\frac{tu}{s^2}\right)\Bigg\}. \end{aligned} \tag{A.15}$$

### A.2.5. $q\bar{q} \to q\bar{q}$

Apart from the $c_1^\mu$, $c_2$ and $c_3$, which are the same as before, we have

$$\begin{aligned} A^c = \frac{\alpha_S^3}{\pi} 2\frac{C_F}{N_C} \Bigg\{ & \frac{t^2+u^2}{s^2} \left[-\frac{1}{N_C^3} \ln\left|\frac{st}{u^2}\right| + 4\frac{C_F^2}{N_C} \ln\left(\frac{-t}{s}\right) + 4\frac{C_F}{N_C^2} \ln\left(\frac{-u}{s}\right)\right] \\ & - \frac{s^2+u^2}{t^2} \frac{1}{N_C} \ln\left|\frac{st}{u^2}\right| + \frac{u^2}{st} \left[\frac{2}{N_C^2} \ln\left|\frac{st}{u^2}\right| - 4\frac{C_F}{N_C} \ln\left(\frac{-u}{s}\right)\right]\Bigg\}. \end{aligned} \tag{A.16}$$

### A.2.6. $q\bar{q} \to gg$

Since for the first time there are gluons involved, the coefficients change with respect to the last sections. In particular, one finds (compare to Sec. 4.3.2 in [12])

$$c_3 = 4C_F - 2C_A, \tag{A.17}$$

$$c_2 = -C_F \left[ \ln\left(\frac{\mu_a^2}{p_T^2}\right) + \ln\left(\frac{\mu_b^2}{p_T^2}\right) \right] - \frac{\beta_0}{2} - 2C_F - 2C_A - 2C_A \ln\left(\frac{p_T^2}{s}\right), \tag{A.18}$$

while

$$T_2 = c_2 + C_F \left[ \ln\left(\frac{\mu_a^2}{s}\right) + \ln\left(\frac{\mu_b^2}{s}\right) \right], \tag{A.19}$$

and $c_1^\mu$ is given in Eq. (3.109). For $T_1$ see the virtual corrections in [7]. We complete this section with

$$\begin{aligned} A^c = &\frac{\alpha_S^3}{\pi} \frac{C_F}{2N_C} \left[ -4\left(\frac{t}{u} + \frac{u}{t}\right) + N_C^2 \left( \frac{s^2+t^2+u^2}{tu} + 8\frac{tu}{s^2} - 6 \right) \right] \ln\left(\frac{tu}{s^2}\right) \\ &+ C_F N_C \left( 2\frac{t-u}{s} + \frac{t}{u} - \frac{u}{t} \right) \ln\left(\frac{u}{t}\right). \end{aligned} \tag{A.20}$$

### A.2.7. $qg \to qg$

For this process the coefficients are (see Sec. 4.3.3 of [12])

$$c_3 = C_F + C_A \tag{A.21}$$

and

$$c_2 = -C_F \ln\left(\frac{\mu_a^2}{p_T^2}\right) - C_A \ln\left(\frac{\mu_b^2}{p_T^2}\right) - \frac{11}{4}C_F - 2C_A - \frac{\beta_0}{4} - 2C_F \ln\left(\frac{-u}{s}\right) - 2C_A \ln\left(\frac{-t}{s}\right), \tag{A.22}$$

so we have

$$T_2 = c_2 + C_F \ln\left(\frac{\mu_a^2}{s}\right) + C_A \ln\left(\frac{\mu_b^2}{s}\right). \tag{A.23}$$

Furthermore,

$$c_1^\mu = -\left[ C_F \ln\left(\frac{-t}{s}\right) + \frac{3}{4}C_F \right] \ln\left(\frac{\mu_a^2}{s}\right) - \left[ C_A \ln\left(\frac{-u}{s}\right) + \frac{\beta_0}{4} \right] \ln\left(\frac{\mu_b^2}{s}\right) + \frac{\beta_0}{2} \ln\left(\frac{\mu_R^2}{s}\right), \tag{A.24}$$

and

$$\begin{aligned} A^c = &-\frac{\alpha_S^3}{\pi} \frac{C_F + N_C}{N_C^2} \left( \frac{t^2}{su} - 2 \right) \ln\left(\frac{-t}{s}\right) + N_C \left( -1 - 2\frac{s}{t} + \frac{u}{2s} - \frac{s}{2u} \right) \ln\left(\frac{-u}{s}\right) \\ &+ \left[ C_F \ln\left(\frac{-t}{s}\right) + \frac{N_C}{2} \ln\left(\frac{-u}{s}\right) \right] \left[ \left( \frac{2}{N_C^2} - 1 \right) \left( \frac{t^2}{su} - 2 \right) + 2\left( 1 - 2\frac{su}{t^2} \right) \right]. \end{aligned} \tag{A.25}$$

Note that all these results are identical for the process $\bar{q}g \to \bar{q}g$.

### A.2.8. $gg \to q\bar{q}$

While the $c$-coefficients are given by (compare to Sec. 4.3.2 in [12])

$$c_3 = 4C_A - 2C_F, \tag{A.26}$$

$$c_2 = -C_A \left[ \ln\left(\frac{\mu_a^2}{p_T^2}\right) + \ln\left(\frac{\mu_F^2}{p_T^2}\right) \right] - \frac{7}{2} C_F - 2C_A - 2C_F \ln\left(\frac{p_T^2}{s}\right), \tag{A.27}$$

$T_2$ therefore being

$$T_2 = c_2 + C_A \left[ \ln\left(\frac{\mu_a^2}{p_T^2}\right) + \ln\left(\frac{\mu_b^2}{p_T^2}\right) \right], \tag{A.28}$$

and

$$c_1^\mu = -\left[ C_A \ln\left(\frac{-t}{s}\right) + \frac{\beta_0}{4} \right] \ln\left(\frac{\mu_a^2}{s}\right) - \left[ C_A \ln\left(\frac{-u}{s}\right) + \frac{\beta_0}{4} \right] \ln\left(\frac{\mu_b^2}{s}\right) + \frac{\beta_0}{2} \ln\left(\frac{\mu_R^2}{s}\right); \tag{A.29}$$

the expression for $A^c$ is simply the one for the inverse process $q\bar{q} \to gg$ multiplied by a factor $\frac{1}{4C_F^2}$ which takes into account the different polarization averages due to the change of the initial partons.

### A.2.9. $gg \to gg$

Finally, the purely gluonic process has the coefficients (Sec. 4.3.4 of [12])

$$c_3 = 2N_C, \tag{A.30}$$

$$c_2 = -2N_C \ln\left(\frac{\mu_F^2}{s}\right) - \frac{\beta_0}{2} - 4N_C \tag{A.31}$$

and

$$c_1^\mu = -\left[ C_A \ln\left(\frac{-t}{s}\right) + \frac{\beta_0}{4} \right] \ln\left(\frac{\mu_a^2}{s}\right) - \left[ C_A \ln\left(\frac{-u}{s}\right) + \frac{\beta_0}{4} \right] \ln\left(\frac{\mu_b^2}{s}\right) + \frac{\beta_0}{2} \ln\left(\frac{\mu_R^2}{s}\right). \tag{A.32}$$

In addition, we have

$$\begin{aligned} A^c = \frac{\alpha_S^3}{\pi} \Bigg\{ & \frac{27}{8} \left[ 2\ln\left(\frac{-t}{s}\right) + 5\ln\left(\frac{-u}{s}\right) \right] \left( 1 - \frac{tu}{s^2} - \frac{st}{u^2} + \frac{t^2}{su} \right) \\ & + \left[ 3\ln\left(\frac{-t}{s}\right) + \frac{3}{2}\ln\left(\frac{-u}{s}\right) \right] \left[ \frac{27}{4} - 9\left( \frac{su}{t^2} + \frac{tu}{4s^2} + \frac{st}{4u^2} \right) \right. \\ & \left. + \frac{9}{2}\left( \frac{u^2}{st} + \frac{s^2}{tu} - \frac{t^2}{2su} \right) \right] - \frac{27}{4} \ln\left(\frac{-u}{s}\right) \left( \frac{st}{u^2} - \frac{tu}{s^2} + \frac{u^2}{st} - \frac{s^2}{tu} \right) \Bigg\}. \end{aligned} \tag{A.33}$$

## B. Boundary terms for the plus distributions

In this section, we quote the analytical expressions of the additional boundary terms, which have to be included if the integration over the plus distribution is done numerically. Due to convolution of the different integrals, the distributions are given by (see Eq. (3.102))

$$\int_0^1 dz\,[f(z)]_+ g(z) = \int_x^1 dz\, f(z)g(z) - \int_0^1 dz\, f(z)g(1), \tag{B.1}$$

so that in case the numerical integration is performed over the interval $[x,1]$ for both integrals, the remaining part

$$\int_0^x dz\, f(z)g(1) \tag{B.2}$$

has to be calculated separately and subtracted from the numerical result. We find (e.g. using `Mathematica`):

$$\int_0^{x_i} dz_i\, \frac{z_i}{1-z_i} = -x_i - \ln(1-x_i), \tag{B.3}$$

$$\begin{aligned}\int_0^{x_i} dz_i\, \frac{z_i}{1-z_i} \ln\left(\frac{-s}{u_i}\frac{z_i}{1-z_i}\right) =& \frac{\pi^2}{6} - \mathrm{Li}_2(1-x_i) + \ln(1-x_i) - x_i \ln\left(\frac{-s}{u_i}\frac{1-x_i}{x_i}\right) \\ &- \frac{1}{2}\left[\ln^2\left(\frac{-s}{u_i}(1-x_i)\right) - \ln^2\left(\frac{-s}{u_i}\right)\right],\end{aligned} \tag{B.4}$$

$$\begin{aligned}\int_0^{x_i} dz_i\, \frac{z_i}{1-z_i} \ln^2\left(\frac{-s}{u_i}\frac{z_i}{1-z_i}\right) =& -\left[x_i + \ln(1-x_i)\right]\ln^2(x_i) + 2x_i \ln(x_i) \ln\left(\frac{-s}{u_i}(1-x_i)\right) \\ &+ \ln\left(\frac{-s}{u_i}\right)\left[\frac{\pi^2}{3} - \ln\left(\frac{-s}{u_i}\right) + \frac{1}{3}\ln^2\left(\frac{-s}{u_i}\right)\right] \\ &- \ln^2\left(\frac{-s}{u_i}(1-x_i)\right)\left[-1 + x_i + \frac{1}{3}\ln\left(\frac{-s}{u_i}(1-x_i)\right)\right] \\ &- 2\left[-1 + \ln\left(\frac{-s}{t_i}(1-x_i)\right)\right]\mathrm{Li}_2(x_i) \\ &+ 2[\mathrm{Li}_3(1-x_i) + \mathrm{Li}_3(x_i)] - \frac{\pi^2}{3} - 2\zeta_3,\end{aligned} \tag{B.5}$$

and finally

$$\begin{aligned}\int_0^{x_i} dz_i\, \frac{z_i}{1-z_i} \ln^3\left(\frac{-s}{u_i}\frac{z_i}{1-z_i}\right) =& \frac{1}{4}\ln\left(\frac{-s}{u_i}\right)\left\{\ln\left(\frac{-s}{u_i}\right)\left[2\pi^2 + \left(-4 + \ln\left(\frac{-s}{u_i}\right)\right)\ln\left(\frac{-s}{u_i}\right)\right]\right. \\ &\left. -4\pi^2\right\} + 3\ln(x_i)\ln^2\left(\frac{-s}{u_i}\frac{1-x_i}{x_i}\right) \\ &+ \left[1 - x_i - \ln(x_i)\right]\ln^3\left(\frac{-s}{u_i}\frac{1-x_i}{x_i}\right) - \frac{1}{4}\ln^4\left(\frac{-s}{u_i}\frac{1-x_i}{x_i}\right) \\ &+ 3\left[-2 + \ln\left(\frac{-s}{u_i}\frac{1-x_i}{x_i}\right)\right]\ln\left(\frac{-s}{u_i}\frac{1-x_i}{x_i}\right)\mathrm{Li}_2\left(\frac{1-x_i}{x_i}\right) \\ &- 6\left[-1 + \ln\left(\frac{-s}{u_i}\frac{1-x_i}{x_i}\right)\right]\mathrm{Li}_3\left(\frac{1-x_i}{x_i}\right) \\ &+ 6\,\mathrm{Li}_4\left(\frac{1-x_i}{x_i}\right) + \frac{7\pi^4}{60}.\end{aligned} \tag{B.6}$$

# C. Comments on the FORTRAN code

This section contains a few comments on how we arranged the new NNLO contributions in the code, and documents some modifications we made in the original program.

## C.1. Structure of the NNLO contributions

Since the soft and virtual corrections to be added are all derived in the soft limit, where only flavour-diagonal splitting contributes, most of the new terms are proportional to the Born cross section of the original underlying $2 \to 2$ hard scattering process. Hence, the outer structure of the NNLO contributions has simply been copied from the leading order contributions. Nevertheless, we have introduced new functions for the NNLO contributions, which are

Listing 1: New NNLO functions

| | |
|---|---|
| `mkoyg2qb(s,t,u,z,x,iab)` | for $\gamma g \to q\bar{q}$, |
| `mkoyq2qg(s,t,u,z,x,iab)` | for $\gamma q \to gq$, |
| `mkoqp2qp(s,t,u,z,x,iab)` | for $qq' \to qq'$, |
| `mkoqr2qr(s,t,u,z,x,iab)` | for $q\bar{q}' \to q\bar{q}'$, |
| `mkoqb2pr(s,t,u,z,x,iab)` | for $q\bar{q} \to q'\bar{q}'$, |
| `mkoqq2qq(s,t,u,z,x,iab)` | for $qq \to qq$, |
| `mkoqb2qb(s,t,u,z,x,iab)` | for $q\bar{q} \to q\bar{q}$, |
| `mkoqb2gg(s,t,u,z,x,iab)` | for $q\bar{q} \to gg$, |
| `mkoqg2qg(s,t,u,z,x,iqg,iab)` | for $qg \to qg$, |
| `mkogg2qb(s,t,u,z,x,iab)` | for $gg \to q\bar{q}$, |
| `mkogg2gg(s,t,u,z,x,iab)` | for $gg \to gg$. |

Note that we have calculated proton-electron collisions, so that contrary to the discussion in the rest of this the is $a$ is related to the proton and $b$ to the photon. The arguments of the new functions are the Mandelstam variables $s'$, $t'$ and $u'$, the threshold variable $z$, which can be given by either $z_a$ or $z_b$, and the momentum fraction $x$, which is used for $x_a$, $x_b$ or $y_b$. Furthermore, the flag `iab` is needed within the functions to choose between $\mu_a$ and $\mu_b$, as well as $t_a$ and $t_b$. An additional flag has been defined exclusively for the $qg \to qg$ process, which is the only process with different types of partons in the initial state. Thus, `iqg` is used to fix if $a$ and $b$ are quark and gluon, or vice versa.
Although at leading order it is sufficient to have five different functions for all cross sections due to the crossing relations, at NNLO these relations do not hold. In particular, all terms derived from the anomalous dimension matrix $\Gamma'_S$ have to be calculated separately for each of these processes; for this reason, we have had to define more than five new functions for the NNLO contributions. All c coefficients (see Appx. A) are defined within the functions listed above, whereas the $A^c$ are calculated externally for each resolved process by the functions `acqp2qp(s,t,u)`, `acqr2qr(s,t,u)`, etc., analogous to the prescription we introduced above.
The transformed plus distributions from Eq. (3.99) as well as the boundary terms from Appx. B are called within the functions introduced above via `d0(z,x)`, `d1(s,ti,z,x)`, `d2(s,ti,z,x)` and `d3(s,ti,z,x)`, for $\mathcal{D}_0(z)$, $\mathcal{D}_1(z)$, $\mathcal{D}_2(z)$ and $\mathcal{D}_3(z)$, respectively. If the new global flag `idelta` is set to `.true.`, the d functions return the corresponding boundary term, which is calculated by $s'$, $t'_i$ and $x_i$. These terms require no additional integration. For `idelta = .false.`, the actual plus distribution integrands are returned, which depend on $s$, $t'_i$ (except $\mathcal{D}_0$) and $z_i$. Two further newly introduced flags, `innloa` and `innlob`, serve to switch on and off the contributions related to parton $a$ and $b$, respectively. Hence, for each process the functions in are called four times:

| | |
|---|---|
| innloa & idelta | for boundary terms belonging to parton $a$, |
| innloa & ¬idelta | for integration over plus distributions of $z_a$, |
| innlob & idelta | for boundary terms belonging to parton $b$, |
| innlob & ¬idelta | for integration over plus distributions of $z_b$. |

In the case of direct photoproduction, only the first two options are realized.

## C.2. Modifications to the original code

In the context of the extension, we have also effected slight changes to the original code. First, we note that the integrations of the various parts are have different dimensions, since the initial state corrections, in contrast to the leading order and virtual contributions, require an additional integration over $z_a$ and $z_b$, respectively. As in the original version of the program, all contributions were calculated within one VEGAS call, this led to the fact that e.g. the leading order cross sections are evaluated through an integration that had two surplus dimensions. The latter caused an increased numerical error; therefore, we have decided to split up the old integration in kernel 1,

Listing 2: Old VEGAS call

```
call vegas (kern1,eps,int1,ipoin1,itt,iprn,igraph)

ipoin1= ipoin1*itt*max0(ipt,iy1,iy2,icosth,imjj,11)

ifill   = 1

call vegas1(kern1,eps,int1,ipoin1,  1,iprn,igraph)

ifill   = 0

sngly   = avgt

sngldy  = errt
```

into three consecutive integrations. The first part includes the Born, virtual and final state contributions, plus the boundary terms of the NNLO corrections, if the flag innlo is set to one in the input file. Initial state contributions of parton $a$ are integrated over in the second part, together with possible NNLO contributions related to the same initial particle. In the third part, the corresponding contributions for particle $b$ are taken into account. The modified code then takes the form:

Listing 3: New VEGAS call

```
if(iborn.eq.1.OR.ivirt.eq.1.OR.ifina.eq.1.OR.innlo.eq.1)then
  iaini = iaini-1
  ibini = ibini-1
  idelta        = .true.
  innloa        = .true.
  innlob        = .true.
    call vegas (kern1,eps,int1,ipoin1,itt,iprn,igraph)
    ipoin1      = ipoin1*itt*max0(ipt,iy1,iy2,icosth,imjj,11)
    ifill       = 1
    call vegas1(kern1,eps,int1,ipoin1,  1,iprn,igraph)
    ifill       = 0
    sngly       = avgt
    sngldy      = errt
  iaini = iaini+1
  ibini = ibini+1
```

```
  idelta        = .false.
  innloa        = .false.
  innlob        = .false.
endif

if(iaini.eq.1.OR.innlo.eq.1)then
  iborn = iborn-1
  ivirt = ivirt-1
  ifina = ifina-1
  ibini = ibini-1
  innloa        = .true.
  int1=int1+1
    ipoin1      = ipoin
    call vegas (kern1,eps,int1,ipoin1,itt,iprn,igraph)
    ipoin1= ipoin1*itt*max0(ipt,iy1,iy2,icosth,imjj,11)
    ifill       = 1
    call vegas1(kern1,eps,int1,ipoin1,  1,iprn,igraph)
    ifill       = 0
    sngly       = sngly+avgt
    sngldy      = sqrt(sngldy**2+errt**2)
  int1  = int1-1
  iborn = iborn+1
  ivirt = ivirt+1
  ifina = ifina+1
  ibini = ibini+1
  innloa        = .false.
endif

if(ibini.eq.1)then
  iborn = iborn-1
  ivirt = ivirt-1
  ifina = ifina-1
  iaini = iaini-1
  innlob        = .true.
  int1=int1+1
  ipoin1        = ipoin
    call vegas (kern1,eps,int1,ipoin1,itt,iprn,igraph)
    ipoin1= ipoin1*itt*max0(ipt,iy1,iy2,icosth,imjj,11)
    ifill       = 1
    call vegas1(kern1,eps,int1,ipoin1,  1,iprn,igraph)
    ifill       = 0
    sngly       = sngly+avgt
    sngldy      = sqrt(sngldy**2+errt**2)
  int1  = int1-1
  iborn = iborn+1
  ivirt = ivirt+1
  ifina = ifina+1
  iaini = iaini+1
  innlob        = .false.
endif
```

This change has reduced the numerical error of the VEGAS output by about 10 percent. A disadvantage of this modifications is that the program will run longer, since for every VEGAS call the grid has to be newly calculated. However, the significantly more time-consuming part of the calculation, which is located in kernel 2 of the program, has remained untouched. Therefore, the increase in calculation time is comparatively small.

Apart from this improvement, we have corrected one error in program code. We have removed a factor of 2 in the initial state corrections for direct photons:

Listing 4: Original code, direct contributions

```
c 3.  Hadron  -Elektron-Streuung

      if((iabs(iatyp).ge.1).and.(ibtyp.eq.0))then
      ⋮
c 3.3   Resolved-Direct

        if((iares.ge.1).and.

     .    ((ibres.eq.0).or.(ibres.eq.4)))then
      ⋮
        if(iaini.eq.1)then
      ⋮
          sum = sum+zadjac/zad*
     .          (4.d0*pi*alpha)*(4.d0*pi*alphas)*alphas/(2.d0*pi)*
     .          ( 8.d0*nc*cf**2*fyqa*(mjyq2qgg1(1,s,t,u,zad)
      ⋮
     .          + 4.d0*nc*cf*   fypa*(mjyq2qqb (1,s,t,u,zad)
     .                              +mjyq2qqb (1,s,u,t,zad))
     .          +16.d0*nc*cf**2*fyga*(mjyg2qbg1(1,s,t,u,zad)
     .                              +mjyg2qbg1(1,s,u,t,zad))
     .          - 4.d0*nc**2*cf*fyga*(mjyg2qbg2(1,s,t,u,zad)
     .                              +mjyg2qbg2(1,s,u,t,zad))

      ⋮
     .          )
          endif
      ⋮
        endif
      ⋮
      endif
```

This error has been found by comparing these terms to the corresponding expressions from the resolved contributions, where the photon y replaced by a gluon. The corrected code then is

Listing 5: Modified code, direct contributions

```
      ⋮
     .          + 8.d0*nc*cf**2*fyga*(mjyg2qbg1(1,s,t,u,zad)
     .                              +mjyg2qbg1(1,s,u,t,zad))
      ⋮
```

However, this change has had a negligible effect on the overall result.

## References


[1] ZEUS Collaboration, S. Chekanov et al.,
*A ZEUS Next-to-Leading-Order QCD Analysis of Data on Deep Inelastic Scattering*,
Phys. Rev. **D**67 (2003) 012007

[2] J. Pumplin, D.R. Stump, J. Huston, H.L. Lai, P. Nadolsky, W.K. Tung,
*New Generation of Parton Distributions with Uncertainties from Global QCD Analysis*,
JHEP 0207 (2002) 012

[3] ZEUS Collaboration, H. Abramowicz et al.,
*Inclusive-Jet Photoproduction at HERA and determination of $\alpha_s$*,
Nucl. Phys. **B**864 (2012) 1-37

[4] ZEUS Collaboration, H. Abramowicz et al.,
*Measurement of Heavy-Quark Jet Photoproduction at HERA*,
Eur. Phys. J. **C**71 (2011) 1659

[5] ZEUS Collaboration, S. Chekanov et al.,
*Three- and Four-Jet Final States in Photoproduction at HERA*,
Nucl. Phys. **B**792 (2008) 1-47

[6] H1 Collaboration, C. Adloff et al.
*Measurement of Inclusive Jet Cross Sections in Photoproduction at HERA*,
Eur. Phys. J. **C**29 (2003) 497-513

[7] M. Klasen,
*Photoproduction of Jets at HERA in Next-to-Leading Order QCD*,
Ph.D. thesis, Hamburg 1996

[8] G. Sterman, S. Weinberg,
*Jets from Quantum Chromodynamics*
Phys. Rev. Lett. 39, (1977) 1436–1439

[9] J.E. Huth et al.,
*Toward a Standardization of Jet Definitions, Proceedings of the 1990 Summer Study on High Energy Physics - Research Directions for the Decade - Snowmass, Colorado, June 25-July 13, 1990*

[10] S.D. Ellis, D.E. Soper,
*Successive Combination Jet Algorithm For Hadron Collisions*,
Phys. Rev. **D**48 (1993) 3160-3166

[11] M. Cacciari, G.P. Salam,
*Dispelling the $N^3$ Myth for the $k_T$ Jet-Finder*,
Phys. Lett. **B**641, (2006) 57-61

[12] N. Kidonakis,
*A Unified Approach to NNLO Soft and Virtual Corrections in Electroweak, Higgs, QCD, and SUSY Processes*, Int. J. Mod. Phys. **A**19 (2004) 1793-1821

[13] J. Gao, M. Guzzi, J. Huston, H.L. Lai, Z. Li, P. Nadolsky, J. Pumplin, D. Stump, C.P. Yuan
*The CT10 NNLO Global Analysis of QCD*,
arXiv:1302.6246 [hep-ph]

[14] M. Bonvini,
*Resummation of Soft and Hard Gluon Radiation in Pertubative QCD*,
Ph.D. thesis, Genova 2012

[15] M. Klasen, G. Kramer,
*Inclusive Dijet Production at HERA: Direct Photon Cross Sections in Next-to-Leading Order QCD*,
Z. Phys. **C**72 (1996) 107-122

[16] I. Bojak,
*NLO QCD Corrections to the Polarized Photo- and Hadroproduction of Heavy Quarks*,
Ph.D. thesis, Dortmund 2000, arXiv:hep-ph/0005120v1

[17] Particle Data Group, J. Beringer et al.,
*Review of Particle Physics (RPP)*,
Phys. Rev. **D**86, 010001 (2012)

[18] CMS Collaboration, Serguei Chatrchyan et al.,
*Search for Heavy Quarks Decaying into a Top Quark and a W or Z Boson Using Lepton + Jets Events in pp Collisions at* $\sqrt{s} = 7\,\text{TeV}$,
JHEP 1301 (2013) 154

[19] A. Pich,
*Quantum Chromodynamics*
Lectures given at "Sorrento 1994, High energy physics", 157-207, arXiv:hep-ph/9505231 May 1995

[20] J.B. Dainton, M. Klein, P. Newman, E. Perez, F. Willeke,
*Deep Inelastic Electron Neutron Scattering at the LHC*,
JINST 1 (2006) P10001

[21] Y.L. Dokshitzer,
*Calculation of the Structure Functions for Deep Inelastic Scattering and* $e^+e^-$ *Annihilation by Perturbation Theory in Quantum Chromodynamics*,
Soviet. Phys. JETP 46 (1977) 641-653

[22] V.N. Gribov, L.N. Lipatov,
*Deep Inelastic ep Scattering in Perturbation Theory*,
Sov. J. Phys. 15 (1972) 438-450

[23] V.N. Gribov, L.N. Lipatov,
$e^+e^-$ *Pair Annihilation and Deep Inelastic ep Scattering in Perturbation Theory*,
Sov. J. Phys. 15 (1972) 675-684

[24] G. Altarelli, G. Parisi,
*Asymptotic Freedom in Parton Language*,
Nucl. Phys. **B**126 (1977) 298-330

[25] G. Curci, W. Furmanski, R. Petronzio,
*Evolution of Parton Densities Beyond Leading Order: The Nonsinglet Case*
Nucl. Phys. **B**175 (1980) 27-92

[26] W. Furmanski, R. Petronzio,
*Singlet Parton Densities beyond Leading Order*,
Phys. Lett. 97**B** (1980) 437-447

[27] A. Vogt, S. Moch, J.A.M. Vermaseren,
*The Three-Loop Splitting Functions in QCD: The Nonsinglet Case*,
Nucl. Phys. **B**688 (2004) 101-134

[28] A. Vogt, S. Moch, J.A.M. Vermaseren,
*The Three-Loop Splitting Functions in QCD: The Singlet Case*,
Nucl. Phys. **B**691 (2004) 129-181

[29] T. Sjostrand, J.K. Storrow, A. Vogt,
*Parton Distributions of Real and Virtual Photons*, J. Phys. **G**22 (1996) 893-902

[30] M. Glück, E. Reya, A. Vogt,
*Photonic Parton Distributions*
Phys. Rev. **D**46 (1992) 1973-1979

[31] J.J. Sakurai,
*Theory of Strong Interactions*,
Ann. Phys. 11 (1960) 1

[32] S.D. Ellis, Z.Kunszt, D.E. Soper,
*One-Jet Inclusive Cross Sections at Order* $\alpha_s^3$*: Gluons Only*
Phys. Rev. Lett. 62, 726–729 (1989)

[33] P. Aurechne, R. Baier, A. Douiri, M. Fontannaz, D. Schiff,
*Scheme Invariant Higher Order QCD Predictions for Large $p_T$ Photoproduction Reactions*,
Nucl. Phys. **B**286, (1987) 553-591

[34] H. Baer, J. Ohnemus, J.F. Owens,
*Next-to-Leading-Logarithm Calculation of Jet Photoproduction*,
Phys. Rev. **D**40 (1989) 2844–2855

[35] R.K. Ellis, J.C. Sexton,
*Radiative Corrections to Parton-Parton Scattering*,
Nucl. Phys. **B**269 (1986) 445-484

[36] G. 't Hooft, M. Veltman,
*Regularization and Renormalization of Gauge Fields*,
Nucl.Phys. **B**44 (1972) 189-213

[37] W. Kilian
*Übungen zu Strahlungskorrekturen in Eichtheorien*,
Herbstschule für Hochenergiephysik, Maria Laach 2001

[38] T. Muta,
*Foundations of Quantum Chromodynamics - An Introduction to Perturbative Methods in Gauge Theories*,
World Scientific Lecture Notes in Physics, Vol. 78, Third Edition (2010)

[39] G. 't Hooft,
*Renormalization of Massless Yang-Mills Fields*,
Nucl. Phys. **B**33 (1971) 173-199

[40] G. 't Hooft,
*The Discovery of the Renormalizability of Non-Abelian Gauge Theories*, Proceedings of the International School of Subnuclear Physics, Erice, Italy, 27 Aug - 5 Sep 2000,
http://www.staff.science.uu.nl/ hooft101/lectures/erice00.pdf

[41] T. Kinoshita,
*Mass Singularities of Feynman Amplitudes*,
J. Math. Phys. 3 (1962) 650-677

[42] T.D. Lee, M. Nauenberg,
*Degenerate Systems and Mass Singularities*,
Phys. Rev. 133 (1964) **B**1549-**B**1562

[43] M. Furman,
*Study of a Non-Leading Correction to Hadron Calorimeter Reactions*,
Nucl. Phys. **B**197 (1982) 413-445

[44] J. Debove,
*QCD Resummations for Gaugino-Pair Hadroproduction*,
Ph.D. thesis, Grenoble 2010

[45] N. Kidonakis,
*Electroweak Boson Hadroproduction at Large Transverse Momentum: Factorization, Resummation, and NNLO Corrections*,
Phys. Lett. **B**480 (2000) 87-96

[46] N. Kidonakis, G. Oderda, G. Sterman,
*Threshold Resummation for Dijet Cross Sections*,
Nucl. Phys. **B**525 (1998) 299-332

[47] N. Kidonakis, G. Sterman,
*Threshold Resummation for QCD Hard Scattering*,
Nucl. Phys. **B**505, (1997) 321-348

[48] G. Sterman,
*Summation of Large Corrections to Short-Distance Hadronic Cross Sections*,
Nucl. Phys. **B**281 (1987) 310-364

[49] N. Kidonakis, E. Laenen, S. Moch, R. Vogt,
*Sudakov Resummation and Finite Order Expansions of Heavy Quark Hadroproduction Cross Sections*,
Phys. Rev. **D**64 (2001) 114001

[50] S. Catani, M.L. Mangano, P. Nason,
*Sudakov Resummation for Prompt-Photon Production in Hadron Collisions*,
JHEP 07 (1998) 024

[51] S. Catani, L. Trentadue,
*Resummation of the QCD Perturbative Series for Hard Processes*,
Nucl. Phys. **B**327 (1989) 323-352

[52] A. Vogt,
*Next-to-Next-to-Leading Logarithmic Threshold Resummation for Deep-Inelastic Scattering and the Drell-Yan Process*,
Phys. Lett. **B**497 (2001) 228-234

[53] S. Catani, M.L. Mangano, P. Nason, L. Trentadue,
*The Resummation of Soft Gluons in Hadronic Collisions*,
**B**478 (1996) 273-310

[54] B. Fuks,
*QCD-Resummation and Non-Minimal Flavour-Violation for Supersymmetric Particle Production at Hadron Colliders*,
Ph.D. thesis, Grenoble 2007

[55] N. Kidonakis, J.F. Owens,
*Soft-Gluon Resummation and NNLO Corrections for Direct Photon Production*,
Phys. Rew. **D**61 (2000) 094004

[56] N. Kidonakis,
*Effects of Higher-Order Threshold Corrections in High-$E_T$ Jet Production*,
Phys. Rev. **D**63 (2001) 054019

[57] S.M. Aybat, L.J. Dixon, G. Sterman,
*The Two-Loop Anomalous Dimension Matrix for Soft Gluon Exchange*,
Phys. Rev. Lett. 97 (2006) 072001

[58] N. Kidonakis,
*Next-to-Next-to-Leading Order Soft-Gluon Corrections in Direct Photon Production*,
Int. J. Mod. Phys. **A**19 (2004) 149-158

[59] DØ Collaboration,
*The Inclusive Jet Cross Section in $p\bar{p}$ Collisions at $\sqrt{s} = 1.8\,\mathrm{TeV}$*,
Phys. Rev. Lett. 82 (1999) 2451-2456

[60] M. Klasen, T. Kleinwort, G. Kramer,
*Inclusive Jet Production in $\gamma p$ and $\gamma\gamma$ Processes: Direct and Resolved Photon Cross-Sections in Next-to-Leading Order QCD*,
Eur. Phys. J. direct **C**1 (1998) 1

[61] N. Kidonakis,
*Next-to-Next-to-Next-to-Leading Order Soft-Gluon Corrections in Hard-Scattering Processes Near Threshold*,
Phys. Rev. **D**73 (2006) 034001